Fisheries and Oceans Canada
Pêches et Océans Canada

Ecosystems and Oceans Science
Sciences des écosystèmes et des océans

Canadian Science Advisory Secretariat (CSAS)

Research Document 2026/059

Pacific Region

Seasonal Spatial Densities of Cetaceans in the Southern Salish Sea and on Swiftsure Bank

Christie J. McMillan, Elise A. Keppel, Lisa D. Spaven, Thomas Doniol-Valcroze

Fisheries and Oceans Canada
Pacific Biological Station
3190 Hammond Bay Road
Nanaimo, BC, V9T 6N7

August 2026

Foreword

This series documents the scientific basis for the evaluation of aquatic resources and ecosystems in Canada. As such, it addresses the issues of the day in the time frames required and the documents it contains are not intended as definitive statements on the subjects addressed but rather as progress reports on ongoing investigations.

Published by:

Fisheries and Oceans Canada
Canadian Science Advisory Secretariat
200 Kent Street
Ottawa ON K1A 0E6

http://www.dfo-mpo.gc.ca/csas-sccs/
DFO.CSAS-SCAS.MPO@dfo-mpo.gc.ca

ISSN 1919-5044
ISBN 978-1-100-00261-3 Cat. No. Fs70-5/2026-059E-PDF

Correct citation for this publication:

McMillan, C.J., Keppel, E.A., Spaven, L.D, and Doniol-Valcroze, T. 2026. Seasonal Spatial Densities of Cetaceans in the Southern Salish Sea and on Swiftsure Bank. DFO Can. Sci. Advis. Sec. Res. Doc. 2026/059. x + 70 p.

Aussi disponible en français :

McMillan, C.J., Keppel, E.A., Spaven, L.D, et Doniol-Valcroze, T. 2026. Densités spatiales saisonnières des cétacés dans le sud de la mer des Salish et sur le banc Swiftsure. Secr. can. des avis sci. du MPO. Doc. de rech. 2026/059. xii + 77 p.

TABLE OF CONTENTS

LIST OF TABLES

LIST OF FIGURES

ABSTRACT

Effective assessment and management of anthropogenic threats to marine mammals requires knowledge of the distribution and habitat use of affected species and how their density patterns vary over time. Knowledge of seasonal density and distribution of cetaceans was identified as a data gap by the Canada Energy Regulator, in relation to the need to mitigate impacts of increased shipping traffic associated with the Trans Mountain Expansion Project (TMX). In response, Fisheries and Oceans Canada conducted a series of 29 systematic, multi-species boat-based cetacean surveys across all seasons from August 2020 to August 2024, covering the southern Salish Sea and Swiftsure Bank. Eight species of cetaceans, including six populations listed under the *Species At Risk Act*, were detected. Distance sampling methods and density surface modelling were used to provide the first year-round, spatially explicit density estimates for humpback whales, harbour porpoises, and Dall's porpoises in the southern Salish Sea and on Swiftsure Bank. All three species showed strong spatial and seasonal density patterns. Areas of highest density for humpback whales included Swiftsure Bank in all seasons, and central and western Juan de Fuca Strait in summer and fall. High densities of harbour porpoises occurred in Haro Strait, Boundary Pass, and eastern Juan de Fuca Strait year-round, while Dall's porpoise density was highest in the southern Strait of Georgia in fall and winter, and in the western portion of the study area in spring and summer. These results will be used to inform future risk assessment models and underscore the need for management strategies that are aligned with seasonal density patterns rather than relying on data from a single season or year.

1. INTRODUCTION

The Salish Sea encompasses biologically rich waters in southern British Columbia and northern Washington State that support a diverse assemblage of marine mammals. These coastal waters have witnessed an increase in human activities, including commercial shipping, recreational boating, and industrial development. In particular, the Trans Mountain Expansion Project (TMX) will further increase vessel traffic, raising concerns about potential impacts on cetacean populations through underwater noise, ship strikes, and habitat degradation. Recognizing these risks, the Canada Energy Regulator (CER) asked the Governor in Council to develop an Offset Program to mitigate the effects of increased marine shipping, with Recommendation 6(d) calling for the identification of specific foraging, congregation and migration areas of species listed under the *Species At Risk Act* and consideration of mitigations in those areas (including Swiftsure Bank; National Energy Board 2019). These objectives required that the seasonal spatial densities of cetacean species be quantified for the southern Salish Sea and Swiftsure Bank.

The most recent threat mitigation research on marine mammal species in the region has focused on the endangered Southern Resident killer whale (*Orcinus orca*) population (Joy et al. 2019, Burnham et al. 2021, Vagle et al. 2021, Thornton et al. 2022a, Thornton et al. 2022b). Although this population-specific research has led to the implementation of management measures aimed at reducing the impacts of vessel noise and fisheries on Southern Resident killer whales (Government of Canada 2024), little consideration has been given to whether these measures effectively mitigate threats to other cetacean species in the area. One reason for this gap is the lack of effort-corrected, seasonally resolved data with comprehensive coverage to estimate density and habitat use. Spatially explicit density estimates are needed to identify areas of high cetacean presence and their overlap with human activities. Knowledge of seasonal and inter-annual variation is also essential for assessing the risks posed by anthropogenic stressors.

In addition to Southern Resident killer whales, marine mammal species frequently sighted in the southern Salish Sea include humpback whales (*Megaptera novaeangliae*), harbour porpoises (*Phocoena phocoena*), Dall's porpoises (*Phocoenoides dalli*), harbour seals (*Phoca vitulina*), Steller sea lions (*Eumetopias jubatus*), California sea lions (*Zalophus californianus*) and Bigg's (transient) killer whales (*Orcinus orca*). There is significant and ongoing work underway to assess the abundance and distribution of several of these species, including Steller sea lions, California sea lions, harbour seals, and Bigg's killer whales (e.g. Ford et al. 2013b, Olesiuk 2018, Towers et al. 2019, Majewski and Ellis 2022, DFO 2023, Majewski et al. 2024). There are, however, significant gaps in knowledge of the seasonal abundance and habitat use of humpback whales, harbour porpoises, and Dall's porpoises in the area. Although most humpback whales migrate to warmer waters during winter, there have been sightings of these whales and both porpoise species in the Salish Sea year-round (Hall 2004, Hall 2011, McMillan et al. 2025, Elliser et al. 2025). Humpback whales and harbour porpoises are listed as Special Concern under the *Species at Risk Act* (SARA), while Dall's porpoises are considered Not At Risk. Other less frequently observed cetacean species in the area include fin whales (*Balaenoptera physalus*, Threatened under SARA), grey whales (*Eschrichtius robustus*, Special Concern), minke whales (*Balaenoptera acutorostrata,* Not At Risk), and Pacific white-sided dolphins (*Lagenorhynchus obliquidens*, Not At Risk). Individuals from all of these marine mammal species may be vulnerable to impacts of increasing vessel traffic when present in the southern Salish Sea and on Swiftsure Bank.

The current state of knowledge on cetaceans in the Salish Sea has relied heavily on presence-only data from platforms of opportunity (e.g., Hauser et al. 2007, Olson et al. 2018). These data often contain biases due to uneven spatial effort and targeting of certain species that make them ill-suited for quantification of density patterns. Therefore, several previous studies have used systematic survey designs and density modelling to predict the density of cetaceans in study areas that include the southern Salish Sea (e.g., Best et al. 2015, Nichol et al. 2017, Wright et al. 2021). However, these surveys were often limited to a single season (Williams and Thomas 2007, Jefferson et al. 2016, Wright et al. 2021), yielded small sample sizes requiring data pooling across multiple seasons (Nichol et al. 2017), or were conducted too long ago to inform current management needs (Keple 2002, Hall 2004, Best et al. 2015). As a result, these studies cannot be used to determine the extent to which current cetacean densities vary by season and year. Given the dynamic nature of marine ecosystems and evidence that several species have exhibited significant shifts in their abundance and distribution in the Salish Sea in recent years (Calambokidis et al. 2017a, Wright et al. 2021), such current information is crucial to provide robust risk assessment and mitigation advice.

Fisheries and Oceans Canada (DFO) has addressed these knowledge gaps by initiating regular, year-round, boat-based cetacean surveys in the southern Salish Sea and on Swiftsure Bank. From August 2020 to August 2024, these surveys have used a systematic line-transect design and distance sampling methods to collect data on cetacean abundance and distribution. The specific objectives of this assessment were to provide seasonal, spatially explicit estimates of the density of cetacean species in the TMX marine shipping area (Figure 1), and to identify the sources of uncertainty and variability in the assessment. The results of this study will contribute to the development of spatially explicit data layers for future risk assessment and inform decision-making related to marine conservation. While primarily focused on the TMX marine shipping area, these findings will also provide valuable insights for other major projects in the Salish Sea with marine shipping components.

2. METHODS

2.1. STUDY AREA AND SURVEY DESIGN

The study area was selected specifically to answer management questions related to the TMX marine shipping area and therefore was delineated using a 6 km buffer around the commercial shipping lanes in the southern Salish Sea marine shipping route between Vancouver and Swiftsure Bank (Figure 1). Although the original survey design also included the U.S. side of the shipping lanes, survey effort during the first two years of the study was limited to the Canadian portions of the study area due to restrictions associated with the COVID-19 pandemic. The current analysis is thus limited to this portion of the study area. Given the geographic complexity of the study region, the area was divided into seven sections for the purpose of survey design, and transect lines were generated for each section separately. This enabled the angles of the transect lines to vary among sections, minimizing off-effort transit time and allowing the majority of transect lines to run perpendicular to depth gradients, as recommended by Thomas et al. (2007). Similar designs were used for previous line-transect surveys in the southern Salish Sea (Williams and Thomas 2007, Doniol-Valcroze et al. 2024). The same line spacing was used across the seven sections to maintain even coverage throughout the study area. The sections could thus be combined and analyzed as a single geographic stratum (3,408 km^2).

The Distance Sampling Survey Design (dssd) package (Marshall and Rexstad 2021) in R (R Core Team 2023) was used to generate transect lines based on a complementary equally-spaced zig-zag design. Several options for line spacing between 13 and 20 km were explored, and a distance of 18 km between lines was selected to balance the time required to conduct each survey and the coverage intensity of the study area. The dssd package was used to ensure that all portions of the study area had an equal probability of being included in the sampled transect lines. The chosen design was then used to generate different realizations of the transect lines for each survey, with different random starting points (Buckland et al. 2001).

2.2. DATA COLLECTION

Surveys were conducted year-round, on a monthly basis when possible, in 2020-2022, and every other month in 2023-2024, due to vessel and crew constraints. The 12.8 m research vessel traveled along pre-determined transect lines at approximately 10 knots (18.5 km hr^{-1}) when “on-effort” (actively surveying along transect lines). Data collected when vessel speed was less than 5 knots (9.2 km hr^{-1}) or greater than 13 knots (24.1 km hr^{-1}) were excluded from analyses. Surveys were conducted in “passing” mode (i.e., the research vessel generally did not divert from a consistent speed and direction while on transect lines), but observational effort was halted occasionally when required for species confirmation or in response to marine traffic. The order and direction in which each transect line was surveyed depended primarily on weather conditions. Effort was not conducted when conditions precluded effective surveying, which generally occurred when Beaufort sea state reached 5, or swell height reached 3 metres; however, other factors including wind and swell direction, glare, precipitation, visibility, and tidal effects were also considered in decisions of whether to suspend or continue survey efforts.

Data were collected using standard distance sampling protocols (Buckland et al. 2001). One observer was positioned on either side of the vessel’s bow (285 cm average height of eye from sea level) and used 7x50 Fujinon binoculars equipped with reticles to visually scan for cetaceans from 0-90 degrees on each side of the realized transect line. Each observer worked independently to communicate sightings to the data collection station via in-ear Ultra High Frequency radio headsets. The data recorder was positioned inside the wheelhouse and recorded data from the observers using Mysticetus software (Steckler and Donlan 2018), while also assisting with data quality control (e.g., avoiding entry of duplicate sightings in the case of both observers detecting the same sighting ahead of the vessel). The observers and the data recorder rotated positions after every transect line, or after 45 minutes depending on transect line length, to avoid eye strain and fatigue. All sightings included in the analyses were made by the same three observers throughout the entire study period.

Mysticetus, connected to GPS, automatically collected vessel position and speed every 10 s, and upon each new entry of effort or sightings data. Effort conditions were reported by observers at the start of each transect line, when observers switched positions, and whenever conditions changed. Effort conditions included visibility, Beaufort sea state, cloud cover, glare intensity and extent, precipitation, and swell height (Table 1). Data collected at the time of each cetacean sighting included the angle and reticle reading (or visually estimated radial distance if the sighting was very close to the vessel) to the animal(s), species, and group size (i.e., the number of animals spotted in a single detection). The reticle measurements built into the binoculars were used to determine the distance to each sighting by counting down from the horizon or nearest land mass to the location of the sighting. Rail-mounted, manual protractors were used to measure the angle from the vessel heading to each cetacean sighting, and the boundaries of the glare extent.

2.3. DATA PROCESSING

Radial sighting distances were calculated based on reticle readings, distance to the horizon (or nearest land mass), and the observational height of eye (Buckland et al. 2001). When reticles were measured from the nearest land mass, the distance to the land mass was used to correct the position and distance of sightings using a custom R script. The perpendicular distance of each sighting from the trackline was calculated from the radial sighting distance and the angle to the sighting.

2.4. ANALYTICAL APPROACH

The specific objectives of our analyses focused on generating reliable density surfaces rather than identifying mechanistic drivers of cetacean distribution. Our modelling approach was therefore predictive in nature, rather than explanatory, and as such, was designed to optimize spatial prediction rather than test causal hypotheses. We fit separate density surface models (DSMs) for each cetacean species and season to estimate year-round, spatially explicit densities throughout the study area. “Seasons” were defined as four three-month periods: January - March (winter), April - June (spring), July - September (summer), and October - December (fall). Seasons were delineated to correspond with abundance and distribution patterns of cetacean species in the study area, thus minimizing intra-seasonal variability.

DSMs are a two-stage approach for modeling spatially explicit density using distance sampling data (Miller et al. 2013). First, imperfect detection during survey effort is modeled using detection functions (DFs; Buckland et al. 2001, Marques et al. 2007). Survey data are then divided into segments of continuous effort, and the counts per segment, adjusted for detectability based on the DFs, are used as the response variable in generalized additive models (GAMs) to predict how density varies throughout the study area as a consequence of environmental covariates (Hedley and Buckland 2004, Miller et al. 2013). This approach is frequently used to estimate cetacean abundance (e.g., Williams et al. 2011, Best et al. 2015, Wright et al. 2021), and has been of particular interest in DFO stock assessments for complex geographic regions (Doniol-Valcroze et al. 2015, Marcoux et al. 2019, Thompson et al. 2022). In addition, the resulting maps of predicted density can inform threat risk assessments and mitigation (Nichol et al. 2017, Mayaud et al. 2024).

2.5. DETECTION FUNCTIONS

Detection functions were fit to the perpendicular (relative to trackline) sighting distances of each species using the *ds* function in the Distance R package (Miller 2017). Because the survey platform, protocols, and team of observers remained consistent throughout the study period, DFs were informed by data pooled across all months and years.

DFs were first fit with key-only models (half-normal, hazard-rate, and uniform key functions), considered with and without cosine and polynomial series adjustments. To determine appropriate right-truncation distances, key-only DFs were examined for the perpendicular distance at which the probability of detection was approximately 0.15, as recommended in Buckland et al. (2001). Visibility, Beaufort sea state, swell, glare, individual observer, precipitation, cloud cover, and group size were considered as candidate covariates in the DFs (Marques and Buckland 2003). All detection covariates were considered as categorical variables. Some covariate levels were pooled to ensure sufficient numbers of sightings in each covariate category (i.e., no less than 10 observations for any category) and considering the expected impact on detectability of different species (Table 2). Covariates were added to the key-only models in a stepwise forward selection process. Comparisons were made between the key-only models and each of the covariate models based on Akaike information criterion (AIC) values. Goodness of fit was assessed using Cramer-von Mises (CvM) tests and visual inspection of quantile-quantile (QQ) plots for continuous perpendicular distance data or using chi-squared (χ^2) tests for binned perpendicular distance data.

2.6. SEGMENTATION

DSMs require continuous effort conducted along individual transect lines to be split into smaller segments with homogenous effort conditions. Buckland et al. (2004) and Miller et al. (2013) recommend a segment length of approximately twice the truncation distance used in a species’ detection function, though DSMs tend to be robust to the selection of segment length (Hedley and Buckland 2004). Given the multi-species nature of our analyses, our truncation distances ranged from a minimum of 0.65 km (harbour porpoises) to a maximum of 1.65 km (humpback whales), and we thus selected an intermediate segment length of 2 km that we deemed appropriate for all three species.

We followed methods described in Becker et al. (2010) and used in Wright et al. (2021) to adjust segment lengths to incorporate remaining sections of effort beyond the total transect length divisible by two (i.e., the “extra” distance covered, which ranged from approximately 0.1 km to 1.9 km). If the extra distance covered along a section of continuous effort and conditions was more than 1 km, then the transect was divided such that all segments were 2 km long, with the exception of one segment that was the length of this extra distance (i.e., between 1 - 2 km long). If the extra distance was 1 km or less, then one of the segments along the same continuous transect line was adjusted to include this additional distance (i.e., one segment was randomly selected to be between 2.1 and 2.9 km long, while all others remained at the target length of 2 km).

Segments were generated separately for each species, based on the detectability covariates that were relevant to the detection of the species. For example, if Beaufort sea state was included as an explanatory covariate in a species’ DF, segments for that species comprised portions of effort along a single transect line in which Beaufort sea state did not change.

2.7. ENVIRONMENTAL COVARIATES

While the inclusion of environmental covariates can help with ecological interpretation, we prioritized variables that improved model performance and predictive accuracy, rather than seeking to infer causal relationships. Static environmental covariates considered in our spatial models included depth, slope, rugosity, root mean square (RMS) of tidal current speed, distance to nearest area of high tidal current, and distance to the nearest shore. Each of these temporally static covariates were included based on their influence on cetacean distribution and density in previous studies (e.g., Best et al. 2015, Meynecke et al. 2021, Wright et al. 2021, Bortolotto et al. 2023). Data sources and definitions for each the static covariates are consistent with those described in Wright et al. (2021) and are detailed in Table 3.

In addition, we considered two temporally dynamic covariates: sea surface temperature (SST) and chlorophyll a (chl a) concentration. Given that data on cetacean prey species were not available at the spatial or temporal resolution required to inform our spatial models, we included these variables as potential proxies indicating dynamic areas of higher productivity and prey density (e.g., Schleimer et al. 2019, Meynecke et al. 2021). Data sources and methods of assigning these dynamic covariates to segments are included in Table 3.

Environmental covariates for each season and each species’ segments were examined and outliers were removed. Where covariate value distribution was skewed, covariates were transformed using log or square-root transformations. All environmental covariates and sighting positions were standardized prior to model fitting. Each pair of environmental covariates for each species and season were then examined for collinearity using Pearson’s correlation coefficient. Covariates with strong relationships (Pearson correlation values greater than 0.7) were not included in the same candidate models.

Month and year (considered as factors) were also examined for collinearity with the environmental covariates and with one another, then were included as potential categorical covariates in candidate models. Unlike the environmental covariates, the addition of one or both of these factors did not affect the spatially-varying density patterns throughout the study area but allowed the intercepts to vary between months or years within a season. Intra-season variability could thus be considered in the overall density estimates for the study area, but not in spatially explicit density patterns.

2.8. SPATIAL MODELS

Generalized additive models (GAMs) were fit using the dsm package in R (Miller et al. 2019). Counts per segment for each species and season were modeled using both negative binomial and Tweedie distributions. Models were fit using restricted maximum likelihood (REML). Candidate model sets for each species and season included a spatial-only model (i.e., with a bivariate spatial smoother of sighting position as the only covariate), as well as candidate models that included each potential combination of non-collinear environmental covariates, in addition to the bivariate spatial term. Each candidate model within each distribution was fit twice: once with all environmental covariates initially fit using univariate thin plate regression spline (ts) smooths and once with all environmental covariates fit using univariate Duchon spline (ds) smooths. The ds splines were considered because they can be effective in mitigating edge effects (i.e., unrealistically high predictions of density in areas farthest from most survey effort; Miller et al. 2013). Multiple options for the basis dimension (k) for each smooth term were considered, to explore how increasing or decreasing k impacted the smooth's effective degrees of freedom (EDF), therefore reducing the potential for overfitting. Term selection was conducted using a shrinkage approach (Marra and Wood 2011), which penalizes null space and shrinks non-significant terms toward zero. This approach allows model selection to occur in fewer steps and avoids the path dependency associated with stepwise model selection. Covariates with EDFs < 1 were removed from the candidate models. Any covariates with EDFs approximately equal to one were included in the final candidate models as linear terms rather than higher-order smoothers. Linear terms and factors with p-values < 0.05 were retained in the final candidate models for each season.

Model validation and selection for each species and season followed several steps. Smooth terms within candidate models were checked for concurvity with one another (i.e., the extent to which one smooth term in the model could be explained by one or more of the other smoothers) using the *vis_concurvity* function in the dsm package. QQ plots and residual patterns were examined for the candidate models using various functions (*rqgam.check, gam.check,* and *qq.gam*) in the dsm and mgcv packages. Scaled quantile residuals were created and examined using the DHARMa package in R (Hartig 2024) to further examine residual patterns and to identify potential problems with zero inflation or overdispersion. In addition to the model validation process, we considered both AIC and Bayesian information criterion (BIC) to achieve a balance between model fit and model complexity. Final model selection decisions also considered the relationships between candidate covariates and the response variable based on visual examinations of partial effects plots and the spatial distributions predicted by candidate models relative to our survey sightings, as well as edge effects and estimates of uncertainty.

2.9. ABUNDANCE AND DENSITY PREDICTIONS

Spatially explicit density for each species and season based on the selected model were predicted over a 2 km x 2 km grid that covered the Canadian portions of the survey area. Grid size was selected to correspond with the target length of our segments, and with the available resolution of environmental covariate data. The prediction grid was cropped to exclude any portions located on land, and any resulting grid cells with an area of less than 1 km^2 were excluded from analyses. Environmental covariates were either averaged over each grid cell (for depth, slope, rugosity, and tidal speed), or extracted/calculated for the midpoint of the grid cell (for distance to shore, distance to the nearest high tidal current area, SST, and mean chl a; see Table 3 for sources of these data). Density per cell for each temporal period was predicted separately for any models that included temporally dynamic environmental covariates (i.e., SST, chl a) or month / year terms, and then averaged to estimate density for the season. Colour scales on the resulting density plots were consistent among seasons for a given species but varied between species.

Overall and spatially explicit (per-cell) coefficients of variation (CVs) were estimated for each model. The approach to estimating uncertainty varied among species, based on whether or not detectability covariates were included in their detection functions. If a species' DF did not include covariates, average detectability did not vary spatially; thus, the uncertainty in the DF was assumed to be independent from uncertainty in the GAM, and the delta method was used to combine the estimates of uncertainty from the two models. For species whose DFs did include covariates, uncertainty from the DF model was propagated through the GAM model using methods described in Bravington et al. (2021) and Williams et al. (2011). For any models that included dynamic environmental covariates or month / year terms, we estimated variances for each temporal period separately and averaged these, before converting to an average CV for the study period.

3. RESULTS

3.1. SURVEY EFFORT AND SPECIES SIGHTINGS

In total, 29 surveys were conducted between August 2020 and August 2024, resulting in 8,524 km of effort over 161 days along pre-determined transect lines. Of this effort, 7,370 km were within Canadian portions of the study area and were thus included in the spatial analyses. DFs were informed by all on-effort survey data. All months were represented at least once in the study period. The transect distance covered (i.e., realized effort) varied among surveys, from a low of 138 km in October 2022, to a high of 561 km in March 2024. Coverage by month, season, and year is provided in Table 4 and Figure 2.

A total of 2,306 sightings of eight cetacean species (3,992 individuals), comprised of humpback whales, harbour porpoises, Dall's porpoises, killer whales, Pacific white-sided dolphins, a minke whale, a grey whale, and a fin whale, were made while surveying along pre-determined transect lines (Figures 3 - 7). Additional (incidental) sightings of some species were made while off-effort (Figures 6, 7). Incidental sightings were not used in the DFs or DSMs but provide insight into the seasonal presence of these species in the study area.

The three most frequently detected species were humpback whales, harbour porpoises, and Dall's porpoises. Humpback whales were sighted year-round (553 sightings comprising 903 individuals; Table 5, Figure 3), during all months of the year except March. The highest numbers of humpback whales were detected between August and October. Mean humpback whale group size (i.e., the number of individuals in a single detection) was lowest in winter (mean: 1.2, range: 1 – 2) and highest in fall (mean: 1.9, range: 1 – 8). Harbour porpoises were the most frequently sighted species of cetacean (1,529 sightings of 2,465 individuals; Table 5, Figure 4) and were detected during all surveys. The highest numbers of harbour porpoise sightings in each year occurred during either summer or fall, though the largest group of harbour porpoises detected was a sighting of approximately 45 individuals in April 2021 in eastern Juan de Fuca Strait. Group size for harbour porpoises tended to be lowest in summer (mean: 1.5, range: 1 – 7) and highest in fall (mean: 1.8, range: 1 – 17) and winter (mean: 1.8, range: 1 – 18). Dall's porpoises were also encountered year-round (164 sightings of 437 individuals; Table 5, Figure 5), though less frequently than harbour porpoises. The number of Dall's porpoise detections were highest in winter and lowest in summer. Average Dall's porpoise group size was also largest in winter (mean: 2.9, range: 1 – 9) and smallest in summer (mean: 2.1, range: 1 – 4).

Groups of Southern Resident and Bigg's (transient) killer whales were encountered 21 and 18 times, respectively, while on-effort. Three additional killer whale groups were detected while on-effort, but ecotype could not be confirmed for these sightings. Bigg's killer whales and Southern Resident killer whales were each sighted during all seasons (Table 5, Figure 6). A fin whale, a minke whale, a grey whale, and a group of Pacific white-sided dolphins were each sighted once while on-effort (Table 5, Figure 7). The grey whale sighting occurred in March, the minke whale sighting in July, the fin whale sighting in August, and the Pacific white-sided dolphin sighting in September. Additional killer whales, minke whales, grey whales, Pacific white-sided dolphins, and a fin whale were also detected in the study area while "off-effort" (i.e., transiting between transect lines; Figure 6, Figure 7).

3.2. DETECTION FUNCTIONS

Three species (humpback whales, harbour porpoises, and Dall's porpoises) had sufficient sightings to fit detection functions. Comparisons of the top-performing models with delta AICs of less than five for each species are presented in Tables 6, 7 and 8.

The best performing DF model for humpback whales based on AIC was a half-normal key function with swell and visibility as covariates (Table 6, Figure 8a). Two other models had AIC scores within 2 of the top model:

1. a half-normal key function with swell, visibility, and glare as covariates; and
2. a half-normal model with swell, visibility, and precipitation as covariates.

CvM tests indicated that all three models showed good fit to the data, and the average detectability (i.e., the estimated average probability of detecting an animal given that it is within the survey area) was consistent among all three models. The least complex model with marginally better AIC support was therefore selected. Humpback whale sightings were right-truncated at a distance of 1.65 km and the average detectability was 0.59, resulting in an effective strip width of 0.97 km.

Initial attempts to fit DFs to the harbour porpoise data resulted in CvM p-values that were less than 0.05, indicating poor model fit. Data exploration suggested that this may have been due to heaping or clusters of detections around some perpendicular distances (Buckland et al. 2001, Howe et al. 2019). As recommended by Buckland et al. (2001), we therefore grouped the perpendicular distance data for harbour porpoises into bins and fit detection curves to the binned data. The width of the first bin was 0.1 km, while all subsequent bins widths were 0.05 km (Figure 8b). The top-ranked DF for harbour porpoises based on AIC was a half-normal model with Beaufort sea state, cloud cover, and observer as covariates; however, this model failed the chi-squared goodness of fit test. The next highest ranked model was therefore selected - a half-normal key function with no detectability covariates but including cosine series adjustment terms of order 2,3. (Table 7, Figure 8b). Harbour porpoise sightings were right-truncated at a distance of 0.65 km and the average detectability for the selected model was 0.48, resulting in an esw of 0.32 km.

The DF models with the lowest AIC scores for Dall's porpoises were:

1. half-normal and hazard-rate models with glare and swell as covariates;
2. a half-normal model with glare as the only covariate;
3. half-normal and uniform models with no detectability covariates; and
4. a hazard rate model with swell as the only covariate (Table 8).

CvM tests indicated that all of the top-ranked models exhibited relatively good fit to the data; however, the hazard-rate models fitted large spikes near zero perpendicular distance. Given that Dall's porpoises are known to show responsive movement toward vessels to bow-ride (Best et al. 2015), there was concern that this model would result in overestimation of abundance due to this potential responsive movement. We thus excluded the hazard-rate models from further consideration. Average detectability was very similar among the remaining top-ranked models and the model with slightly stronger support, the half-normal model with swell and glare as covariates, was selected (Table 8, Figure 8c). Sightings were right-truncated at a distance of 0.8 km and the average detectability of the selected model was 0.57, resulting in an esw of 0.46 km.

3.3. SPATIAL MODELS

3.3.1. Humpback Whales

We fit humpback whale density models to the selected four three-month seasonal periods: January - March (winter), April - June (spring), July - September (summer), and October - December (fall). Although initially included in the candidate models for each season, many of the static environmental covariates were removed from the models either because of low EDFs or high concurvity with the bivariate spatial smoother. The selection of the top model had little impact on humpback whale density estimates (Table 9) and on overall spatial patterns in all seasons.

The selected humpback whale DSM for winter was a Tweedie model with the bivariate smoother of X and Y as the only smooth term, fit using a ds spline (Table 9). All three of the candidate negative binomial models had higher CVs than the Tweedie models and exhibited some edge effects toward the western portion of the study area and thus were not considered further. The three candidate Tweedie models had equal support based on AIC, and the spatial-only ds model was selected because it minimized edge effects (Figure 9).

The top-ranked Tweedie humpback model for spring based on AIC included the bivariate smoother of X and Y and a smooth of slope, with month as a factor and fit using ds splines (Table 9). Again, the Tweedie models were selected over the negative binomial models as they minimized CVs and edge effects. Among the Tweedie models, one other model was within ΔAIC of 2 of the selected model – the ds model with the bivariate smoother of X and Y as the only smooth term, and month as a factor. Examination of the predicted density plot (Figure 10) and the partial effect plot (Figure 11) supported the inclusion of slope in the selected model, and the addition of slope reduced the CV compared to the model without slope. We therefore selected the Tweedie model with marginally better AIC support that included the smooth of slope.

The selected summer DSM for humpback whales was a negative binomial model with the bivariate smoother of X and Y as the only covariate, fit using a ts spline (Figure 12). This model had the lowest BIC and among the lowest CVs of all negative binomial models (Table 9). The model that included SST as a linear term and year as a factor had the lowest AIC of the negative binomial models, but the highest BIC. Given that the inclusion of SST did not change the predicted spatial density patterns and resulted in a higher CV, we selected the simpler model with the lowest BIC score, rather than the more complex model with the lowest AIC score. The Tweedie model with the lowest BIC also included the bivariate smoother of X and Y as the only covariate, fit using a ts spline; however, this model exhibited some edge effects in the southwestern portion of the study area and was thus not selected. The Tweedie models with the lowest AIC included a smooth of chl a, a covariate that did not show any clear relationship with counts per segment in summer and resulted in very high CVs and edge effects in parts of the study area.

Data exploration of the effect of month on counts per segment for humpbacks whales during fall indicated that this covariate was influenced by the lower number of sightings and less effort in December and was thus not a reliable predictor for this season. Candidate models that included month as a factor were therefore not considered further. The highest ranked negative binomial models failed model validation tests; thus, we selected the Tweedie model with the bivariate smoother of X and Y, fit using a ts spline, with SST included as a linear term and year as a factor (Table 9, Figures 13, 14, A2). This model minimized edge effects and had among the lowest AIC, BIC, and CVs of all candidate Tweedie models.

Humpback whale spatial models indicated strong seasonal differences in density patterns (Figures 9, 10, 12, 13), though the western portion of the study area, which includes Swiftsure Bank, was highlighted as an area of high relative density year-round. The number of humpback whale sightings, and thus the estimated abundance and density throughout the study area, were low in winter, with an estimated total of only 14 (CV = 0.36) humpback whales, but the highest density of these humpbacks was predicted to occur around Swiftsure Bank. As the abundance of humpbacks in the study area increased through spring (81, CV = 0.14), summer (221, CV = 0.19), and fall (347, CV = 0.18), the density of humpback whales predicted around Swiftsure Bank remained high. The summer and fall models further indicated that humpback whale density was not uniformly high throughout the Swiftsure Bank area, but rather that the highest density areas corresponded to the eastern portion of the Bank, characterized by abrupt changes in depth (Figure A1). High densities of humpback whales were also predicted in central and western Juan de Fuca Strait in summer and fall (up to 0.31 and 0.91 whales per km^2, respectively). The Strait of Georgia and eastern Juan de Fuca Strait had moderately high densities of humpback whales in spring, summer and fall. Humpback whale density was low in Haro Strait year-round.

3.3.2. Harbour Porpoises

The environmental covariates with good predictive power for harbour porpoises varied seasonally but were similar to humpback whales in that many of the temporally static covariates were removed from candidate models due to low EDFs or high concurvity with the spatial smooths.

The selected harbour porpoise model for winter was a negative binomial model with the bivariate smoother of X and Y as the only smooth term and month as a factor, fit using a ts spline (Table 10; Figure 15). Model validation tests indicated that all Tweedie models for this season were overdispersed; thus, only negative binomial models were considered further. Among the candidate negative binomial models, the top-ranked models based on AIC both included SST as a smooth term; however, the smooth plot of SST indicated no clear relationship between this covariate and the response variable. Additionally, the inclusion of SST resulted in some edge effects at the southeastern portion of the study area. We therefore selected the top-ranked negative binomial model based on BIC, which had a lower CV and lack of edge effects compared to the models that included SST.

Model validation tests indicated that the negative binomial models for harbour porpoises in spring out-performed the Tweedie models; thus, the Tweedie models were not considered in further model selection decisions for this season. The negative binomial model with the lowest AIC score included the bivariate smoother of X and Y and a smoother of chl a, both fit with ts splines, and slope as a linear term (Table 10). However, this model had a higher CV than many of the other candidate models and displayed some edge effects in parts of the study area. The three top-ranked negative binomial harbour porpoise models for spring based on BIC were all fit with ts splines and included the bivariate smoother of X and Y as the only smooth term. These included:

1. a model with rugosity as a linear term;
2. a model with no linear terms or factors; and
3. a model with slope as a linear term.

Selection among these three models had little impact on spatial patterns, CVs, or estimates of overall density. We therefore selected the model with marginally better BIC support and the lowest AIC score among the three: the negative binomial model with the bivariate smoother of X and Y fit with a ts smooth, and rugosity as a linear term (Figure 16, Figure 17).

The selected summer model for harbour porpoises was a Tweedie model with the bivariate X, Y smoother fit with a ts spline, with RMS tidal current speed as a linear term and year as a factor (Table 10, Figure 18, Figure 19). The Tweedie models were selected over negative binomial models because model validation tests indicated deviations in the residuals of almost all candidate negative binomial models. The Tweedie models with the lowest AIC scores were complex models with smooths of SST and chl a in addition to the bivariate spatial smoother, and month and year as factors. These models had very high CVs compared to all other candidate models and resulted in some edge effects in the southeastern parts of the study area. We therefore selected the Tweedie model with the lowest BIC score, which showed no sign of edge effects and had a much lower CV.

Model validation tests indicated that all candidate Tweedie models for harbour porpoises during fall were overdispersed, so further model selection was carried out among the negative binomial models only. The top-ranked negative binomial model for this season based on AIC included smooths of SST and chl a in addition to the spatial smoother, with month as a factor (Table 10). Spatially-varying CVs for this model were very high, however, particularly toward the western portion of the study area. Additionally, the smooth plot of SST indicated no clear relationship between this covariate and the response variable. The next best model based on AIC was also the top-ranked model based on BIC, had a lower CV than the top-ranked model based on AIC alone, and its predicted density plot showed a better fit to the sightings and lack of edge effects. We therefore selected this model, which used a ts spline, and included the bivariate smoother of X and Y as the only smooth term and month as a factor (Figure 20).

Harbour porpoise density was high in Boundary Pass, Haro Strait, and eastern Juan de Fuca Strait year-round (Figures 15, 16, 18, 20). Harbour porpoise densities in this area were particularly high during summer and fall; portions of these areas had predicted densities of more than three harbour porpoises per km^2 (Figure 18, Figure 20). The western portions of the study area (western Juan de Fuca Strait and Swiftsure Bank) had low densities of harbour porpoises predicted year-round, though uncertainty in these areas was high, owing to the very small number of harbour porpoise detections in this portion of the study area during all months. The Strait of Georgia also had areas of moderately high density predicted during most bimonthly periods, with particularly high densities in the eastern portion of the Strait during fall (Figure 20).

Estimated overall abundance of harbour porpoises was highest during fall (1,552, CV = 0.23) and lowest during winter (637, CV = 0.29). A total of 1,335 (CV = 0.11) and 1,192 (CV = 0.17 harbour porpoises were estimated in the study area in spring and summer, respectively.

3.3.3. Dall's Porpoises

Based on AIC scores, the top-ranked Tweedie and negative binomial winter Dall's porpoise models included smooths of SST in addition to the bivariate spatial smoothers, and no other linear terms or factors (Table 11). The top-ranked negative binomial models based on AIC showed signs of over-fitting, however, with very high CVs at the western portion of the study area. Of the highest-ranked Tweedie models, the models fit with ds splines exhibited less evidence of edge effects than those fit with using ts splines. The selected model for this season was therefore a Tweedie model with the bivariate smoother of X and Y and a smoother of SST, both fit using ds splines (Figures 21, 22, A3).

The selected Dall's porpoise DSM for spring was a Tweedie model with the bivariate smoother of X and Y as the only smooth term, fit using a ds spline and included month as a factor (Table 11, Figure 23). An almost identical model that differed only in terms of the factor used (i.e., year rather than month) was within ΔAIC of 2 of the selected model, but had a higher CV. The top-ranked negative binomial model (a ds model with the bivariate spatial smoother as the only covariate) resulted in very similar density patterns to the selected model but had a higher CV. All models fit with ts splines exhibited edge effects at the western portion of the study area and were thus not selected.

All candidate summer Dall's porpoise Tweedie models were within ΔAIC of 2 of one another, as were all candidate negative binomial models (Table 11). For both distributions, the models fit using ts splines exhibited edge effects in the western portion of the study area and the models that included a smooth of SST in addition to the spatial smoother resulted in density plots that did not align well with the Dall's porpoise sightings. We therefore selected the Tweedie model with the bivariate ds smooth of X and Y as the only covariate (Figure 24), as the corresponding negative binomial model had a much higher CV.

Many of the candidate models for Dall's porpoises during fall exhibited edge effects in the Strait of Georgia, particularly in the northern-most part of the study area. The highest-ranked model that did not have these edge effects was a Tweedie model with the bivariate spatial smoother fit using a ds spline and including year as a factor (Table 11, Figure 25). This model performed well in all model validation tests and exhibited good fit to the data and was thus selected.

Predicted areas of highest Dall's porpoise density varied among seasons but generally included the northern or western portions of the study area (Figures 21, 23 - 25). The Strait of Georgia, south of Vancouver, had the highest predicted densities of Dall's porpoises in both fall and winter (Figures 21, 25). This area was not predicted to have high densities of Dall's porpoises in spring and summer, however, at which times the highest density areas for Dall's porpoises were in the western portions of the study area, including Juan de Fuca Strait and Swiftsure Bank (Figures 22, 23). Eastern and western Juan de Fuca Strait were also predicted to have high densities of Dall's porpoises in winter. Predicted density of Dall's porpoises in most of Haro Strait was low year-round.

Estimated Dall's porpoise abundance within the study area was highest in winter at 336 (CV = 0.40) and lowest in summer at 76 (CV = 0.35). Spring and fall estimated abundances based on the selected DSMs were 201 (CV = 0.22) and 283 (CV = 0.47), respectively.

4. DISCUSSION

In regions with intensive human activity, quantitative information on cetacean density is essential for assessing population-level impacts of threats such as entanglement in fishing gear, vessel strikes, and underwater noise. In this study, we provide the first year-round spatially explicit estimates of the seasonal distribution and abundance of three species - humpback whales, harbour porpoises, and Dall's porpoises - in the southern Salish Sea and on Swiftsure Bank. The analysis was informed by 8,500 km of repeated systematic boat-based surveys conducted over multiple years and seasons, covering the area in and around the shipping lanes. The results highlighted strong spatial and seasonal patterns in cetacean distribution, underscoring the importance of year-round monitoring and management strategies that are aligned with seasonal density patterns.

4.1. METHODOLOGICAL APPROACH, UNCERTAINTY AND CAVEATS

While presence-only data or qualitative distribution maps can highlight areas of species occurrence, they do not usually provide robust information for quantifying geographic overlap with stressors or evaluating risk-mitigation measures (Rocchini et al. 2011). The main issues with non-systematic data include sampling biases, lack of survey effort assessment, lack of coverage of the entire area or time period of interest, and the difficulty of ascertaining whether areas with few or no observations truly represent lower densities (Ruete 2015). Moreover, results must account for the imperfect detection of animals in survey data, and for the variability due to the dynamic nature of species distributions in the marine environment. Therefore, this study was designed specifically to address these issues by

1. delineating the study area in a manner relevant to management aims,
2. using a systematic sampling design,
3. ensuring repeated effort over multiple seasons and years,
4. using distance sampling methods, and
5. accounting for imperfect detection at varying distances in the spatial models (Miller et al. 2013).

It is also critical that major sources of uncertainty be clearly accounted for and propagated through the different phases of any assessment of abundance, density or habitat use (Miller et al. 2022). Indeed, maps of point estimates (e.g., density) are usually not sufficient for robust conservation without some measure of uncertainty (Jansen et al. 2022), because management objectives and frameworks are often probabilistic (Taylor et al. 2000, Hammill et al. 2024). One advantage of DSMs is that they include methods to incorporate the uncertainty from the fitting of detection functions with the uncertainty associated with estimating smooths and factors in the spatial GAMs (Bravington et al. 2021). Following recommendations in Miller et al. (2022), we also accounted for the variability in dynamic environmental covariates across months or years in the models that retained SST, by estimating spatially varying densities for each temporal period and averaging the resulting variances. The resulting maps of CV, included as insets in the spatial density plots for each species and season, provide information to managers about the robustness of our predicted densities and can be used to identify gaps in space and time where additional effort could increase confidence. The CV maps will also be crucial for any risk-assessment model that uses the calculated densities as quantitative inputs (e.g., a model of ship strike risk).

Distance sampling and DSMs are well-established approaches for estimating cetacean density, but certain assumptions and caveats should be considered when interpreting our results. Distance sampling assumptions include that all animals are available at the surface to be detected and counted by observers, and that all available animals on the trackline are detected (Buckland et al. 2001). Violation of these assumptions can lead to availability bias or perception bias, respectively. Availability bias in cetacean surveys generally occurs due to animals being underwater during the window of time that they are within detection range of observers on the moving vessel. Humpback whales, harbour porpoises, and Dall's porpoises are all species that engage in relatively short-duration dives (e.g., average dives times of 65 s to 2.4 min; Dolphin 1987, Westgate et al. 1995). Estimates of the proportion of time available at the surface during visual surveys conducted in 2018 from a larger vessel (similar speed but a higher observation platform) were 0.989 for humpback whales and 0.975 for porpoises (Doniol-Valcroze et al. 2024). We lack the required data to calculate availability bias for our survey platform in the Salish Sea, recognizing that diving behaviour in particular has a large impact on these calculations but can vary spatially and temporally. However, given these previous results and considering the relatively slow survey speed (~10 knots) of our research vessel, it is expected that availability bias did not impact our abundance estimates as much as it would for species with longer dive times (e.g., sperm whales, beaked whales) or for faster moving observation platforms (e.g., aerial surveys).

Perception bias occurs due to animals on the trackline remaining undetected by observers even when they are available to be sighted. Imperfect detection on the trackline primarily affects estimates for small and cryptic species, including porpoises, as they are more likely to be missed due to factors such as weather conditions. Perception bias was minimized to the extent possible during our surveys, with all visual effort conducted by a consistent team of three experienced observers throughout the study period, who were instructed to focus primarily on the area between the trackline and 45 degrees to the port or starboard side of the vessel's bow. Our results may still underestimate overall abundance for these small cetacean species to some extent, but the validity of the general density patterns would only be affected if this bias varies spatially (i.e., if perception bias is stronger in some parts of the study area). Western Juan de Fuca Strait and Swiftsure Bank tended to have higher sea states and swell heights than the rest of the survey area thereby creating a possible negative bias in density estimates for those locations that could not be fully accounted for with the use of detectability variables in the DFs. Collection of passive acoustic monitoring data is ongoing to improve future detection and understanding of habitat use of small cetaceans in our study area.

The majority of the selected models included a bivariate spatial smooth as the only smooth term (i.e., they did not include a modelled environmental relationship). Poor performance of environmental variables as predictors is a common occurrence in cetacean habitat models (Becker et al. 2020) due to a variety of reasons. In our study, most covariates, especially static ones such as depth or distance to shore, exhibited strong concurvity with the spatial smooths and thus contributed little additional explanatory power if included alongside the spatial smooth. These environmental variables could still be ecologically important, as their concurvity with s(x,y) could suggest that the biological processes they represent actually underlie some of the observed distribution patterns. Because our modelling objective was primarily predictive, we prioritized spatial fit and model performance over mechanistic interpretation. For explanatory purposes, alternative model formulations that constrain or omit spatial smooths could be used to better identify environmental drivers of cetacean distribution. A more general issue with environmental variables is that they are often not adequate proxies for the actual drivers of habitat selection, or that the presence of multiple behaviours or prey preferences makes it challenging to identify straightforward explanatory relationships (Doniol-Valcroze et al. 2012). Another explanation could be the relatively small size of our study area and the lack of strong environmental gradients perpendicular to its main axis (i.e., inshore to offshore along the shipping route from Vancouver to Swiftsure Bank). This lack of contrast in habitat characteristics could make it difficult for any variable to hold strong explanatory power, and could reflect a scale-dependent process in which habitat selection has already occurred at a broader scale, with the southern Salish Sea having been selected for a range of habitat characteristics that differ from other parts of the northeastern Pacific but do not vary much within the area. Ultimately, understanding the mechanistic drivers of cetacean distribution in any region could greatly enhance our ability to predict how their spatial distribution may vary over time in response to changes in the ecosystem.

In future work focused on explaining habitat relationships, the inclusion of more detailed or dynamic environmental variables could improve interpretability. For example, fine-scale oceanographic features such as tidal eddies, current shear zones, and subsurface prey distributions are likely to influence cetacean habitat use but were not captured by the covariates used here. High-resolution physical-biological model outputs (e.g., from the SalishSeaCast

NEMO model at 500 m resolution, Suchy et al. 2023), as well as spatial data on vessel noise or traffic density, may provide better understanding of the mechanisms shaping cetacean distribution in coastal habitats. However, as previously stated, the goal of this study was not to produce habitat models explaining the underlying biological drivers of cetacean spatial distribution, but to quantify their current patterns of density. As such, the lack of strong observed environmental relationships does not preclude the use of the resulting outputs for further research and management processes.

4.2. HUMPBACK WHALES

Humpback whales were detected in the study area during all seasons, and in all months except March. Most humpback whales that feed in the waters off southern B.C. between spring and fall are known to migrate to Hawaii, Mexico, or Central America for the winter (Calambokidis et al. 2008, Barlow et al. 2011, McMillan et al. 2023). However, humpback whale migratory timing is staggered (Craig et al. 2003), and our results confirm that not all individuals leave the area in late fall/early winter. The presence of humpbacks in the study area year-round is an important consideration for any measures to address the threats of vessel strikes and noise to this population.

The selected spring humpback whale spatial model included a smooth of slope, and the fall model included SST as a linear term, but there were no other environmental covariates in the selected humpback whale DSMs. Previous models of humpback whale density in the northeastern Pacific have included depth, distance to shore, chl a concentration, and other static and dynamic terms as explanatory covariates, often in addition to SST and slope (Becker et al. 2010, Dalla-Rosa et al. 2012, Best et al. 2015). These previous models, however, were based on data collected over much larger areas and thus the ranges of these covariates varied more than they did within our Salish Sea study area. Some of the areas identified by our models as having very high humpback whale densities, including the eastern edge of Swiftsure Bank, are characterized by steep slopes and abrupt changes in depth (Figure A1). These features likely serve to concentrate humpback whale prey (small schooling fish and krill) and contribute to the high predicted humpback whale densities. However, the high concurvity with the spatial smoothers precluded these covariates from being included in the candidate DSMs for most seasons.

Our models highlighted Swiftsure Bank and the entrance to Juan de Fuca Strait as areas with high humpback whale density in all seasons. Given that the winter humpback whale DSMs were based on a very limited number of sightings (n=13), the degree of confidence in predicted habitat use is lower at this time of year than during other seasons. Overall, though, our results predict use of the western portion of our study area by humpbacks whales year-round. Although models based on broad-scale cetacean surveys conducted in summer 2018 did not predict high densities of humpback whales around Swiftsure Bank (Wright et al. 2021), earlier studies did predict a high concentration of humpbacks in this area (Dalla-Rosa et al. 2012, Nichol et al. 2017). Nichol et al. (2017) also assessed Swiftsure Bank and the entrance to Juan de Fuca Strait as areas off the west coast of Vancouver Island that pose the highest risk of lethal ship strikes to humpbacks. Our results build on these previous assessments by incorporating season-specific insights into humpback whale use of the Swiftsure Bank area, highlighting its importance to humpback whales year-round.

Moderate to high densities of humpback whales were also predicted in the Strait of Georgia and central/western Juan de Fuca Strait in summer and fall (Figure 12, Figure 13). Central and western Juan de Fuca Strait were identified as areas of high humpback density by Wright et al. (2021), but the southern Strait of Georgia was predicted to have relatively low humpback whale abundance based on summer 2018 survey data. No humpback whales were detected in the southern Strait of Georgia during systematic marine mammal surveys conducted in 2000, 2001 and 2004 (Keple et al. 2002, Williams et al. 2007, Best et al. 2015) but systematic and opportunistic efforts conducted in recent years have documented the return of humpback whales to this area (Calambokidis et al. 2017a, McMillan et al. 2022, McMillan et al. 2025). Our models indicate that the southern Strait of Georgia has become increasingly important to humpback whales, particularly during fall.

Our DSMs provide valuable information regarding temporal and spatial presence of humpback whales in and around the shipping lanes from Swiftsure Bank to Vancouver – information required to inform effective management actions. However, quantification of vessel strike risk for humpback whales and other cetaceans can be improved by considering behavioural factors, for example patterns in dive behaviour (Calambokidis et al. 2019, Keen et al. 2019, Keen et al. 2023). Collection and analysis of humpback whale dive behaviour based on data-logging tags is underway and will further inform vessel strike risk to humpback whales in this area.

Humpback whales are listed as a species of special concern under SARA, and the primary threats to this population in Canadian waters include vessel strikes and entanglement in fishing gear (COSEWIC 2022). Humpback whales are the species of cetacean most often documented in vessel strikes in Canadian waters and worldwide are second only to fin whales in terms of documented strikes (Jenson and Silber 2003, COSEWIC 2022). The relatively recent return of high densities of humpback whales to the Salish Sea (Calambokidis et al. 2017a, McMillan et al. 2025, this study), particularly in areas of high vessel traffic including Swiftsure Bank and Juan de Fuca Strait, have resulted in increasing overlap between members of this population and anthropogenic activities.

4.3. HARBOUR PORPOISES

Predicted harbour porpoise abundance was high in Haro Strait and eastern Juan de Fuca Strait in all seasons, with particularly high densities in summer and fall (Figure 18, Figure 20). These areas were also identified in previous studies, some based on data collected as far back as the early 1990s, as high density or “hotspot” areas for harbour porpoises (Hall 2004, Hall 2011, Best et al. 2015, Wright et al. 2021). Our current models, combined with the results of this previous research, highlight the long-term importance of these portions of the southern Salish Sea to harbour porpoises, and confirm that these are areas where high densities of harbour porpoises can be expected year-round.

Areas of moderate to high harbour porpoise density were also predicted in the southern Strait of Georgia, south of Vancouver, year-round (Figures 15, 16, 18, 20). In winter and fall, these waters were predicted to have some of the highest densities of harbour porpoises in the study area. Based on surveys conducted in 2004 and 2018, Best et al. (2015) and Wright et al. (2021) predicted relatively low densities of harbour porpoises in this part of the Strait of Georgia. Both previous surveys were conducted in summer only, however, and thus could not have documented the higher harbour porpoise densities that we predicted in this area in other seasons.

Harbour porpoise sightings were rare in the western portions of our study area (western Juan de Fuca Strait and Swiftsure Bank) at all times of year (Figures 15, 16, 18, 20). Consequently, predicted harbour porpoise densities in this area were low, and spatially explicit CVs were high, in all four of the selected DSMs. The small body size, low profile, and often cryptic behaviour of harbour porpoises means that they are rarely detected in sea states above Beaufort 2, and thus the impact of higher sea states on detectability may not be sufficiently captured in harbour porpoise detection functions, leading to underestimates of harbour porpoise density in this area. Efforts are underway to characterize porpoise presence using acoustic methods, which will provide additional information about seasonal habitat use by porpoises of the Swiftsure Bank area.

Harbour porpoises are listed as a species of Special Concern under SARA. The main threats identified for this species include acoustic disturbance, entanglement, habitat degradation, toxic spills, and chemical contamination (Fisheries and Oceans Canada 2009). A previous, rapid decline in harbour porpoise abundance and distribution in the Salish Sea in the 1970s may have resulted from one or a combination of these anthropogenic threats (Jefferson et al. 2016, Elliser and Hall 2021). There is evidence that harbour porpoises are highly vulnerable to acoustic disturbance (Wisniewska et al. 2018, Frankish et al. 2023, Pigeault et al. 2024), highlighting the importance of mitigating underwater noise, particularly in areas of high harbour porpoise density.

4.4. DALL'S PORPOISES

Previous Dall's porpoise density models have included static covariates (e.g., distance to shore, depth, and slope), as explanatory terms (Best et al. 2015, Wright et al. 2021). Depth in particular (and by association, distance from shore), has been identified as a factor that may influence Dall's porpoise distribution (Hall 2011, Nichol et al. 2013, Wright et al. 2021). Based on stomach content analysis, it has been suggested that Dall's porpoises in the Salish Sea prey on species that are found in deeper water than harbour porpoises do, and that this may represent evidence of habitat partitioning between these two species (Nichol et al. 2013). As previously stated, depth could not be considered in many of our candidate models due to its concurvity with the spatial smoother. However, our models do provide some evidence of spatial and temporal habitat partitioning of Dall's and harbour porpoises. Predicted Dall's porpoise density was relatively low in Haro Strait in all seasons (Figures 21, 23-25), whereas the area was predicted to have some of the highest densities of harbour porpoises year-round. The highest densities of Dall's porpoises in spring and fall were predicted in the western portion of our study area (Figures 23, 25), which had low predicted density of harbour porpoises year-round. Although the southern Strait of Georgia was highlighted as a high density area for both species during some times of year, the highest densities of Dall's porpoises in this area, as well as the highest abundance of Dall's porpoises in the overall study area, occurred during winter, the season with the lowest harbour porpoise abundance.

Unlike harbour porpoises, that exhibit long-term patterns of having high densities in Haro and eastern Juan de Fuca Straits, our models resulted in predictions of Dall's porpoise patterns that differ from some of these earlier studies. Hall (2011) identified central and northern Haro Strait as hotspot areas for Dall's porpoises, while our models predicted low densities of Dall's porpoises in these areas in all seasons (Figures 21, 23-25). Wright et al. (2021), however, also predicted low densities of Dall's porpoises in Haro Strait, indicating that the lower abundance of Dall's porpoises in this area may be more consistent in recent years. Aerial surveys conducted in portions of the Salish Sea in the late 1990s resulted in no sightings of Dall's porpoises in the Strait of Georgia at all (Calambokidis et al. 1997). In comparison, our predicted densities of Dall's porpoises were highest in the Strait of Georgia in winter and fall (Figures 21, 25). It is unknown whether these differing results may represent a shift in Dall's porpoise abundance/distribution, or whether they are reflective of how survey timing can impact predictions of Dall's porpoise density patterns.

4.5. ADDITIONAL SPECIES

A total of 42 groups of killer whales were detected while surveying along transect lines. We attempted to fit detection functions to these sightings using models that were specific to ecotype, as well as DFs for all killer whales pooled together, but neither sample size was large enough to fit reliable DFs. Our study area is well-known for its importance to this species and includes critical habitat of both Southern and Northern Resident killer whales (Ford et al. 2017), and habitat of special importance to Bigg's (transient) killer whales (Ford et al. 2013b). The relatively low number of killer whale detections during our survey efforts do not therefore reflect a lack of importance of this area to killer whales and instead may result from the limitations of distance sampling as an approach for studying these small populations. All three killer whale ecotypes are well-studied in this area using other methods, including photo-identification and acoustic monitoring (e.g., Ford et al. 2017, Riera et al. 2019, Towers et al. 2019) and previous work has already led to measures to mitigate anthropogenic threats to killer whales. For example, areas of important foraging habitat have been identified for the endangered Southern Resident killer whale population in the southern Salish Sea and Swiftsure Bank (Thornton et al. 2022b, Stredulinsky et al. 2023), and management measures including fishing closures and slowdown zones have been implemented in these areas since 2018 (Government of Canada 2024). Although we do not yet have the recommended sample size to inform a reliable DF (approximately 60-80 sightings; Buckland et al. 2001), it is possible that the ongoing systematic, year-round data collected during our surveys may be able help address data gaps for killer whales in the future, as our number of detections for this species increases.

Pacific white-sided dolphins were detected only twice in our study area; once as an on-effort sighting in September 2023, and once while off-effort in fall 2020. Though very few were reported in inshore B.C. waters for several decades prior to the 1990s (Heise 1996), this species has been documented somewhat regularly in the Salish Sea since the late 1990s, with confirmed sightings in the Strait of Georgia year-round (Rechsteiner 2012, Ford 2014). There is evidence that Pacific white sided dolphins have undergone distributional shifts on both decadal and seasonal scales off the coast of B.C. Since the 1990s they tend to be found further offshore in summer than during the rest of the year (Rechsteiner 2012). The reasons for these apparent shifts, however, are not well-understood.

Fin whales were encountered just twice in the study area (once on-effort and once off-effort), both times in Juan de Fuca Strait during summer 2021. Higher densities of fin whales tend to be found in deeper waters to the west and north of our survey area (Nichol et al. 2017), where ships must pass through prior to entering the shipping lanes into Vancouver. These waters adjacent to our study area have been identified as high risk areas for lethal collisions with fin whales (Nichol et al. 2017). No fin whales were detected in the Salish Sea during systematic cetacean surveys conducted in 2004 and 2018 (Williams and Thomas 2007, Wright et al. 2021). However, fin whales have been documented several times in the waters between Vancouver Island and the mainland since 2005, including in parts of Juan de Fuca Strait (Towers et al. 2018). The highest impact threats to fin whales (listed as Threatened under SARA) are vessel strikes and vessel noise (COSEWIC 2019). Twelve dead fin whales, all with evidence of vessel strikes, were documented in the southern Salish Sea between 1986 and 2017 (Towers et al. 2018). Despite their relatively infrequent presence in the area, fin whales are highly susceptible to vessel strikes and thus should be considered in measures to mitigate impacts of increasing vessel traffic.

Grey whales were also infrequently detected during our surveys even though large numbers are known to use southwestern Vancouver Island waters, which are directly adjacent to the study area, during their spring migration (Poole 1984, Green et al. 1995, Shelden and Laake 2002, Perryman et al. 2002, Ford et al. 2013a). Moreover, numerous individuals from the Pacific Coast Feeding Group feed in this area throughout the summer (Darling et al. 1998, Calambokidis et al. 2017b). Grey whales tend to be found very close to shore along the west coast of Vancouver Island (Darling 1984) and thus were likely to be missed during our survey efforts, which crossed over the shipping lanes farther offshore in the western part of our study area (Figure 1). Eastern

North Pacific grey whales are currently listed as a species of Special Concern under SARA, and the Committee on the Status of Endangered Wildlife in Canada (COSEWIC) recently re-assessed these grey whales as comprising three distinct management units, including two designated as Endangered (COSEWIC 2017). Vessel strikes and entanglement are considered the principal threats to the survival and recovery of grey whales (Gavrilchuk and Doniol-Valcroze 2021), and the high and increasing levels of anthropogenic activity in this area may impact a greater portion of this population than was detected during our survey efforts.

Minke whales are known to feed in parts of our study area, including southern Haro and eastern Juan de Fuca Straits (Towers et al. 2013), though we detected only one minke whale while surveying along pre-determined transect lines. Their low profile, erratic surfacing patterns, and lack of a visible blow make minke whales difficult to detect during line-transect surveys, especially in poor sea states. Sightings of minke whales have been infrequent even during surveys covering much larger portions of western Canadian waters (Williams and Thomas 2007, Best et al. 2015, Doniol-Valcroze et al. 2024). Accurate assessments of abundance and habitat use are therefore challenging for this species, and additional effort is required to inform the extent to which increasing anthropogenic activity in the southern Salish Sea may be impacting the minke whale population.

5. CONCLUSIONS AND FUTURE WORK

This multiyear study provides the first year-round spatially explicit estimates of the seasonal distribution and abundance of humpback whales, harbour porpoises and Dall's porpoises in the southern Salish Sea and on Swiftsure Bank. These results are intended to inform a subsequent planned assessment of vessel strike risk. The temporal variability observed in cetacean distributions within the TMX marine shipping area underscores the need for management strategies that are aligned with seasonal density patterns rather than relying on data from a single season or year. The seasonal density layers can further inform ecosystem studies, recovery planning, environmental response planning, and impact assessments of threats such as entanglement in fishing gear and underwater noise.

Additional data collection and analyses are underway to produce spatio-temporal predictions of vessel strike risk to cetaceans in the TMX marine shipping area. The density layers from the current analysis will be combined with data from data-logging tags, and additional boat-based survey efforts to address some of the sources of uncertainty identified herein. Specifically, these data will:

1. provide additional insight into habitat use of cetaceans, particularly in areas where more challenging weather conditions have contributed to higher uncertainty in density estimates;
2. allow incorporation of behavioural factors, specifically humpback whale dive behaviour, into the vessel strike risk analysis; and
3. potentially allow for inclusion of additional areas (e.g., the U.S. portions of the southern Salish Sea and Swiftsure Bank) and species (e.g., killer whales) into future vessel strike risk assessments.

6. ACKNOWLEDGEMENTS

We would like to thank Stacey Hrushowy, Captain of the R/V Manyberries, for their skilled operation and maintenance of the vessel and their dedication to this program. We are grateful to Brianna Wright and Eva Stredulinsky for developing and sharing R code for data processing and analysis and providing advice on adapting code for our requirements. James Pilkington, Jackie

Hildering, Wendy Szaniszlo, Katy Gavrilchuk, and Daniel Williams provided assistance with survey efforts. We are grateful to Benjamin Snow, Seaton Taylor, and DFO Science's Non-Destructive Survey Tools Program for making this work possible through sharing the use, maintenance, and expenses of the R/V Manyberries. We are appreciative for the ongoing efforts by OrcaNetwork and OceanWise Sightings Network to maintain opportunistic sightings records available publicly or upon request as their records were used to confirm killer whale ecotypes when this could not be done during the course of survey effort. Thank you also to the numerous kind and helpful people we met at docks in Nanaimo and throughout the Salish Sea – Riley Hardy and Chris Flynn; the crews of the Kitsilano Lifeboat Station; as well as Mike, Sarah, Merle, Ted, and Sherry. Funding for this work was provided by Fisheries and Oceans Canada's OPP 2.0/ TMX initiative.

7. REFERENCES CITED

Barlow, J., Calambokidis, J., Falcone, E.A., Baker, C.S., Burdin, A.M., and Clapham, P.J. 2011. Humpback whale abundance in the North Pacific estimated by photographic capture-recapture with bias correction from simulation studies. Marine Mammal Science, 27: 793-818.

Becker E.A., Carretta J.V., Forney K.A., Barlow, J., Brodie, S., Hoopes, R., Jacox, M.G., Maxwell, S.M., Redfern, J.V., Sisson, N.B., Welch, H., and Hazen, E.L. 2020. Performance evaluation of cetacean species distribution models developed using generalized additive models and boosted regression trees. Ecology and Evolution, 10: 5759–5784.

Becker, E.A., Forney, K.A., Ferguson, M.C., Foley, D.G., Smith, R.C., Barlow, J., and Redfern, J.V. 2010. Comparing California Current cetacean-habitat models developed using in situ and remotely sensed sea surface temperature data. Marine Ecology Progress Series, 413:163-183.

Best, B.D., Fox, C.H., Williams, R.W., Halpin, P.N., and Paquet, P.C. 2015. Updated marine mammal distribution and abundance estimates in British Columbia. Journal of Cetacean Research and Management, 15: 9-26.

Bortolotto, G., Zerbini, A., Thomas, L., Andriolo, A., and Hammond, P. 2023. Distribution and habitat use modelling from satellite tracking data of humpback whales in Brazil agree with shipboard survey data modelling. Marine Ecology Progress Series, 720: 161–174.

Bravington, M.V., Miller, D.L., and Hedley, S.L. 2021. Variance propagation for density surface models. Journal of Agricultural, Biological, and Environmental Statistics 26: 306–323.

Buckland, S.T., Anderson, D.R., Burnam, K.P., Laake, J.L., Borchers, D.L., and Thomas, L. 2001. Introduction to distance sampling: Estimating abundance of biological populations. Oxford University Press: Oxford, UK.

Buckland, S.T., Anderson, D.R., Burnham, K.P., Laake, J.L., Borchers, D.L., and Thomas, L. 2004. Advanced Distance Sampling. Oxford University Press: Oxford, UK.

Burnham, R.E., Vagle, S., O'Neill, C., and Trounce, K. 2021. The efficacy of management measures to reduce vessel noise in critical habitat of Southern Resident killer whales in the Salish Sea. Frontiers in Marine Science, 8.

Calambokidis, J., Osmek, S., and Laake, J.L. 1997. Aerial surveys for marine mammals in Washington and British Columbia inside waters. Final Report for Contract 52ABNF-6-00092.

Calambokidis, J., Falcone, E.A., Quinn, T.J., Burdin, A.M., Clapham, P.J., Ford, J.K.B., Gabriele, C.M., LeDuc, R., Mattila, D., Rojas-Bracho, L., Straley, J.M., Taylor, B.L., Urbán, J.R., Weller, D., Witteveen, B.H., Yamaguchi, M., Bendlin, A., Camacho, D., Flynn, K., Havron, A., Huggins, J., and Maloney, N. 2008. SPLASH: Structure of Populations, Levels of Abundance and Status of Humpback Whales in the North Pacific. Report to U.S. Dept of Commerce, Seattle, Washington. 57 pp.

Calambokidis, J., Barlow, J., Flynn, K., Dobson, E., and Steiger, G.H. 2017a. Update on abundance, trends, and migrations of humpback whales along the US West Coast. Report to the International Whaling Commission SC/A17/NP/13.

Calambokidis, J., Laake, J., and Perez, A. 2017b. Updated analysis of abundance and population structure of seasonal gray whales in the Pacific Northwest, 1996-2015. Report to the International Whaling Commission SC/A17/GW/05.

Calambokidis, J., Fahlbusch, J.A., Szesciorka, A.R., Southall, B.L., Cade, D.E., Friedlaender, A.S., and Goldbogen, J.A. 2019. Differential vulnerability to ship strikes between day and night for blue, fin, and humpback whales based on dive and movement data from medium duration archival tags. Frontiers in Marine Science 6, 543.

COSEWIC. 2017. COSEWIC assessment and status report on the Grey Whale *Eschrichtius robustus*, Northern Pacific Migratory population, Pacific Coast Feeding Group population and the Western Pacific population, in Canada. Committee on the Status of Endangered Wildlife in Canada.

COSEWIC. 2019. COSEWIC assessment and status report on the Fin Whale, *Balaenoptera physalus*, Atlantic population and Pacific population, in Canada. Committee on the Status of Endangered Wildlife in Canada.

COSEWIC. 2022. COSEWIC assessment and status report on the humpback whale (*Megaptera novaeangliae kuzira*) in Canada 2022. Committee on the Status of Endangered Wildlife in Canada.

Craig, A.S., Herman, L.M., Gabriele, C.M., and Pack, A.A. 2003. Migratory timing of humpback whales (*Megaptera novaeangliae*) in the central North Pacific varies with age, sex and reproductive status. Behaviour, 140: 981–1001.

Dalla Rosa, L., Ford, J.K.B., and Trites, A.W. 2012. Distribution and relative abundance of humpback whales in relation to environmental variables in coastal British Columbia and adjacent waters. Continental Shelf Research, 36: 89–104.

Darling, J.D. 1984. Gray whales off Vancouver Island, British Columbia. In M.L. Jones, S. L. Swartz, and S. Leatherwood Eds. The Gray Whale pp. 267-287. Academic Press.

Darling, J.D., Keogh, K.E., and Steeves, T.E. 1998. Gray whale (*Eschrichtius robustus*) habitat utilization and prey species off Vancouver Island, B.C. Marine Mammal Science, 14: 692-720.

DFO. 2023. California Sea Lion Abundance Estimation in Canada, 2020–21. DFO Can. Sci. Advis. Sec. Sci. Advis. Rep. 2023/016.

Dolphin, W.F. 1987. Dive behavior and estimated energy expenditure of foraging humpback whales in southeast Alaska. Canadian Journal of Zoology, 65: 354–362.

Doniol-Valcroze, T., Lesage, V., Giard, J., and Michaud, R. 2012. Challenges in marine mammal habitat modelling: evidence of multiple foraging habitats from the identification of feeding events in blue whales. Endangered Species Research, 17: 255-268.

Doniol-Valcroze, T., Gosselin, J.-F., Pike, D., and Lawson, J. 2015. Spatial modelling of narwhal density in fiords during the 2013 High Arctic Cetacean Survey (HACS). DFO Can. Sci. Advis. Sec. Res. Doc. 2015/059. v + 31 p.

Doniol-Valcroze, T., Nichol, L., Wright, B., Stredulinsky, E., Spaven, L., and Abernethy, R. 2024. Abundance estimates of cetaceans from the 2018 Pacific Region International Survey of Marine Megafauna. DFO Can. Sci. Advis. Sec. Res. Doc. 2024/043. iv + 34 p.

Elliser, C.R., and Hall, A.M. 2021. Return of the Salish Sea Harbor Porpoise, *Phocoena phocoena*: Knowledge gaps, current research, and what we need to do to protect their future. Frontiers in Marine Science, 8: 1–18.

Elliser, C.R., White, K.H., and Hansen, M.C. 2025. Resident harbor porpoises (*Phocoena phocoena vomerina*) in the Salish Sea: Photo-identification shows long-term site fidelity, natal philopatry, and provides insights into longevity and behavior. Oceans, 6(1): 9.

Fisheries and Oceans Canada. 2009. Management plan for the Pacific harbour porpoise (*Phocoena phocoena*) in Canada. Species at Risk Act Management Plan Series, Fisheries and Oceans Canada.

Ford, J.K.B. 2014. Marine Mammals of British Columbia. Royal BC Museum Handbook, Mammals of BC, volume 6. Royal BC Museum, Victoria. 460 pp.

Ford, J.K.B., Durban, J.W., Ellis, G.M., Towers, J.R., Pilkington, J.F., Barrett-Lennard, L.G., and Andrews, R.D. 2013a, New insights into the northward migration route of gray whales between Vancouver Island, British Columbia, and southeastern Alaska. Marine Mammal Science, 29: 325-337.

Ford, J.K.B., Ellis, G.M., and Stredulinsky, E.H., 2013b. Information in support of the identification of critical habitat for transient killer whales (*Orcinus orca*) off the west coast of Canada. DFO Can. Sci. Advis. Sec. Res. Doc. 2012/155. iv + 46 p.

Ford, J.K., Pilkington, J.F., Reira, A., Otsuki, M., Gisborne, B., Abernethy, R.M., Stredulinsky, E.H., Towers, J.R., and Ellis, G.M., 2017. Habitats of special importance to resident killer whales (*Orcinus orca*) off the West Coast of Canada. DFO Can. Sci. Advis. Sec. Res. Doc. 2017/035. viii + 57 p.

Foreman, M.G.G., Crawford, W.R., Cherniawksy, J.Y., Henry, R.F. and Tarbotton, M.R. 2000. A high-resolution assimilating tidal model for the northeast Pacific Ocean. Journal of Geophysical Research 105(C12): 28629-28651.

Frankish, C.K., von Benda-Beckmann, A.M., Teilmann, J., Tougaard, J., Dietz, R., Sveegaard, S., Binnerts, B., de Jong, C.A.F., and Nabe-Nielsen, J. 2023. Ship noise causes tagged harbour porpoises to change direction or dive deeper. Marine Pollution Bulletin, 197: 115755.

Gavrilchuk, K., and Doniol-Valcroze, T. 2021. Recovery Potential Assessment for the Grey Whale (*Eschrichtius robustus*): Pacific Coast Feeding Group and Western Pacific Population in Canadian Waters. DFO Can. Sci. Advis. Sec. Res. Doc. 2021/020. iv + 52 p.

Government of Canada. 2024. Management measures to protect Southern Resident killer whales.

Green, G.A., Brueggeman, J.J., Grotefendt, R.A., and Bowlby, C.E. 1995. Offshore distances of gray whales migrating along the Oregon and Washington coasts, 1990. Northwest Science, 69: 223–227.

Hall, A.M. 2004. Seasonal abundance, distribution and prey species of Harbor Porpoise (*Phocoena phocoena*) in southern Vancouver Island waters [Unpublished master's thesis]. University of British Columbia.

Hall, A.M. 2011. Foraging behaviour and reproductive season habitat selection of northeast Pacific porpoises [Unpublished PhD thesis]. University of British Columbia.

Hammill, M.O., Stenson, G.B., Doniol-Valcroze, T., and Lang, S.L.C. 2024. Application of the precautionary approach to the management of marine mammals in northern Canada. NAMMCO Scientific Publications, 13.

Hauser, D.D., Logsdon, M.G., Holmes, E.E., VanBlaricom, G.R., and Osborne, R.W. 2007. Summer distribution patterns of Southern Resident killer whales *Orcinus orca*: core areas and spatial segregation of social groups. Marine Ecology Progress Series, 351: 301-310.

Hartig, F. 2024. DHARMa: Residual diagnostics for hierarchal (multi-level/ mixed) regression models. R package version 0.4.7.

Hedley, S.L., and Buckland, S.T. 2004. Spatial models for line transect sampling. Journal of Agricultural, Biological, and Environmental Statistics, *9*(2): 181–199.

Heise, K.A. 1996. Life history parameters of the Pacific white-sided dolphin (*Lagenorhynchus obliquidens*) and its diet and occurrence in the coastal waters of British Columbia. [Unpublished M.Sc. Thesis]. University of British Columbia, Vancouver, BC.

Hijmans R (2025). raster: Geographic Data Analysis and Modeling. R package version 3.6-32.

Horn, B.K.P. 1981. Hill shading and the reflectance map. Proceedings of the Institute of Electrical and Electronics Engineers, 69:14-47.

Howe, E.J., Buckland, S.T., Després-Einspenner, M.L., and Kühl, H.S. 2019. Model selection with overdispersed distance sampling data. Methods in Ecology and Evolution, 10(1): 38–47.

Huang, B., Liu, C., Banzon, V., Freeman, E., Graham, G., Hankins, B., Smith, T., and Zhang, H.M. 2021. Improvements of the Daily Optimum Interpolation Sea Surface Temperature (DOISST) Version 2.1. Journal of Climate, 34: 2923-2939.

Jansen, J., Woolley, S.N.C., Dunstan, P.K., Foster, S.D., Hill, N.A., Haward, M., and Johnson, C.R. 2022. Stop ignoring map uncertainty in biodiversity science and conservation policy. Nature Ecology & Evolution, 6: 828–829.

Jensen, A.S., and Silber, G.K. 2003. Large Whale Ship Strike Database. U.S. Department of Commerce. NOAA Technical Memorandum. NMFS-OPR-25. 37 pp.

Jefferson, T.A., Smultea, M.A., Courbis, S.S., and Campbell, G.S. 2016. Harbor porpoise *Phocoena phocoena* recovery in the inland waters of Washington: estimates of density and abundance from aerial surveys, 2013-2015. Canadian Journal of Zoology, 94: 505-515.

Joy, R., Tollit, D., Wood, J., MacGillivray, A., Li, Z., Trounce, K., and Robinson, O. 2019. Potential benefits of vessel slowdowns on endangered Southern Resident killer whales. Frontiers in Marine Science, 6.

Keen, E.M., Mahony, É.O., Nichol, L.M., Wright, B.M., Shine, C., Hendricks, B., Meuter, H., Alidina, H.M., and Wray, J. 2023. Ship-strike forecast and mitigation for whales in Gitga'at First Nation territory. Endangered Species Research, 51: 31–58.

Keen, E.M., Scales, K.L., Rone, B.K., Hazen, E.L., Falcone, E.A., and Schorr, G,S. 2019. Night and day: diel differences in ship strike risk for fin whales (*Balaenoptera physalus*) in the California current system. Frontiers in Marine Science, 6: 730.

Keple, A.R. 2002. Seasonal abundance and distribution of marine mammals in the southern Strait of Georgia, British Columbia [Unpublished master's thesis]. University of British Columbia.

Majewski, S. P. and Ellis, G.M. 2022. Abundance and distribution of Harbour Seals (*Phoca vitulina*) in the Strait of Georgia, British Columbia; synthesis of the 2014 aerial survey and long-term trends. DFO Can. Sci. Advis. Sec. Res. Doc. 2022/060. iv + 59 p.

Majewski, S., Szaniszlo, W., Nordstrom, C.A., Abernethy, R. M., and Tucker, S. 2024. Abundance and Distribution of Steller Sea Lions (*Eumetopias jubatus*) in British Columbia: Updates from 2016-17 Aerial Surveys. DFO Can. Sci. Advis. Sec. Res. Doc. 2024/047. iv + 29 p.

Marcoux, M., Matthews, C.J.D., Montsion, L.M., and Dunn, J.B. 2019. Estimate of the abundance of the Eclipse Sound narwhal (*Monodon monoceros*) summer stock from the 2016 photographic aerial survey. DFO Can. Sci. Advis. Sec. Res. Doc. 2019/028. iv + 16 p

Marques, T.A., and Buckland, S.T. 2003. Incorporating covariates into standard line transect analyses. Biometrics, 59: 924–35.

Marques, T.A., Thomas, L., Fancy, S.G., and Buckland, S.T. 2007. Improving estimates of bird density using multiple-covariate distance sampling. The Auk, 124(4): 1229.

Marra, G., and Wood, S.N. 2011. Practical variable selection for generalized additive models. Computational Statistics and Data Analysis, 55: 2372-2387.

Marshall, L., and Rexstad, E. 2021. Distance sampling survey design. R package version 0.3.1.

Mayaud, R., Peel, D., Smith, J.N., Wilson, C., and Nash, S.B. 2024. The need to consider recreational vessels in risk assessments of vessel strikes to humpback whales (*Megaptera novaeangliae*). Ocean and Coastal Management, 259(October): 107419.

McMillan, C.J., Ford, J.K.B., Cheeseman, T., Calambokidis, J., Audley, K., Birdsall, C., Byington, J.K., Currie, J., Darling, J.D., De Weerdt, J., Doe, N., Doniol-Valcroze, T., Dracott, K., Finn, R., Frisch-Jordán, A., Gabriele, C., Goodwin, B., Hildering, J., Jones, M., Lyman, E., Malleson, M., Martinez Loustalot, P., Pack, A.A., Quintana-Rizzo, E., Ransome, N., Shaw, T.J.H., Stack, S., Urbán R., J., Wray, J., Wright, B.M., and Yano, K.M. 2023. Spatial patterns in the migratory destinations of humpback whales (*Megaptera novaeangliae*) encountered in Canadian Pacific waters, based on photo-identification data and ocean basin-wide collaboration. Can. Tech. Rep. Fish. Aquat. Sci. 3519: v + 27 p.

McMillan, C.J., Keppel, E.A., Spaven, L.D., and Doniol-Valcroze, T. 2022. Preliminary report on the seasonal abundance and distribution of cetaceans in the southern Salish Sea in response to TMX Recommendations 5 and 6. Canadian Technical Report of Fisheries and Aquatic Sciences 3474, Fisheries and Oceans Canada.

McMillan, C.J., Keppel, E.A., Spaven, L.D., Hrushowy, S.M., and Doniol-Valcroze, T. 2025. Seasonal abundance and distribution of cetaceans in a high traffic shipping corridor. Marine Mammal Science, e70061.

Meynecke, J.O., de Bie, J., Barraqueta, J.L.M., Seyboth, E., Dey, S.P., Lee, S.B., Samanta, S., Vichi, M., Findlay, K., Roychoudhury, A., and Mackey, B. 2021. The role of environmental drivers in humpback whale distribution, movement and behavior: A Review. Frontiers in Marine Science, 8 (November).

Miller, D.L. 2017. Distance: Distance sampling detection function and abundance estimation. R package version 0.9.7.

Miller D.L., Becker E.A., Forney K.A., Roberts J.J., Cañadas A., and Schick, R.S. 2022. Estimating uncertainty in density surface models. PeerJ, 10:e13950.

Miller, D.L., Burt, M.L., Rexstad, E.A., and Thomas, L. 2013. Spatial models for distance sampling data: recent developments and future directions. Methods in Ecology and Evolution, 4:1001-1010.

Miller, D.L., Rexstad, E., Thomas, L., Marshall, L., and Laake, J.L. 2019. Distance sampling in R. Journal of Statistical Software, 89(1): 1–28.

National Energy Board. 2019. Reconsideration Report - Trans Mountain Pipeline ULC - MH-052-2018.

Nichol, L.M., Hall, A.M., Ellis, G.M., Stredulinsky, E., Boogaards, M., and Ford, J.K.B. 2013. Dietary overlap and niche partitioning of sympatric harbor porpoises and Dall's porpoises in the Salish Sea. Progress in Oceanography, 115: 202-210.

Nichol, L.M., Wright, B.M., O'Hara, P., and Ford, J.K.B. 2017. Assessing the risk of lethal ship strikes to humpback (*Megaptera novaeangliae*) and fin (*Balaenoptera physalus*) whales off the west coast of Vancouver Island, Canada. DFO Can. Sci. Advis. Sec. Res. Doc. 2017/007. vii + 33 p.

NOAA CoastWatch and NOAA NESDIS Ocean Color Science Team. 2024-11-26. Chlorophyll (Gap-filled DINEOF), NOAA S-NPP NOAA-20 VIIRS and Copernicus S-3A OLCI, Science Quality, Global 2km, 2018-recent, Daily. National Centers for Environmental Information (NCEI). Downloaded from ERDDAP.

NOAA CoastWatch and NOAA Center for Satellite Applications and Research. 2024-12-17. Chlorophyll, NOAA S-NPP VIIRS, Science Quality, Global 4km, Level 3, 2012-present, Weekly. National Centers for Environmental Information (NCEI). Downloaded from ERDDAP.

NOAA PSL 2024-11-27. OISST V2 High Resolution Dataset. NOAA Physical Sciences Laboratory, Boulder, Colorado, USA.

Olesiuk, P.F. 2018. Recent trends in abundance of Steller sea lions (*Eumetopias jubatus*) in British Columbia. DFO Can. Sci. Advis. Sec. Res. Doc. 2018/006. v + 67 p.

Olson, J.K., Wood, J., Osborne, R.W., Barrett-Lennard, L., and Larson, S. 2018. Sightings of Southern Resident killer whales in the Salish Sea 1976–2014: the importance of a long-term opportunistic dataset. Endangered Species Research, 37: 105-118.

Perryman, W.L., Donahue, M.A., Perkins, P.C., and Reilly, S.B. 2002. Gray whale calf production 1994–2000: are observed fluctuations related to changes in seasonal ice cover? Marine Mammal Science, 18(1): 121–144.

Pigneault, R., Ruser, A., Ramírez-Martínez, N.C., Geelhoed, S.C.V., Haelters, J., Nachtsheim, D.A., Schaffeld, T., Sveegaard, S., Siebert, U., and Gilles, A. 2024. Maritime traffic alters distribution of the harbour porpoise in the North Sea. Marine Pollution Bulletin, 208: 116925.

Poole, M.M. 1984. Migration corridors of gray whales along the central California coast, 1980–1982. In M. L. Jones, S. L. Swartz, and S. Leatherwood Eds., The Gray Whale, *Eschrichtius robustus*. Pp. 389-407. Academic Press.

R Core Team. 2023. R: A language and environment for statistical computing. R Foundation for Statistical Computing, Vienna, Austria.

Rechsteiner, E.U. 2012. Resting metabolism, energetics, and seasonal distribution of Pacific white-sided dolphins. [Unpublished M.Sc. Thesis]. University of British Columbia, Vancouver, BC.

Riera, A., Pilkington, J.F., Ford, J.K.B., Stredulinsky, E.H., and Chapman, N.R. 2019. Passive acoustic monitoring off Vancouver Island reveals extensive use by at-risk Resident killer whale (*Orcinus orca*) populations. Endangered Species Research, 39: 221-234.

Rocchini, D., Hortal, J., Lengyel, S., Lobo, J. M., Jiménez-Valverde, A., Ricotta, C., Bacaro, G., and Chiarucci, A. 2011. Accounting for uncertainty when mapping species distributions: The need for maps of ignorance. Progress in Physical Geography: Earth and Environment, 35(2): 211-226.

Ruete, A. 2015. Displaying bias in sampling effort of data accessed from biodiversity databases using ignorance maps. Biodiversity Data Journal, 3: e5361.

Schleimer, A., Ramp, C., Plourde, S., Lehoux, C., Sears, R., and Hammond, P.S. 2019. Spatio-temporal patterns in fin whale *Balaenoptera physalus* habitat use in the northern Gulf of St. Lawrence. Marine Ecology Progress Series, 623: 221-234.

Shelden, K.E.W., and Laake, J.L. 2002. Comparison of the offshore distribution of southbound migrating gray whales from aerial survey data collected off Granite Canyon, California, 1979–96. Journal of Cetacean Research and Management, 4: 53–56.

Simons, R.A., and John, C. 2022. ERDDAP. Monterey, CA: NOAA/NMFS/SWFSC/ERD.

Steckler, D., and Donlan, P. 2018. Mysticetus LLC. Version 2.0.

Stredulinsky, E.H., Toews, S., Watson, J., Noren, D.P., Holt, M.M., and Thornton, S.J. 2023. Delineating important killer whale foraging areas using a spatiotemporal logistic model. Global Ecology and Conservation, 48: e02726.

Suchy, K.D., Olson, E., Allen, S.E., Galbraith, M., Herrmann, B.E.L., Keister, J.E., Perry, I.R., Sastri, A.R., and Young, K. 2023. Seasonal and regional variability of model-based zooplankton biomass in the Salish Sea and evaluation against observations. Progress in Oceanography 219.

Taylor, B.L., Wade, P.R., De Master, D.P., and Barlow, J. 2000. Incorporating uncertainty into management models for marine mammals. Conservation Biology,14(5):1243–1252.

Thomas, L., Williams, R., and Sandilands, D. 2007. Designing line transect surveys for complex survey regions. Journal of Cetacean Research and Management, 9: 1–13.

Thompson, P.L., Anderson, S.C., Nephin, J., Robb, C.K., Proudfoot, B., Park, A.E., Haggarty, D.R., and Rubidge, E.M. 2023. Integrating trawl and longline surveys across British Columbia improves groundfish distribution predictions. Canadian Journal of Fisheries and Aquatic Sciences. 80(1): 195-210.

Thornton, S.J., Toews, S., Burnham, R., Konrad, C.M., Stredulinsky, E., Gavrilchuk, K., Thupaki, P., and Vagle, S. 2022a. Areas of elevated risk for vessel-related physical and acoustic impacts in Southern Resident Killer Whale (*Orcinus orca*) critical habitat. DFO Can. Sci. Advis. Sec. Res. Doc. 2022/058. vi + 47 p.

Thornton, S.J., Toews, S., Stredulinsky, E., Gavrilchuk, K., Konrad, C., Burnham, R., Noren, D. P., Holt, M.M., and Vagle, S. 2022b. Southern Resident Killer Whale (*Orcinus orca*) summer distribution and habitat use in the southern Salish Sea and the Swiftsure Bank area (2009 to 2020). DFO Can. Sci. Advis. Sec. Res. Doc. 2022/037. v + 56 p.

Towers, J.R., Malleson, M., McMillan, C.J., Cogan, J., Berta, S., and Birdsall, C. 2018. Occurrence of fin whales *Balaenoptera physalus* between Vancouver Island and continental North America. Northwestern Naturalist, 99: 49-57.

Towers, J.R, McMillan, C.J., Malleson, M., Hildering, J., Ford, J.K.B., and Ellis, G.M. 2013. Seasonal movements and ecological markers as evidence for migration of common minke whales photo-identified in the eastern North Pacific. Journal of Cetacean Research and Management, 13: 221-229.

Towers, J.R., Sutton, G.J., Shaw, T.J.H., Malleson, M., Matkin, D., Gisborne, B., Forde, J., Ellifrit, D., Ellis, G.M., Ford, J.K.B., and Doniol-Valcroze, T. 2019. Photo-identification catalogue, population status, and distribution of Bigg's killer whales known from coastal waters of British Columbia, Canada. Canadian Technical Report of Fisheries and Aquatic Sciences 3311: vi + 299 p.

Vagle, S., Burnham, R., Thupaki, P., Konrad, C., Toews, S., and Thornton, S.J. 2021. Vessel presence and acoustic environment within Southern Resident Killer Whale (*Orcinus orca*) critical habitat in the Salish Sea and Swiftsure Bank area. DFO Can. Sci. Advis. Sec. Res. Doc. 2021/058. x + 66 p.

Westgate, A.J., Read, A.J., Berggren, P., Koopman, H.N., and Gaskin, D.E. 1995. Diving behaviour of harbour porpoises, *Phocoena phocoena*. Canadian Journal of Fisheries and Aquatic Sciences, 52(5): 1064-1073.

Williams, R., and Thomas, L. 2007. Distribution and abundance of marine mammals in the coastal waters of British Columbia, Canada. Journal of Cetacean Research and Management, 9: 15-28.

Williams, R., Hedley, S.L., Branch, T.A., Bravington, M.V., Zerbini, A.N., and Findlay, K.P. 2011. Chilean blue whales as a case study to illustrate methods to estimate abundance and evaluate conservation status of rare species. Conservation Biology, 25(3): 526–35.

Wisniewska, D.M., Johnson, M., Teilmann, J., Siebert, U., Galatius, A., Dietz, R., and Madsen, P.T. 2018. High rates of vessel noise disrupt foraging in wild harbor porpoises *Phocoena phocoena*. Proceedings of the Royal Society B, 285: 20172314.

Wright, B.M., Nichol, L.M., and Doniol-Valcroze, T. 2021. Spatial density models of cetaceans in the Canadian Pacific estimated from 2018 ship-based surveys. DFO Can. Sci. Advis. Sec. Res. Doc. 2021/049. viii + 46 p. (Erratum: March 2022).

8. TABLES

Table 1. Environmental conditions collected during line-transect surveys.

Environmental condition	Level	Definition
Beaufort sea state	0	Glassy (calm, flat, no wave height, <1 kt wind)
Beaufort sea state	1	Ripples (light air, no wave crests, 0.1 m wave height, 1 - 3 kts wind)
Beaufort sea state	2	Small wavelets (light breeze, glassy unbreaking crests, 0.2 - 0.3 m wave height, 4 - 6 kts wind)
Beaufort sea state	3	Scattered whitecaps (gentle breeze, large wavelets, 0.6 - 1 m wave height, 7 - 10 kts wind)
Beaufort sea state	4	Frequent whitecaps (moderate breeze, small waves, 1 - 1.5 m wave height, 11-16 kts wind)
Beaufort sea state	5	Many whitecaps/ little spray (fresh breeze, 2-2.5 m wave height, 17 - 21 kts wind)
Cloud cover	Clear	No clouds from 0° to +/-90° out to the horizon
Cloud cover	<25%	Less than 25% of the sky from 0° to +/-90° is covered by clouds
Cloud cover	25% - 50%	Roughly 25% to 50% of the sky from 0° to +/-90° is covered by clouds
Cloud cover	50% - 75%	Roughly 50% to 75% of the sky from 0° to +/-90° is covered by clouds
Cloud cover	75% - 99%	Roughly 75% to 99% of the sky from 0° to +/-90° is covered by clouds
Cloud cover	100%	The entire sky from 0° to +/-90° is covered by clouds
Glare	None	No glare at all
Glare	Mild	There is glare, but you can see through it without sunglasses
Glare	Severe	There is glare, and you cannot see into it without sunglasses
Precipitation	Clear	There is no precipitation or weather obstruction from 0 to +/-90° out to the horizon
Precipitation	Fog	“Fog” best describes the weather obstruction from 0 to +/-90° out to the horizon
Precipitation	Mist	Precipitation is best described as “mist” from 0 to +/-90° out to the horizon
Precipitation	Light Rain	Light rain is leaving small water droplets on binoculars, but observers can see fine through them without frequent wiping
Precipitation	Heavy Rain	Heavy rain is leaving water droplets on binoculars, and they require frequent wiping
Precipitation	Snow	Precipitation is best described as “snow” from 0 to +/-90° out to the horizon
Precipitation	Haze	“Haze” or smog best describes the weather condition from 0 to +/-90° (typically at the horizon)
Precipitation	Smoke	“Smoke” best describes the weather condition from 0 to +/-90° out to the horizon
Swell height	None	No swell
Swell height	Low	< 1 m swell
Swell height	Moderate	1 - 2 m swell
Swell height	Large	> 2 m swell
Visibility	Good	The horizon is unobstructed in the entire field of view from 0° to +/- 45°
Visibility	Moderate	The horizon is partially obstructed from 0° to +/- 45°, but with no less than 2 Nm visibility
Visibility	Poor	There is <2 Nm visibility from 0° to +/- 45°

Table 2. *Covariates considered in the candidate detection functions (DFs) for humpback whales (HW), harbour porpoises (HP), and Dall's porpoises (DP). Categories 1-3 indicate how covariate levels were grouped for analyses, where applicable. "No clear patterns" indicates covariates that showed no relationship with the perpendicular distance data for the species, and which were thus not considered in candidate DFs. "Insufficient data" indicates covariates that could not be considered in candidate DFs due to having insufficient sightings at more than one covariate level, regardless of how data were grouped. "n/a" = not applicable.*

Species	Covariate	Category 1	Category 2	Category 3	Comments
HW	Beaufort	n/a	n/a	n/a	No clear patterns
HW	Visibility	Good, Moderate	Poor	-	-
HW	Swell	Swell	No Swell	-	-
HW	Glare	Glare	No Glare	-	-
HW	Cloud cover	n/a	n/a	n/a	No clear patterns
HW	Precipitation	Light Rain, Mist, Snow	Fog, Haze, Smoke	-	-
HW	Observer	No grouping	No grouping	No grouping	-
HW	Group size	n/a	n/a	n/a	No clear patterns
HP	Beaufort	0-1	2	>2	-
HP	Visibility	Good	Moderate	-	No sightings in poor visibility
HP	Swell	Swell	No Swell	-	-
HP	Glare	Glare	No Glare	-	-
HP	Cloud cover	Clear	1-50%	>50%	-
HP	Precipitation	Light Rain, Mist, Snow	Fog, Haze, Smoke	-	-
HP	Observer	No grouping	No grouping	No grouping	-
HP	Group size	1	2	>2	-
DP	Beaufort	0-1	2	>2	-
DP	Visibility	n/a	n/a	n/a	Insufficient data
DP	Swell	No/Low Swell	>1 m Swell	-	-
DP	Glare	Glare	No Glare	-	-
DP	Glare	No/Mild Glare	Severe Glare	-	-
DP	Cloud cover	n/a	n/a	n/a	No clear patterns
DP	Precipitation	Precipitation	No Precipitation	-	-
DP	Observer	No grouping	No grouping	No grouping	-
DP	Group size	1	2	>2	-

Table 3. Environmental covariates considered in candidate spatial models. "Type" indicates whether the covariate was considered as a temporally static value (i.e., a single value per segment) or as temporally dynamic values (i.e., monthly values for each segment)

Type	Covariate name	Data source	Definition
Static	Depth (m)	BC Digital Elevation Model 75 m x 75 m resolution	Depth at the midpoint of survey segments.
Static	Slope (radians)	BC Digital Elevation Model 75 m x 75 m resolution	Represents the steepness of the seafloor, estimated as the rate of change in depth using Horn's method (Horn 1981) for each raster cell of the digital elevation model relative to its eight neighbouring cells. Slope was extracted for the midpoint of each survey segment using the terrain function in the R package raster (Hijmans 2025), option = "slope".
Static	Rugosity (index)	BC Digital Elevation Model 75 m x 75 m resolution	Mean of the absolute differences between the depth value of a raster cell and the value of the eight surrounding cells. Calculated for the midpoint of survey segments using the terrain function in the R package raster, option = "TRI" (Terrain Ruggedness Index).
Static	Distance from shore (km)	Coastal chart.	Euclidean distance to the nearest shoreline from the midpoint of survey segments.
Static	RMS tidal current speed (m/s)	British Columbia Marine Conservation Atlas (Foreman et al. 2000).	Modelled values represent average (root mean square, RMS) tidal speeds with variable resolution from a minimum of 80 m (nearshore) to a maximum of 80 km (offshore). Extracted for the midpoint of survey segments.
Static	Distance to nearest high tidal current area (km)	British Columbia Marine Conservation Atlas (Foreman et al. 2000) - modelled values categorized into polygons of high tidal current speed areas.	Euclidean distance from the midpoint of survey segments to the edge of the nearest high tidal current polygon (defined as having tidal current speeds of 0.332-2.801 m/s).
Dynamic	Sea surface temperature (°C)	NOAA OI SST V2 High Resolution Dataset data provided by the NOAA PSL, Boulder, Colorado, USA, from their website at https://psl.noaa.gov by the NOAA Physical Sciences Laboratory (NOAA PSL 2024-11-27) and the NOAA/OISST dataset, 0.25 x 0.25 degree resolution (Huang et al. 2021).	Monthly mean SST for each month and year throughout our study period calculated at the midpoint of survey segments (Huang et al. 2021).

Type	Covariate name	Data source	Definition
Dynamic	Chlorophyll a concentration (mg/cm3)	Data provided by the NOAA CoastWatch program, NOAA NESDIS Ocean Color Science Team (NOAA 2024-11-26), and NOAA's Center for Satellite Applications and Research (STAR) (NOAA 2024-12-17) through the ERDDAP portal (Simons and John 2022).	2 km daily mean data were averaged for each month and year over the study period (NOAA 2024-11-26) except for January data which were 4 km weekly data (NOAA 2024-12-17) and December for which no data were available. December data were approximated by averaging the mean values from the previous November and following January.

Table 4. Survey effort by year and month, including number of effort days and distance surveyed (km). Seasons were defined as Winter (January through March), Spring (April through June), Summer (July through September), and Fall (October through December).

Survey #	**Year**	Month	**Season**	**Start Date (GMT)**	**End Date (GMT)**	**Effort Days**	**Distance (km)**
1	2020	Aug/Sep	Summer	8/28/2020	9/13/2020	5	303
2	2020	Oct	Fall	10/14/2020	10/20/2020	6	339
3	2021	Jan	Winter	1/19/2021	1/25/2021	6	287
4	2021	Feb	Winter	2/8/2021	2/13/2021	4	170
5	2021	Mar	Winter	3/2/2021	3/6/2021	4	273
6	2021	Apr	Spring	4/23/2021	4/29/2021	7	373
7	2021	May	Spring	5/14/2021	5/20/2021	6	320
8	2021	Jun	Spring	6/4/2021	6/17/2021	6	243
9	2021	Jul	Summer	7/9/2021	7/14/2021	6	249
10	2021	Aug	Summer	8/20/2021	8/25/2021	4	229
11	2021	Oct	Fall	10/13/2021	10/18/2021	6	280
12	2021	Nov	Fall	11/17/2021	11/22/2021	6	265
13	2022	Jan	Winter	1/21/2022	1/27/2022	6	235
14	2022	Feb	Winter	2/9/2022	2/13/2022	5	312
15	2022	Apr/May	Spring	4/25/2022	5/1/2022	6	357
16	2022	Jun	Spring	6/7/2022	6/11/2022	5	273
17	2022	Jul	Summer	7/19/2022	7/29/2022	5	161
18	2022	Aug	Summer	8/23/2022	8/28/2022	5	251
19	2022	Sep	Summer	9/20/2022	9/23/2022	3	159
20	2022	Oct	Fall	10/3/2022	10/16/2022	3	138
21	2022	Dec	Fall	12/4/2022	12/7/2022	4	204
22	2023	Feb	Winter	2/11/2023	2/16/2023	5	245
23	2023	May	Spring	5/22/2023	5/29/2023	6	354
24	2023	Jul	Summer	7/16/2023	7/20/2023	5	245
25	2023	Sep	Summer	9/6/2023	9/14/2023	6	291
26	2023	Nov	Fall	11/20/2023	11/28/2023	9	506
27	2024	Mar	Winter	3/18/2024	3/26/2024	8	561
28	2024	Jun	Spring	6/12/2024	6/19/2024	7	508
29	2024	Aug	Summer	8/6/2024	8/16/2024	7	393

Table 5. On-effort sightings of cetacean species by year and month with monthly totals across years. "n/a" indicates months in which no survey effort was conducted. Species sighted include humpback whales (HW), harbour porpoises (HP), Dall's porpoises (DP), porpoises for which species was not confirmed (UP), Bigg's killer whales (KW – Bigg's), Southern Resident killer whales (KW – SRKW), killer whales for which ecotype was not confirmed (KW – UNKN), Pacific white-sided dolphins (PWSD), fin whales (FW), grey whales (GW), minke whales (MW).

Species	Year	Jan	Feb	Mar	Apr	May	Jun	Jul	Aug	Sep	Oct	Nov	Dec	Total
HW	All years	9	5	0	20	2	60	20	116	81	151	55	34	553
HW	2020	n/a	n/a	n/a	n/a	n/a	n/a	n/a	1	15	37	n/a	n/a	53
HW	2021	8	0	0	12	2	23	2	24	n/a	42	22	n/a	135
HW	2022	1	4	n/a	8	n/a	12	16	70	1	72	n/a	34	218
HW	2023	n/a	1	n/a	n/a	0	n/a	2	n/a	64	n/a	33	n/a	100
HW	2024	n/a	n/a	0	n/a	n/a	25	n/a	22	n/a	n/a	n/a	n/a	47
HP	All y	33	29	121	94	170	235	97	197	241	178	78	56	1529
HP	2020	n/a	n/a	n/a	n/a	n/a	n/a	n/a	8	108	104	n/a	n/a	220
HP	2021	13	11	59	69	67	23	17	31	n/a	73	26	n/a	389
HP	2022	20	15	n/a	25	n/a	56	16	86	61	1	n/a	56	336
HP	2023	n/a	3	n/a	n/a	103	n/a	64	n/a	64	n/a	52	n/a	286
HP	2024	n/a	n/a	62	n/a	n/a	156	n/a	80	n/a	n/a	n/a	n/a	298
DP	All years	21	19	16	9	7	32	6	7	1	25	18	3	164
DP	2020	n/a	n/a	n/a	n/a	n/a	n/a	n/a	0	1	20	n/a	n/a	21
DP	2021	8	2	14	7	4	5	3	4	n/a	4	4	n/a	55
DP	2022	13	13	n/a	2	0	8	2	1	0	1	n/a	3	43
DP	2023	n/a	4	n/a	n/a	3	n/a	1	n/a	0	n/a	14	n/a	22
DP	2024	n/a	n/a	2	n/a	n/a	19	n/a	2	n/a	n/a	n/a	n/a	23
UP	All years	0	2	2	2	2	1	0	0	0	5	0	0	14
UP	2020	n/a	n/a	n/a	n/a	n/a	n/a	n/a	0	0	4	n/a	n/a	4
UP	2021	0	1	2	2	1	0	0	0	n/a	1	0	n/a	7

Species	Year	Jan	Feb	Mar	Apr	May	Jun	Jul	Aug	Sep	Oct	Nov	Dec	Total
UP	2022	0	1	n/a	0	n/a	1	0	0	0	0	n/a	0	2
UP	2023	n/a	0	n/a	n/a	1	n/a	0	n/a	0	n/a	0	n/a	1
KW – Bigg's	All years	0	0	4	1	0	2	3	2	3	2	1	0	18
KW – Bigg's	2020	n/a	n/a	n/a	n/a	n/a	n/a	n/a	0	1	0	n/a	n/a	1
KW – Bigg's	2021	0	0	4	0	0	1	1	0	n/a	1	0	n/a	7
KW – Bigg's	2022	0	0	n/a	1	n/a	1	0	1	2	1	n/a	0	5
KW – Bigg's	2023	n/a	0	n/a	n/a	0	n/a	2	n/a	0	n/a	1	n/a	3
KW – Bigg's	2024	n/a	n/a	0	n/a	n/a	0	n/a	1	n/a	n/a	n/a	n/a	1
KW - SRKW	All years	8	0	5	0	0	2	0	1	0	3	2	0	21
KW - SRKW	2020	n/a	n/a	n/a	n/a	n/a	n/a	n/a	0	0	1	n/a	n/a	1
KW - SRKW	2021	7	0	0	0	0	0	0	1	n/a	1	2	n/a	11
KW - SRKW	2022	1	0	n/a	0	n/a	0	0	0	0	1	n/a	0	2
KW - SRKW	2024	n/a	n/a	5	n/a	n/a	2	n/a	0	n/a	n/a	n/a	n/a	7
KW - UNKN	All years	0	0	0	0	0	0	1	0	1	1	0	0	3
KW - UNKN	2022	0	0	n/a	0	n/a	0	1	0	0	1	n/a	0	2
KW - UNKN	2023	n/a	0	n/a	n/a	0	n/a	0	n/a	1	n/a	0	n/a	1
PWSD	All years	0	0	0	0	0	0	0	0	1	0	0	0	1
PWSD	2023	n/a	0	n/a	n/a	0	n/a	0	n/a	1	n/a	0	n/a	1
FW	All years	0	0	0	0	0	0	0	1	0	0	0	0	1
FW	2021	0	0	0	0	0	0	0	1	n/a	0	0	n/a	1
GW	All years	0	0	1	0	0	0	0	0	0	0	0	0	1
GW	2024	n/a	n/a	1	n/a	n/a	0	n/a	0	n/a	n/a	n/a	n/a	1
MW	All years	0	0	0	0	0	0	1	0	0	0	0	0	1
MW	2023	n/a	0	n/a	n/a	0	n/a	1	n/a	0	n/a	0	n/a	1

Table 6. Comparison among humpback whale detection function models with strong support (i.e., ΔAIC less than five compared to the top-ranked model). Truncation distance for all models was 1.65 km. Formula = covariates in model, CvM p-value = Cramer-von Mises test p-value, Average detectability = estimated average probability of detecting an animal that is in the survey area, SE (Average detect.) = standard error of the average detectability. ΔAIC = difference in AIC from the top performing model. The selected detection function for humpback whales is a half-normal key function with swell and visibility as covariates, indicated in bold.

Key function	***Formula***	***CvM p-value***	***Average detectability***	***SE (Average detect.)***	***ΔAIC***
Half-normal	**~Swell + Visibility**	**0.51**	**0.59**	**0.03**	**0**
Half-normal	~Swell + Visibility + Glare	0.52	0.59	0.03	1.4
Half-normal	~Swell + Visibility + Precipitation	0.52	0.59	0.03	2.0
Half-normal	~Swell + Visibility + Observer	0.50	0.59	0.03	3.5
Half-normal	~Visibility	0.57	0.60	0.03	4.5

Table 7. Comparison among harbour porpoise detection function models with strong support (i.e., ΔAIC less than five compared to the top-ranked model). All models had a truncation distance of 0.65 km. Formula = covariates in model, χ^2 = Chi-squared p-value, Average detectability = estimated average probability of detecting an animal that is in the survey area, SE (Average detect.) = standard error of the average detectability. ΔAIC = difference in AIC from the top performing model. The selected detection function for harbour porpoises is a half-normal key function with cosine series adjustment terms of order 2,3, indicated in bold. "N/A" = not applicable.

Key function	Formula	χ^2 p-value	Average detectability	SE (Average detect.)	*ΔAIC*
Half-normal	~Beaufort + Cloud + Observer	1.04 e-07	0.58	0.01	0
Half-normal cos 3	**~1**	**0.07**	**0.48**	**0.02**	**2.1**
Half-normal	~Beaufort + Cloud	7.50 e-07	0.59	0.01	3.8
Uniform cos 3	N/A	0.04	0.50	0.02	4.2
Half-normal	~Beaufort + Observer	1.75 e-06	0.59	0.01	4.4
Hazard-rate	~Beaufort + Observer	4.00 e-04	0.50	0.03	4.7

Table 8. Comparison among Dall's porpoise detection function models with strong support (i.e., ΔAIC less than five compared to the top-ranked model). All models were right-truncated at a distance of 0.80 km. Formula = covariates in model, CvM p-value = Cramer-von Mises test p-value, Average detectability = estimated average probability of detecting an animal that is in the survey area, SE(Average detect.) = standard error of the average detectability. ΔAIC = difference in AIC from the top performing model. The selected detection function for Dall's porpoises is a half-normal model with swell and glare as covariates, indicated in bold. "N/A" = not applicable.

Key function	Formula	CvM p-value	Average detectability	SE (Average detect.)	ΔAIC
Half-normal	**~ Glare + Swell**	**0.40**	**0.57**	**0.04**	**0**
Hazard-rate	~ Glare + Swell	0.80	0.37	0.09	0.46
Half-normal	~ Glare	0.40	0.57	0.04	0.53
Half-normal	~1	0.39	0.58	0.04	0.58
Uniform cos 1	N/A	0.38	0.58	0.03	0.71
Hazard-rate	~Swell	0.73	0.38	0.09	0.88
Half-normal	~ Glare + Swell + Beaufort	0.40	0.57	0.04	2.0
Hazard-rate	~ Glare + Swell + Precipitation	0.74	0.38	0.09	2.1
Hazard-rate	~ Glare + Swell + Beaufort	0.79	0.37	0.09	2.4
Half-normal	~ Glare + Swell + Group Size	0.38	0.57	0.04	2.4
Half-normal	~ Glare + Swell + Precipitation	0.42	0.57	0.04	2.9
Hazard-rate	~1	0.51	0.43	0.08	3.3
Hazard-rate	~ Glare + Swell + Group Size	0.76	0.36	0.09	3.4
Half-normal	~ Glare + Swell + Group Size	0.41	0.57	0.04	3.5
Hazard-rate	~ Glare + Swell + Group Size	0.80	0.37	0.09	4.3

Table 9. Candidate generalized additive models considered for humpback whales after removal of collinear terms, terms with high concurvity with the spatial smoother, and terms with effective degrees of freedom (EDFs) less than one. The selected model for each season (Winter = January through March, Spring = April through June, Summer = July through September, and Fall = October through December) is indicated in bold. "Family" indicates the probability distribution of each model, either negative binomial (NB) or Tweedie (TW). Terms considered as smoothers are included with their respective EDFs. "sst" = sea surface temperature; "sqr.slope" = square root of slope; "sqr.chl" = square root of chlorophyll a concentration; "chl" = chlorophyll a concentration; "n/a" = not applicable. "Basis" indicates the type of smoothing spline used for each smooth term in the model, either penalized thin-plate regression splines (ts) or Duchon splines (ds). Estimated density per km² for the full study area and its associated coefficient of variation (CV) are included for each candidate model.

Season	Family	Smooths	Linear terms/ Factors	Basis	ΔAIC	ΔBIC	Density	CV
Winter	NB	s(x,y, 1.48), s(sst, 1.4)	n/a	ds	0.0	8.7	0.004	0.44
Winter	NB	s(x,y, 1.49)	n/a	ds	0.5	0.0	0.004	0.42
Winter	NB	s(x,y, 1.52)	n/a	ts	0.6	0.3	0.004	0.42
Winter	TW	s(x,y, 1.46), s(sst, 1.4)	n/a	ds	0.0	8.3	0.004	0.38
Winter	TW	s(x,y, 1.52)	n/a	ts	0.5	0.0	0.004	0.36
Winter	**TW**	**s(x,y, 2.45)**	**n/a**	**ds**	**1.8**	**9.2**	**0.004**	**0.36**
Spring	NB	s(x,y, 8.29)	month	ds	0.0	0.0	0.022	0.36
Spring	NB	s(x,y, 7.41)	month	ts	3.5	1.6	0.022	0.22
Spring	NB	s(x,y, 7.71), s(sst, 2.3)	n/a	ds	14.4	22.0	0.020	0.22
Spring	NB	s(x,y, 6.47)	sst	ts	15.6	3.7	0.022	0.23
Spring	NB	s(x,y, 8.27)	n/a	ds	20.9	11.2	0.023	0.21
Spring	NB	s(x,y, 7.14)	n/a	ts	24.4	11.1	0.024	0.22
Spring	**TW**	**s(x,y, 9.13), s(sqr.slope, 1.13)**	**month**	**ds**	**0.0**	**8.6**	**0.024**	**0.14**
Spring	TW	s(x,y, 8.94)	month	ds	1.2	0.0	0.023	0.17
Spring	TW	s(x,y, 7.89)	month	ts	5.2	1.4	0.024	0.15
Spring	TW	s(x,y, 8.13), s(sqr.slope, 1.07), s(sst, 2.41)	n/a	ds	16.4	31.3	0.023	0.18
Spring	TW	s(x,y, 6.92)	sst	ts	18.8	4.9	0.024	0.17
Spring	TW	s(x,y, 9.3)	n/a	ds	26.4	18.8	0.024	0.13
Spring	TW	s(x,y, 7.9)	n/a	ts	31.4	20.1	0.024	0.17
Summer	NB	s(x,y, 13.8)	sqr.sst, year	ds	0.0	28.0	0.081	0.24
Summer	NB	s(x,y, 12.6)	sqr.sst, year	ts	0.5	22.0	0.082	0.25
Summer	NB	s(x,y, 12.1)	month, year	ds	3.7	28.7	0.063	0.21
Summer	NB	s(x,y, 10.8)	month, year	ts	4.5	22.9	0.065	0.22
Summer	NB	s(x,y, 11.1)	n/a	ds	14.7	5.5	0.063	0.18
Summer	**NB**	**s(x,y, 9.9)**	**n/a**	**ts**	**15.1**	**0.0**	**0.065**	**0.19**
Summer	TW	s(x,y, 15.4), s(sqr.chl, 7)	year	ds	0.0	40.5	0.089	0.28
Summer	TW	s(x,y, 14.9), s(sqr.chl, 6.07)	year, month	ds	0.5	46.5	0.078	0.22
Summer	TW	s(x,y, 20.2), s(sqr.sst, 5.73)	year	ds	3.5	71.4	0.094	0.28
Summer	TW	s(x,y, 13.1), s(sqr.chl, 5.73)	year, month	ts	4.7	42.7	0.087	0.2
Summer	TW	s(x,y, 15.7)	sqr.sst, year	ts	14.7	21.0	0.090	0.31

Season	Family	Smooths	Linear terms/ Factors	Basis	ΔAIC	ΔBIC	Density	CV
Summer	TW	s(x,y, 12.5)	n/a	ds	41.0	9.3	0.067	0.15
	TW	s(x,y, 10.7)	n/a	ts	42.0	0.0	0.068	0.15
Fall	NB	s(x,y, 22), s(chl, 6.85)	month	ds	0.0	38.7	0.138	0.29
Fall	NB	s(x,y, 21.3)	year	ts	8.3	3.7	0.096	0.33
Fall	NB	s(x,y, 20.6)	month	ts	10.6	0.0	0.118	0.26
Fall	NB	s(x,y, 20.5), s(sst, 1.35)	year	ds	16.6	33.7	0.092	0.26
Fall	NB	s(x,y, 21.4)	sst	ts	20.7	8.2	0.104	0.21
Fall	NB	s(x,y, 20.4)	sst	ds	21.8	5.2	0.107	0.21
Fall	NB	s(x,y, 21.5)	n/a	ts	25.4	10.1	0.087	0.17
Fall	NB	s(x,y, 20.9)	n/a	ds	31.0	23.1	0.088	0.17
Fall	TW	s(x,y, 27.7), s(chl, 8.26)	month	ts	0.0	27.4	0.149	0.23
Fall	TW	s(x,y, 28.1), s(chl, 7.91)	month	ds	0.6	31.5	0.149	0.23
Fall	TW	s(x,y, 27.7), s(sst, 1.74), s(chl, 7.51)	year	ds	7.6	54.6	0.102	0.19
Fall	**TW**	**s(x,y, 26.8)**	**sst, year**	**ts**	**15.9**	**4.8**	**0.102**	**0.18**
Fall	TW	s(x,y, 26.5)	sst, month	ts	17.2	0.0	0.114	0.2
Fall	TW	s(x,y, 26.6)	year	ts	20.1	3.2	0.110	0.24
Fall	TW	s(x,y, 26.6)	year	ds	20.5	5.0	0.110	0.24
Fall	TW	s(x,y, 26.7)	month	ts	23.4	2.4	0.143	0.23
Fall	TW	s(x,y, 26.8)	month	ds	26.4	13.1	0.144	0.23
Fall	TW	s(x,y, 25.8), s(chl, 1.98)	sst	ds	42.2	26.4	0.122	0.19
Fall	TW	s(x,y, 26)	sst	ts	45.2	16.4	0.122	0.16
Fall	TW	s(x,y, 26.1)	n/a	ts	51.8	19.5	0.103	0.13
Fall	TW	s(x,y, 26.2)	n/a	ds	54.2	27.9	0.104	0.13

Table 10. Candidate generalized additive models considered for harbour porpoises after removal of collinear terms, terms with high concurvity with the spatial smoother, and terms with effective degrees of freedom (EDFs) less than one. The selected model for each season (Winter = January through March, Spring = April through June, Summer = July through September, and Fall = October through December) is indicated in bold. "Family" indicates the probability distribution of each model, either negative binomial (NB) or Tweedie (TW). Terms considered as smoothers are included with their respective EDFs. "sst" = sea surface temperature; "sqrtmean" = square root of mean; "sqrtmean.chl" = square root of mean chlorophyll a concentration; "mean.chl" = mean chlorophyll a concentration; "logrug" = log rugosity; "logmean.chl" = log of mean chlorophyll a concentration; "n/a" = not applicable. "Basis" indicates the type of smoothing spline used for each smooth term in the model, either penalized thin-plate regression splines (ts) or Duchon splines (ds). Estimated density per km^2 for the full study area and its associated coefficient of variation (CV) are included for each candidate model.

Season	*Family*	*Smooths*	*Linear terms/ Factors*	*Basis*	*ΔAIC*	*ΔBIC*	*Density*	*CV*
Winter	NB	s(x,y, 10.4), s(sst, 4.92)	n/a	ds	0.0	28.0	0.224	0.38
Winter	NB	s(x,y, 8.43), s(sst, 4.81)	n/a	ts	2.0	20.6	0.227	0.38
Winter	NB	s(x,y, 8.73), s(sqrtmean.chl, 1.62)	month	ds	3.9	17.9	0.186	0.36
Winter	**NB**	**s(x,y, 6.91)**	**month**	**ts**	**7.4**	**0.0**	**0.187**	**0.29**
Winter	NB	s(x,y, 7.47)	sqrtmean.chl, year	ts	11.5	19.0	0.172	0.38
Winter	NB	s(x,y, 10.8)	n/a	ds	26.7	31.8	0.159	0.19
Winter	NB	s(x,y, 8.86)	n/a	ts	27.2	21.8	0.163	0.17
Winter	TW	s(x,y, 13.2), s(sqrtmean, 1.9)	month	ds	0.0	15.6	0.197	0.30
Winter	TW	s(x,y, 11.1)	sqrtmean.chl, month	ts	2.6	0.0	0.201	0.28
Winter	TW	s(x,y, 11.5)	month	ts	7.5	1.5	0.185	0.23
Winter	TW	s(x,y, 13.5)	month	ds	7.6	15.1	0.182	0.22
Winter	TW	s(x,y, 12.6)	n/a	ts	32.3	20.2	0.174	0.14
Winter	TW	s(x,y, 14.1)	n/a	ds	35.1	38.7	0.171	0.14
Spring	NB	s(x,y, 5.89), s(mean.chl, 1.74)	logslope	ts	0.0	10.7	0.405	0.16
Spring	NB	s(x,y, 7.6)	logrug	ds	2.1	7.6	0.387	0.11
Spring	NB	s(x,y, 7.66)	logslope	ds	3.4	9.6	0.385	0.11
Spring	**NB**	**s(x,y, 5.37)**	**logrug**	**ts**	**3.8**	**0.0**	**0.390**	**0.11**
Spring	NB	s(x,y, 4.8)	logslope, year	ts	4.6	11.6	0.413	0.21
Spring	NB	s(x,y, 5.32)	logslope	ts	5.1	0.9	0.389	0.11
Spring	NB	s(x,y, 8.78)	n/a	ds	13.8	25.6	0.358	0.10
Spring	NB	s(x,y, 4.46)	n/a	ts	15.4	0.3	0.368	0.10
Spring	TW	s(x,y, 8.38), s(mean.chl, 2.15)	logslope	ts	0.0	9.2	0.409	0.13
Spring	TW	s(x,y, 21.4)	n/a	ds	1.4	67.2	0.361	0.09
Spring	TW	s(x,y, 14.2), s(logrug, 0.953)	n/a	ds	4.5	43.0	0.390	0.09
Spring	TW	s(x,y, 8.45)	logrug	ts	4.6	0.0	0.396	0.09
Spring	TW	s(x,y, 14.5)	logslope	ds	5.8	46.4	0.390	0.09
Spring	TW	s(x,y, 8.62)	logslope	ts	6.5	3.8	0.394	0.09
Spring	TW	s(x,y, 17)	n/a	ts	11.0	60.4	0.363	0.09

Season	Family	Smooths	Linear terms/ Factors	Basis	ΔAIC	ΔBIC	Density	CV
Summer	NB	s(x,y, 22.8), s(sst, 2.14), s(logmean.chl, 3.66)	month, year	ds	0.0	34.9	0.507	0.49
Summer	NB	s(x,y, 20), s(sst, 1.18), s(logmean.chl, 4.15)	month, year	ts	4.7	21.0	0.483	0.44
Summer	NB	s(x,y, 22.6), s(logmean.chl, 0.352)	year	ds	33.1	23.5	0.376	0.27
Summer	NB	s(x,y, 20.2)	year	ts	33.7	0.0	0.385	0.23
Summer	NB	s(x,y, 23.9), s(logmean.chl, 5.23)	month	ds	33.7	35.1	0.383	0.21
Summer	NB	s(x,y, 20.2), s(logmean.chl, 5.37)	sst, month	ts	35.5	28.9	0.386	0.21
Summer	NB	s(x,y, 16.6), s(logmean.chl, 5.34)	tidal, sst, month	ts	37.7	22.2	0.363	0.21
Summer	NB	s(x,y, 22.9), s(logmean.chl, 4.78)	n/a	ds	52.9	40.7	0.370	0.16
Summer	NB	s(x,y, 23.4), s(sst, 1.77), s(logmean.chl, 4.82)	n/a	ds	53.3	62.4	0.372	0.17
Summer	NB	s(x,y, 21.7)	n/a	ds	59.2	11.3	0.369	0.12
Summer	NB	s(x,y, 20.8), s(logmean.chl, 5.04)	n/a	ts	59.3	42.3	0.374	0.16
Summer	NB	s(x,y, 19.2)	n/a	ts	66.5	10.0	0.374	0.12
Summer	TW	s(x,y, 23.2), s(sst, 2.63), s(logmean.chl, 4.96)	month, year	ds	0.0	27.7	0.567	0.37
Summer	TW	s(x,y, 21.3), s(sst, 2.28), s(logmean.chl, 5.41)	month, year	ts	1.9	18.0	0.561	0.37
Summer	TW	s(x,y, 23.4), s(logmean.chl, 5.11)	year	ds	35.5	32.1	0.388	0.23
Summer	TW	s(x,y, 24.7), s(logmean.chl, 5.76)	month	ds	38.8	33.0	0.388	0.17
Summer	TW	s(x,y, 22.2), s(logmean.chl, 6.33)	sst, month	ts	39.7	31.9	0.418	0.18
Summer	TW	s(x,y, 25), s(sst, 2.58), s(logmean.chl, 5.58)	n/a	ds	50.4	53.6	0.433	0.15
Summer	**TW**	**s(x,y, 17.5)**	**tidal, year**	**ts**	**54.1**	**0.0**	**0.350**	**0.17**
Summer	TW	s(x,y, 23.8), s(sst, 2.49), s(logmean.chl, 5.86)	n/a	ts	54.3	53.7	0.435	0.16
Summer	TW	s(x,y, 20.5), s(logmean.chl, 0.000398)	year	ts	55.4	11.0	0.371	0.23
Summer	TW	s(x,y, 22.4)	n/a	ds	85.5	28.5	0.381	0.09
Summer	TW	s(x,y, 20.7)	n/a	ts	92.2	30.0	0.382	0.09
Fall	NB	s(x,y, 10.6), s(sst, 1.8), s(logmean.chl, 2.61)	month	ds	0.0	25.3	0.455	0.34
Fall	**NB**	**s(x,y, 10.5)**	**month**	**ts**	**4.9**	**0**	**0.455**	**0.23**
Fall	NB	s(x,y, 10.1), s(sst, 2.16), s(logmean.chl, 2.01)	year	ds	6.1	39	0.455	0.44
Fall	NB	s(x,y, 11.4), s(sst, 2.52), s(logmean.chl, 3.07)	n/a	ds	6.5	30.5	0.484	0.38
Fall	NB	s(x,y, 11.7), s(sst, 1.26)	month	ds	7.0	19.4	0.448	0.28
Fall	NB	s(x,y, 8.36), s(sst, 2.07)	year	ts	7.6	15.7	0.443	0.45

Season	*Family*	*Smooths*	*Linear terms/ Factors*	*Basis*	*ΔAIC*	*ΔBIC*	*Density*	*CV*
Fall	NB	s(x,y, 9.64), s(sst, 2.84)	logmean chl	ts	10.2	15	0.602	0.54
Fall	NB	s(x,y, 10.8)	n/a	ts	23.0	8.9	0.456	0.14
Fall	NB	s(x,y, 11.8)	n/a	ds	23.0	13.4	0.451	0.14
Fall	TW	s(x,y, 15.3), s(logmean.chl, 2.31)	month	ds	0.0	19.8	0.472	0.22
Fall	TW	s(x,y, 14.7), s(sst, 1.46), s(logmean.chl, 2.64)	month	ds	1.5	32.9	0.468	0.27
Fall	TW	s(x,y, 13.9)	month	ts	3.6	0.0	0.469	0.18
Fall	TW	s(x,y, 14.8), s(sst, 2.11), s(logmean.chl, 2.43)	year	ds	7.3	52.5	0.393	0.36
Fall	TW	s(x,y, 16.8), s(sst, 2.25), s(logmean.chl, 3.33)	n/a	ds	10.1	46.7	0.481	0.27
Fall	TW	s(x,y, 13.8), s(sst, 0.174)	year	ts	12.9	26.7	0.469	0.23
Fall	TW	s(x,y, 14.2), s(sst, 2.59)	logmean.chl	ts	17.2	29.4	0.536	0.36
Fall	TW	s(x,y, 15.5)	n/a	ds	26.3	19.2	0.472	0.11
Fall	TW	s(x,y, 14.1)	n/a	ts	26.7	13.6	0.474	0.11

Table 11. Candidate generalized additive models considered for Dall's porpoises after removal of collinear terms, terms with high concurvity with the spatial smoother, and terms with effective degrees of freedom (EDFs) less than one. The selected model for each season (Winter = January through March, Spring = April through June, Summer = July through September, and Fall = October through December) is indicated in bold. "Family" indicates the probability distribution of each model, either negative binomial (NB) or Tweedie (TW). Terms considered as smoothers are included with their respective EDFs. "sst" = sea surface temperature; "logsst" = log of sea surface temperature; "dist2shore" = distance to shore; "n/a" = not applicable. "Basis" indicates the type of smoothing spline used for each smooth term in the model, either penalized thin-plate regression splines (ts) or Duchon splines (ds). Estimated density per km² for the full study area and its associated coefficient of variation (CV) are included for each candidate model.

Season	Family	Smooths	Linear terms/ Factors	Basis	ΔAIC	ΔBIC	Density	CV
Winter	NB	s(x,y, 19.8), s(sst, 3.15)	n/a	ds	0.0	40.9	0.077	0.39
Winter	NB	s(x,y, 21)	sst	ts	0.9	31.4	0.070	0.54
Winter	NB	s(x,y, 15.6)	n/a	ts	12.8	5.8	0.070	0.36
Winter	NB	s(x,y, 16.3)	n/a	ds	13.7	13.9	0.075	0.41
Winter	NB	s(x,y, 13.1)	dist2shore	ts	14.8	0	0.067	0.36
Winter	TW	s(x,y, 19.9), s(sst, 2.57)	n/a	ts	0.0	61.9	0.089	0.23
Winter	**TW**	**s(x,y, 9.32), s(sst, 2.92)**	**n/a**	**ds**	**10.3**	**8.4**	**0.099**	**0.40**
Winter	TW	s(x,y, 18.4)	n/a	ts	14.8	51.9	0.080	0.22
Winter	TW	s(x,y, 8.52)	n/a	ds	24.1	0.0	0.087	0.22
Spring	NB	s(x,y, 5.32)	n/a	ds	0.0	15.1	0.058	0.30
Spring	NB	s(x,y, 1.9)	n/a	ts	5.4	0.0	0.091	0.39
Spring	**TW**	**s(x,y, 5.43)**	**month**	**ds**	**0.0**	**5.7**	**0.059**	**0.22**
Spring	TW	s(x,y, 5.94)	year	ds	1.3	14.9	0.080	0.30
Spring	TW	s(x,y, 4.27)	month	ts	3.0	5.4	0.063	0.23
Spring	TW	s(x,y, 5.52)	n/a	ds	3.9	0	0.063	0.22
Spring	TW	s(x,y, 4.43)	year	ts	4.3	12.7	0.089	0.32
Spring	TW	s(x,y, 4.77)	n/a	ts	7.0	2.7	0.066	0.22
Summer	NB	s(x,y, 1.93)	n/a	ts	0.0	0	0.036	0.67
Summer	NB	s(x,y, 3.17), s(logsst, 1.5)	n/a	ds	1.0	22	0.017	0.63
Summer	NB	s(x,y, 4.86)	n/a	ds	1.5	21	0.019	0.53
Summer	TW	s(x,y, 3.88), s(logsst, 1.68)	n/a	ds	0.0	25.7	0.022	0.49
Summer	**TW**	**s(x,y, 5.04)**	**n/a**	**ds**	**1.4**	**21.2**	**0.022**	**0.35**
Summer	TW	s(x,y, 1.79)	n/a	ts	2.0	0.0	0.024	0.36
Fall	NB	s(x,y, 1.84)	n/a	ds	0.0	0.0	0.081	0.37
Fall	NB	s(x,y, 1.95)	n/a	ts	0.3	1.3	0.080	0.37
Fall	TW	s(x,y, 1.95)	year	ts	0.0	6.8	0.088	0.48
Fall	**TW**	**s(x,y, 3.78)**	**year**	**ds**	**2.1**	**23.1**	**0.083**	**0.47**
Fall	TW	s(x,y, 1.95)	n/a	ts	6.9	0.0	0.076	0.24
Fall	TW	s(x,y, 4.57)	n/a	ds	8.6	21.3	0.072	0.24

9. FIGURES

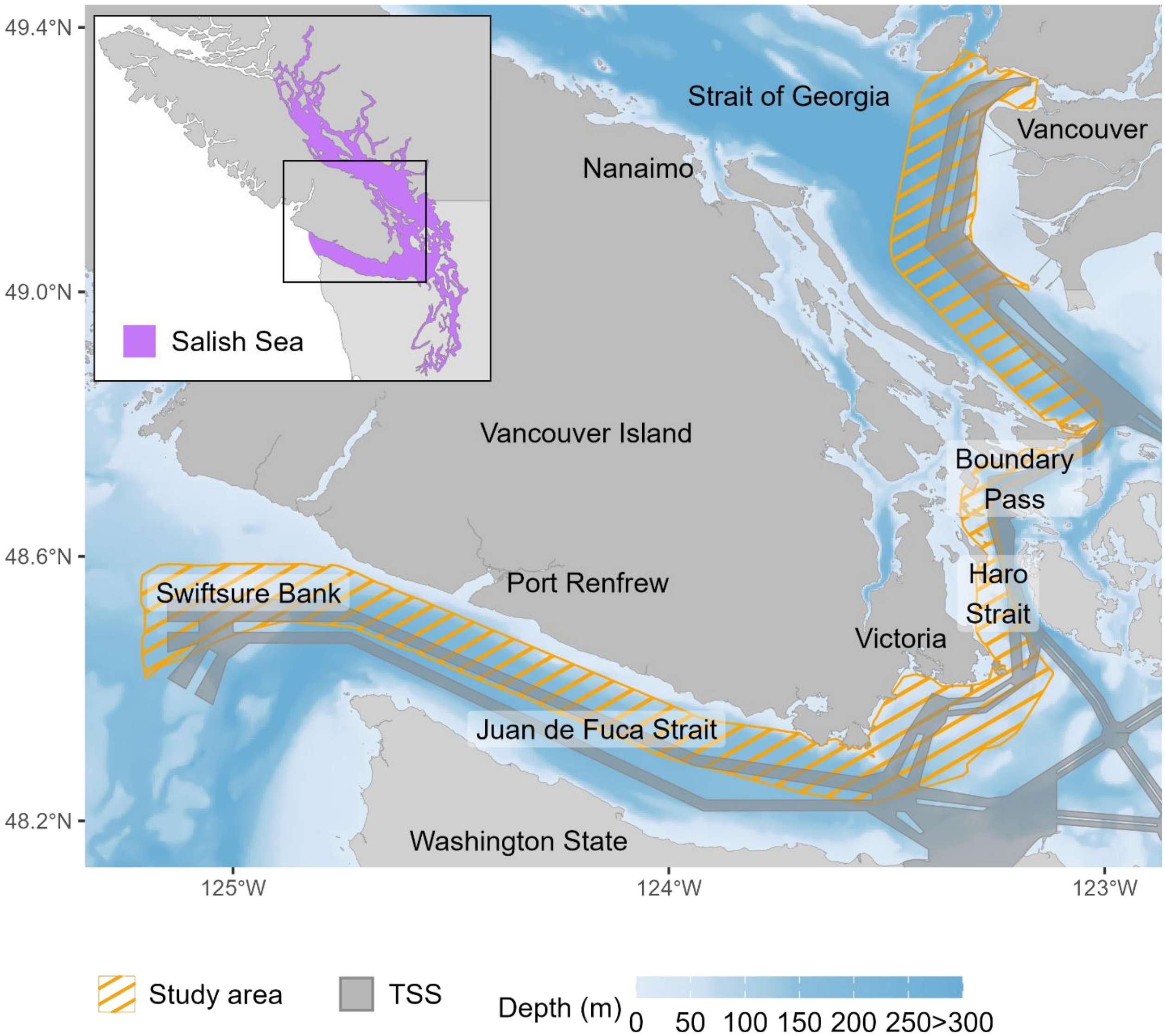

Figure 1. Study area for systematic cetacean line-transect surveys conducted between August 2020 and August 2024 (yellow diagonal lines) and locations of the inbound and outbound shipping lanes (traffic separation scheme (TSS), grey shaded area).The Salish Sea is indicated in purple in the inset.

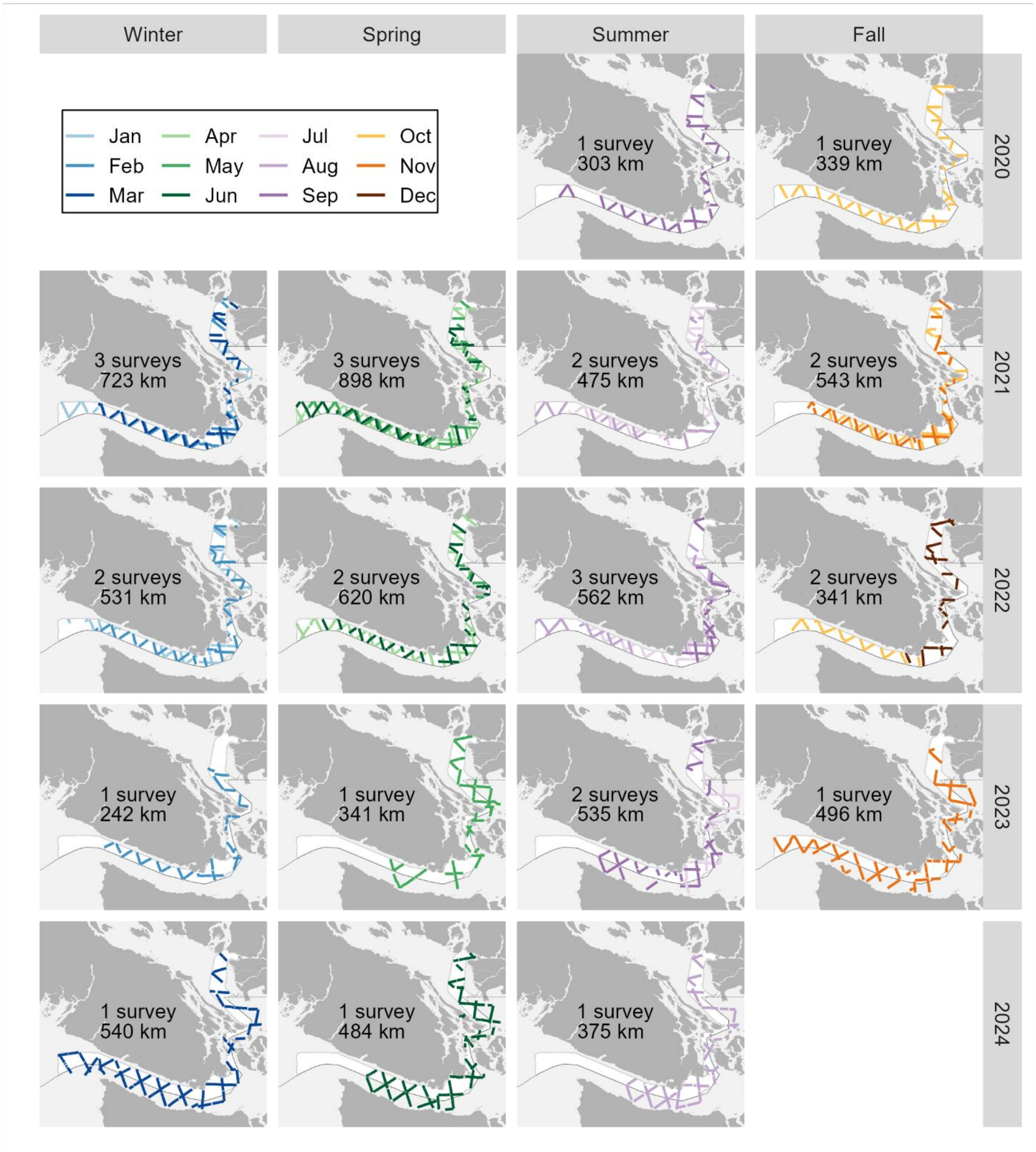

Figure 2. The realized monthly, seasonal, and annual survey effort from August 2020 to August 2024 (coloured transect lines). Number of monthly surveys conducted and total realized effort in km are displayed by season and year. Seasons were defined as Winter (January through March), Spring (April through June), Summer (July through September), and Fall (October through December).

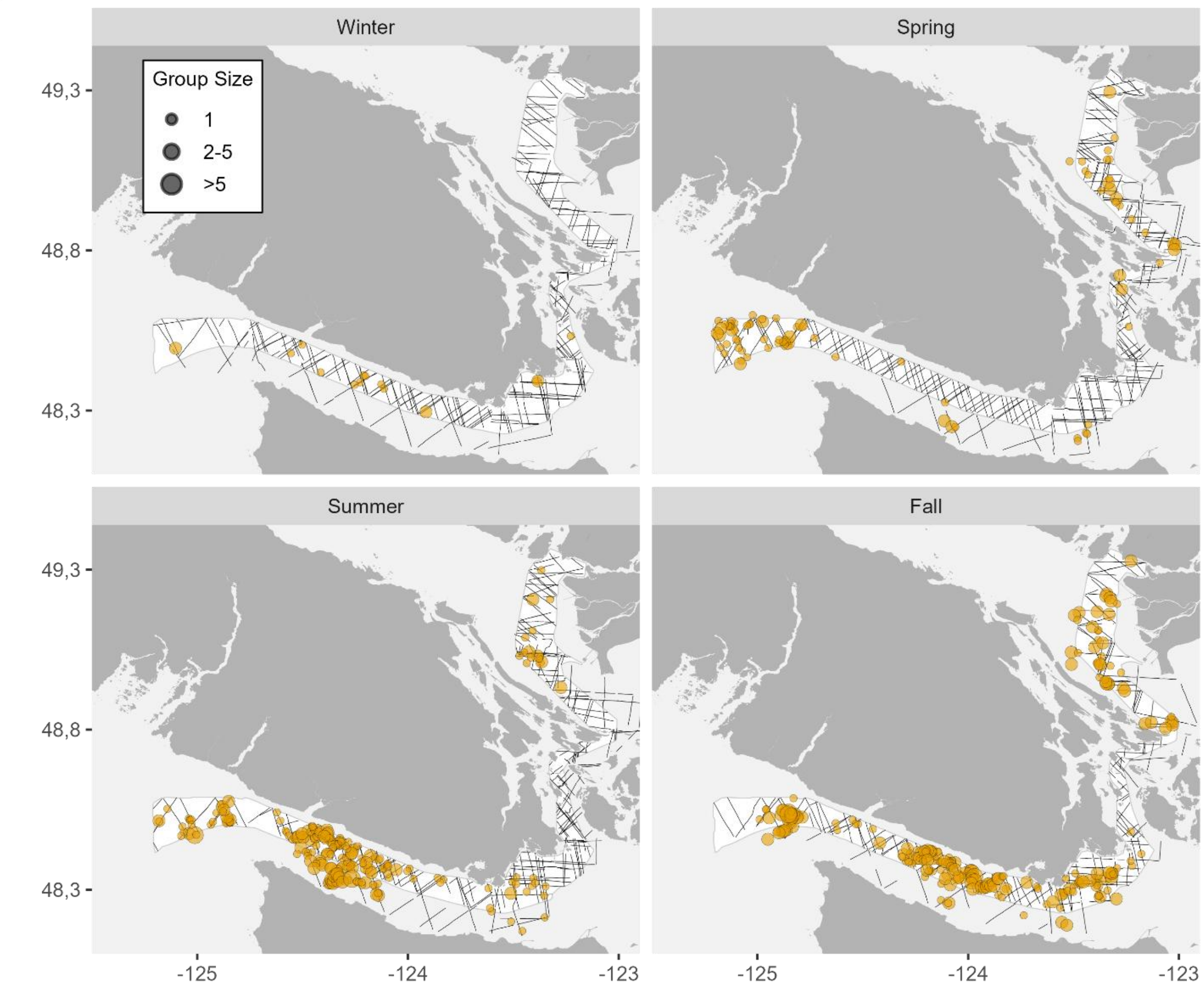

Figure 3. Humpback whale sightings and realized survey effort (black transect lines) by season (winter = January through March, spring = April through June, summer = July through September, fall = October through December) from August 2020 to August 2024. Relative point size (in yellow) indicates group size for each sighting.

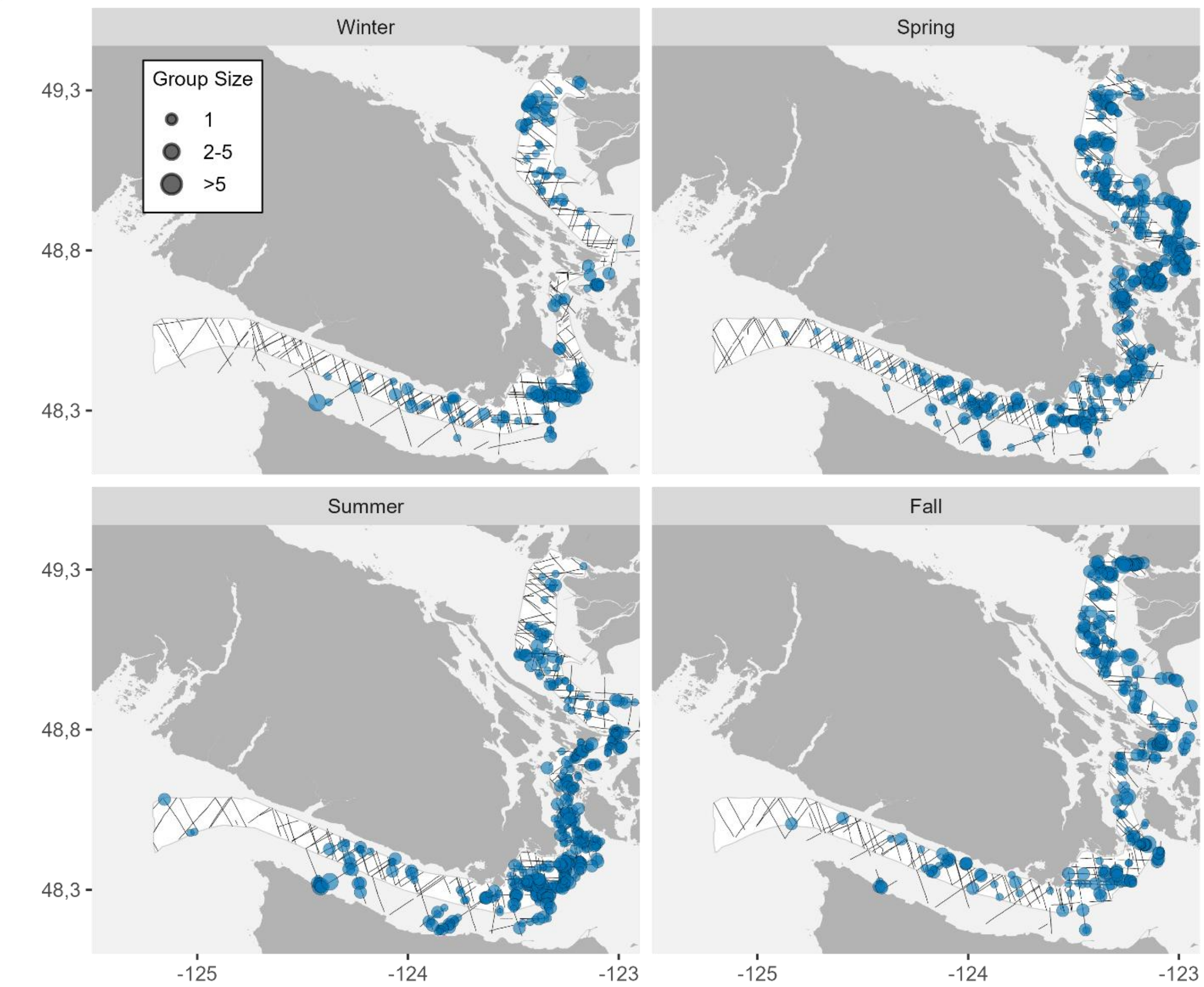

Figure 4. Harbour porpoise sightings and realized survey effort (black transect lines) by season (winter = January through March, spring = April through June, summer = July through September, fall = October through December) from August 2020 to August 2024. Relative point size (in blue) indicates group size for each sighting.

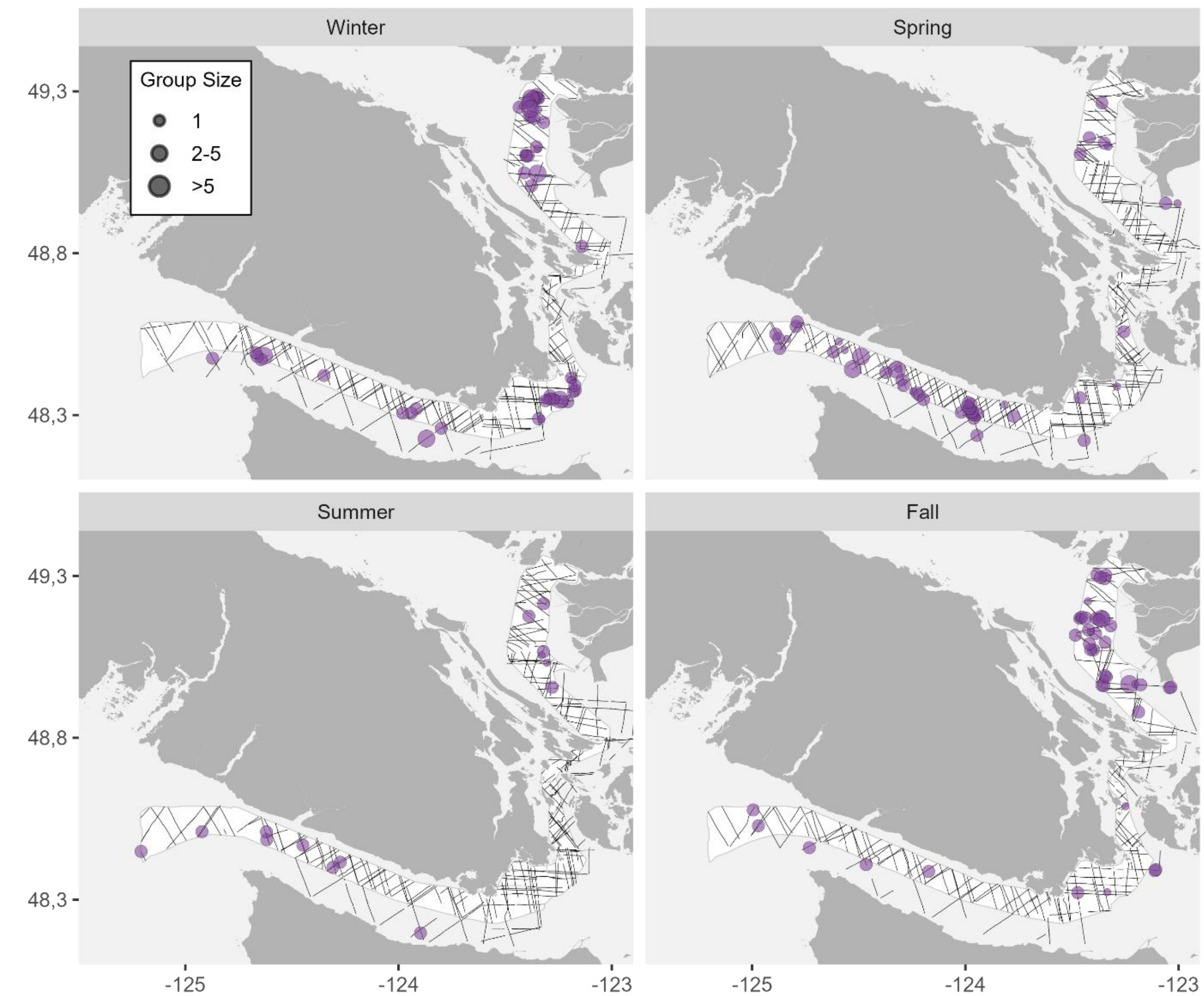

Figure 5. Dall's porpoise sightings and realized survey effort (black transect lines) by season (winter = January through March, spring = April through June, summer = July through September, fall = October through December) from August 2020 to August 2024. Relative point size (in purple) indicates group size for each sighting.

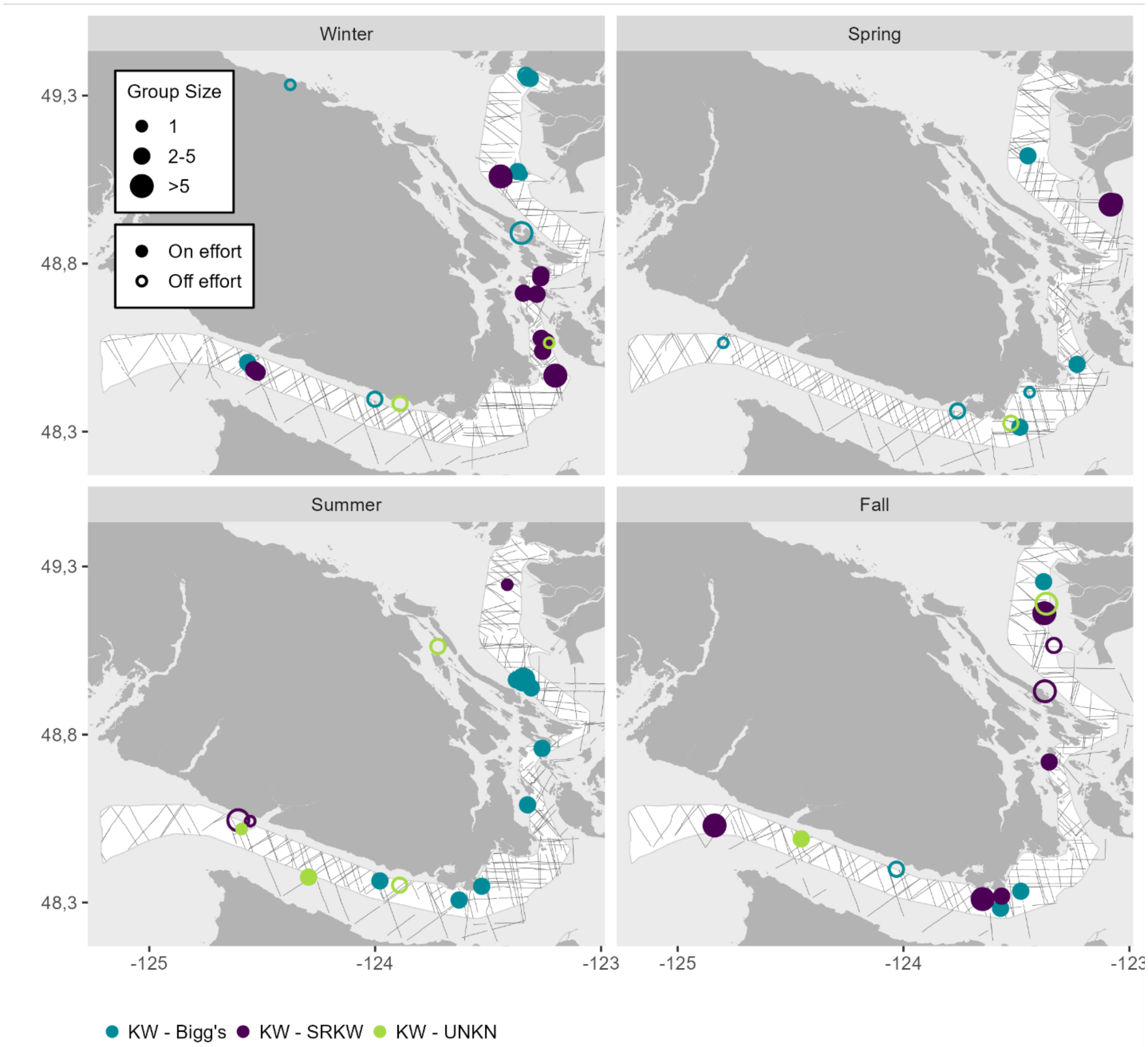

Figure 6. Sightings of killer whales and realized survey effort (grey transect lines) between August 2020 and August 2024. Killer whale ecotypes are denoted by colour (Bigg's killer whales (KW – Bigg's) = blue, Southern Resident killer whales (KW – SRKW) = purple, killer whales of unknown ecotype (KW – UNKN) = green. Closed circles represent on-effort sightings (sightings made while actively surveying along transect lines), while open circles represent incidental sightings (sightings made while transiting between transect lines). Relative point size indicates group size for each sighting.

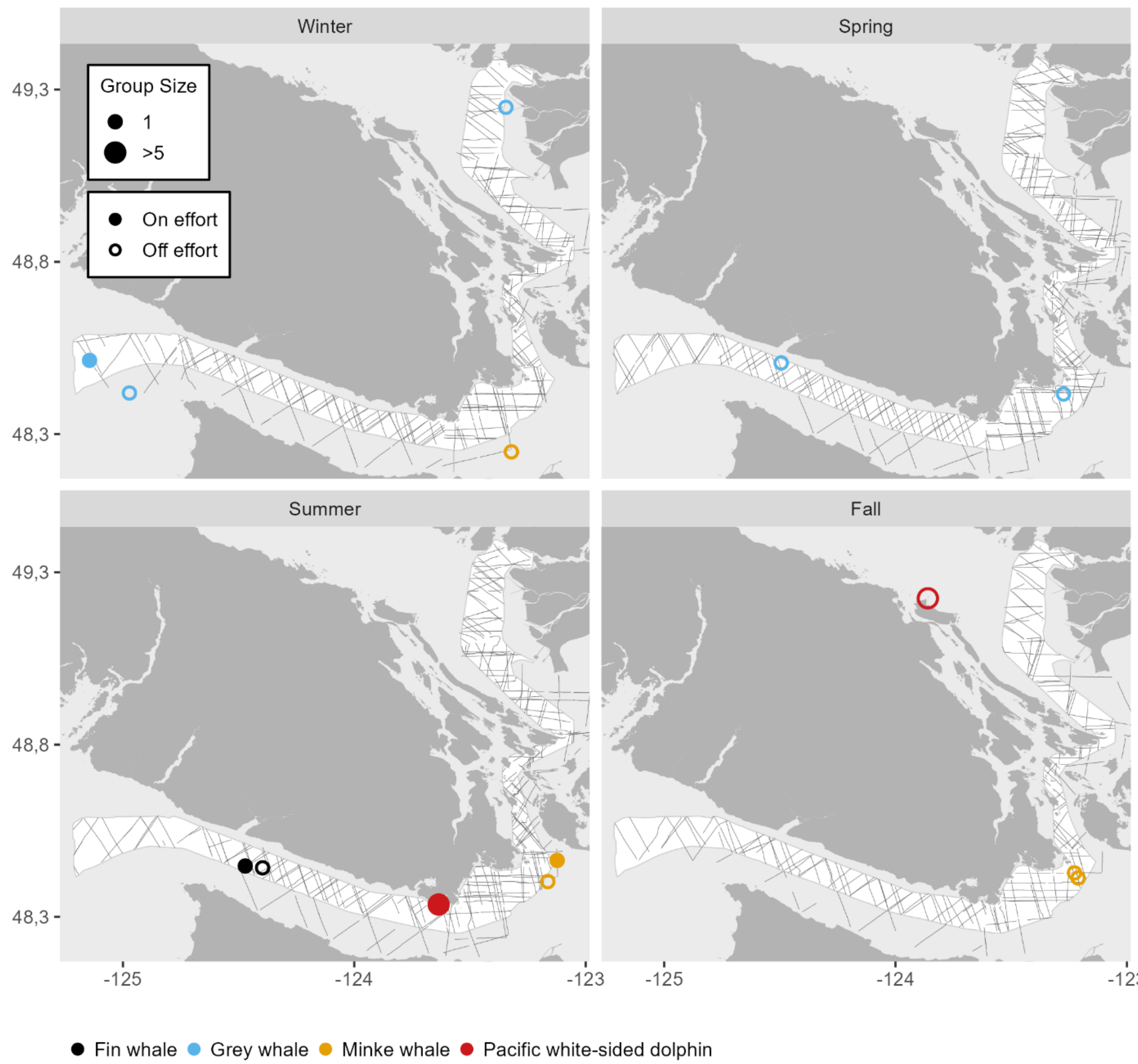

Figure 7. Sightings of species with insufficient sightings to fit detection functions and realized survey effort (grey transect lines), from August 2020 to August 2024. Species are denoted by colour: fin whales = black, grey whales = blue, minke whales = orange, and Pacific white-sided dolphins = red. Closed circles represent on-effort sightings (sightings made while actively surveying along transect lines), while open circles represent off-effort, incidental sightings (sightings made while transiting between transect lines). Relative point size indicates group size for each sighting.

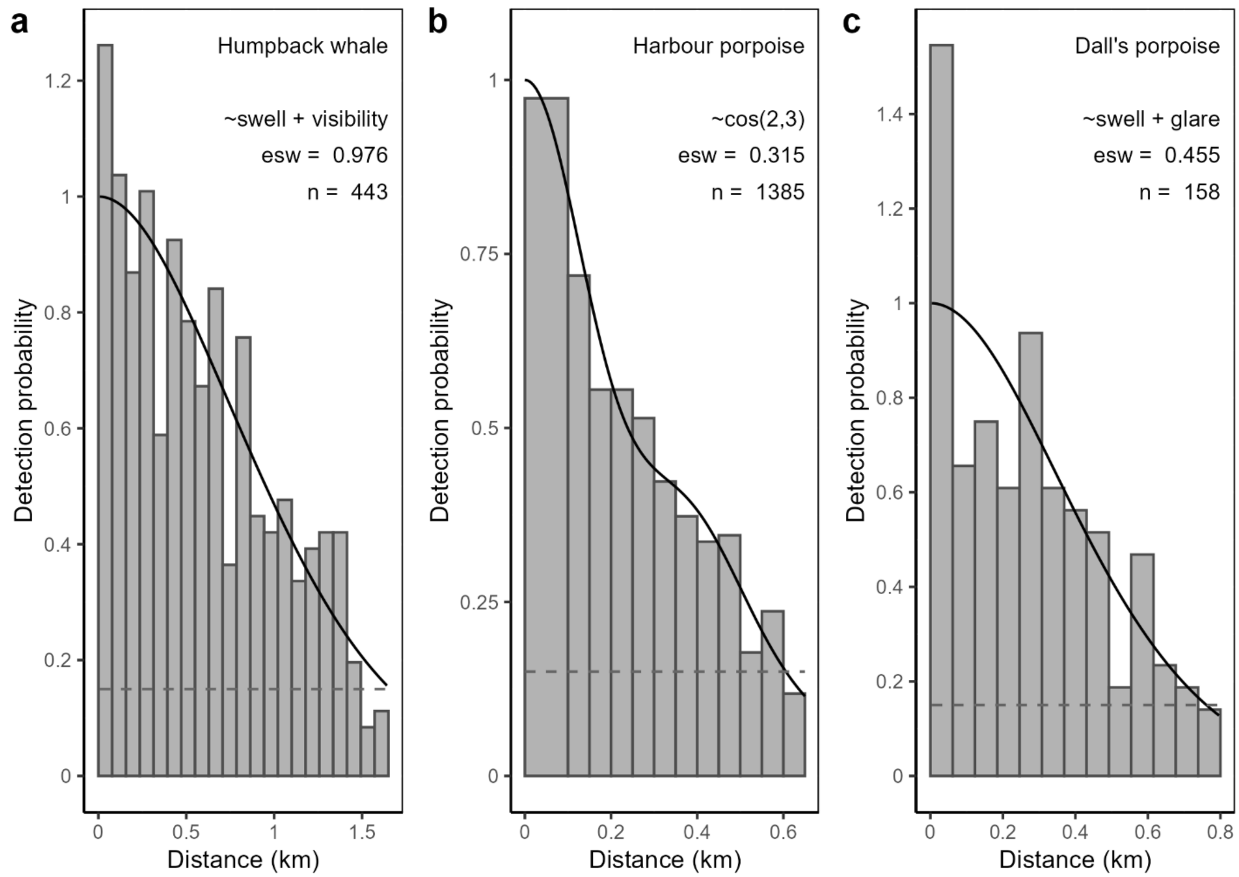

Figure 8. Histograms of perpendicular sighting distances with the selected detection function model for each species: a) humpback whale, a half-normal key function with swell and visibility as covariates and a right-truncation distance of 1.65 km; b) harbour porpoise, a half-normal key function with a cosine series adjustment of order 2,3 and a right-truncation distance of 0.65 km; data were grouped by perpendicular sighting distance for analyses using the bin sizes displayed; c) Dall's porpoise, a half-normal key function with swell and glare as covariates and a right-truncation distance of 0.8 km. For each model, the covariates, effective strip half-width (esw) and number of observations (n) within the truncation distance are shown. The dashed line on each plot indicates where estimated detection probability is 0.15.

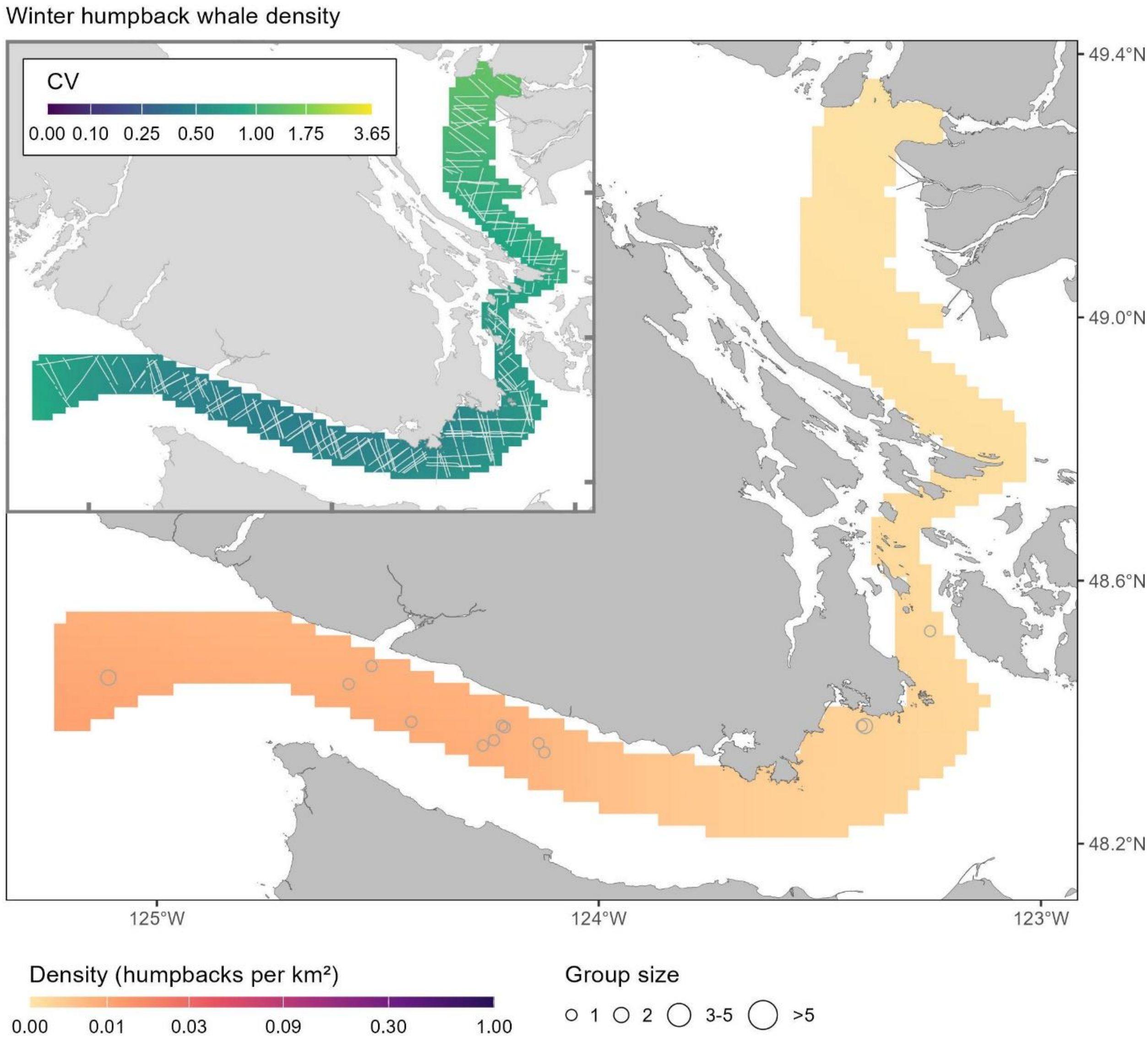

Figure 9. Humpback whale density (whales per km^2) during winter (January, February, March), as predicted by a Tweedie GAM with a bivariate Duchon spline spatial smoother. Total estimated humpback whale abundance during winter was 14 (CV = 0.36). Winter sightings of humpback whales (n = 13) are included as open circles, relative size of circles indicates humpback whale group size. Inset: spatially-varying CVs per 4 km^2 grid cell for the selected winter humpback whale DSM. Completed winter survey effort is indicated by the grey transect lines.

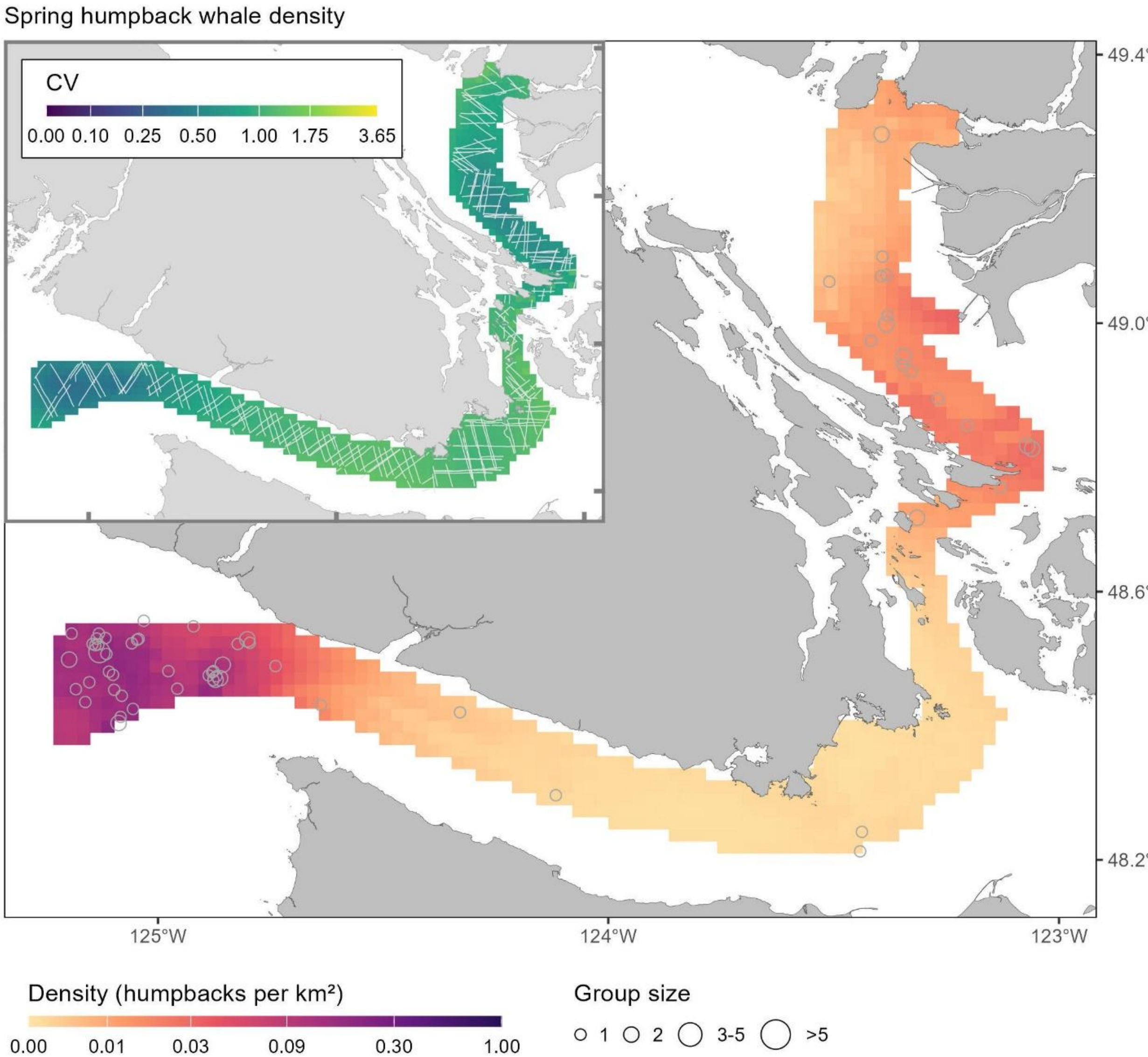

Figure 10. Humpback whale density (whales per km^2) during spring (April, May, June), as predicted by a Tweedie GAM with a bivariate spatial smoother and a smooth of slope, fit using Duchon splines, and including month as a factor. Total estimated humpback whale abundance during spring was 81 (CV = 0.14). Spring sightings of humpback whales (n = 61) are included as open circles, relative size of circles indicates humpback whale group size. Inset: spatially-varying CVs per 4 km^2 grid cell for the selected spring humpback whale DSM. Completed spring survey effort is indicated by the grey transect lines.

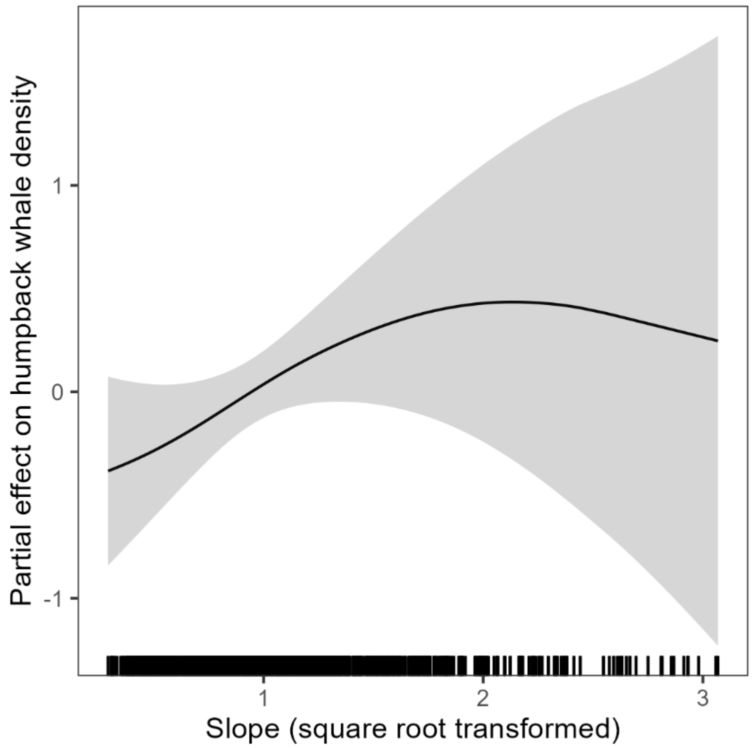

Figure 11. Partial effect of the smooth of slope (square-root transformed) in radians from the selected spring humpback whale DSM. Shaded bands represent 95% confidence intervals. The rug plot along the x-axis indicates the distribution of values for slope.

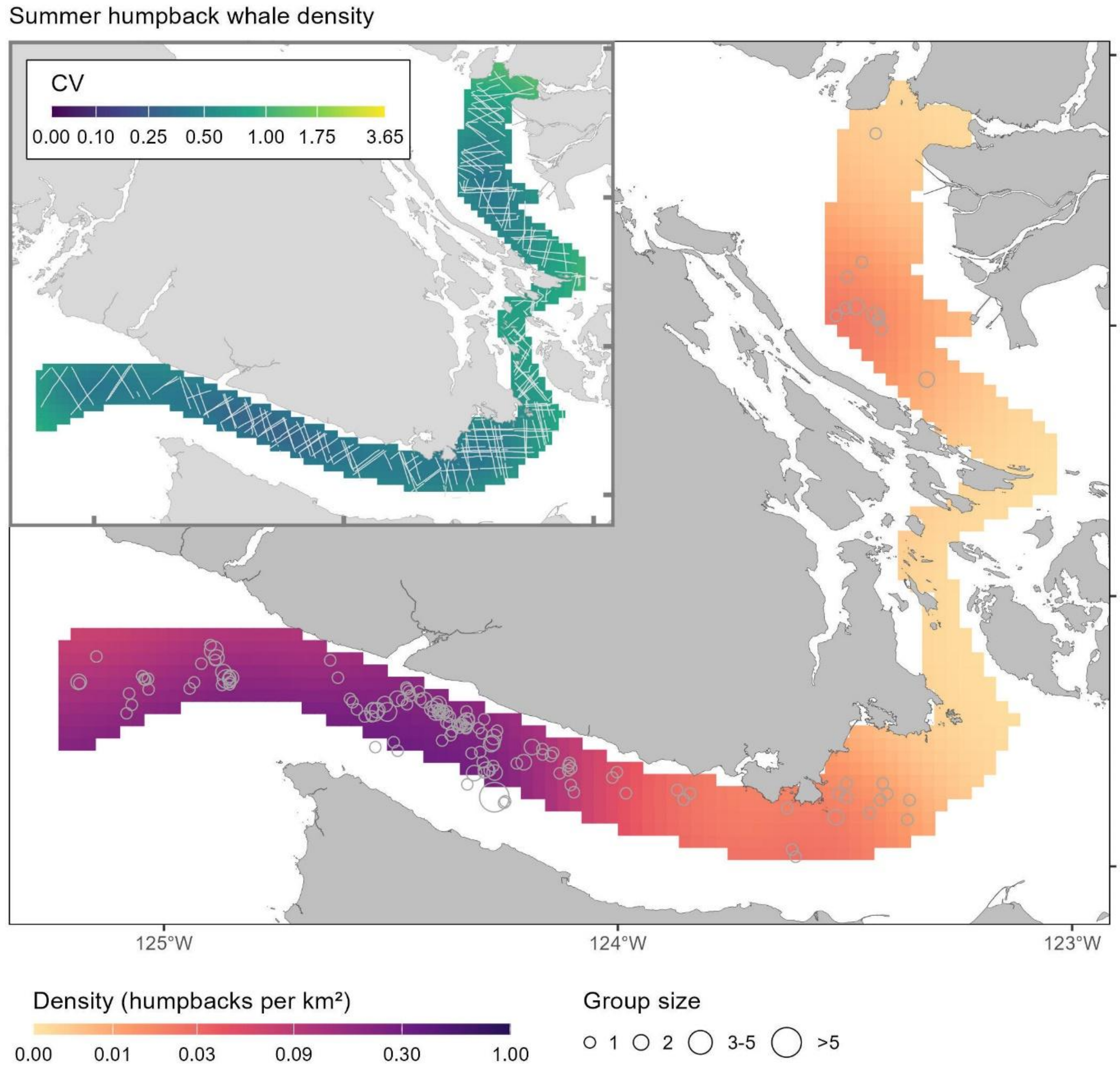

Figure 12. Humpback whale density (whales per km^2) during summer (July, August, September), as predicted by a negative binomial GAM with a bivariate spatial smoother, fit using a thin plate regression spline. Total estimated humpback whale abundance during summer was 221 (CV = 0.19). Summer sightings of humpback whales (n = 144) are included as open circles, relative size of circles indicates humpback whale group size. Inset: spatially-varying CVs per 4 km^2 grid cell for the selected summer humpback whale DSM. Completed summer survey effort is indicated by the grey transect lines.

Fall humpback whale density

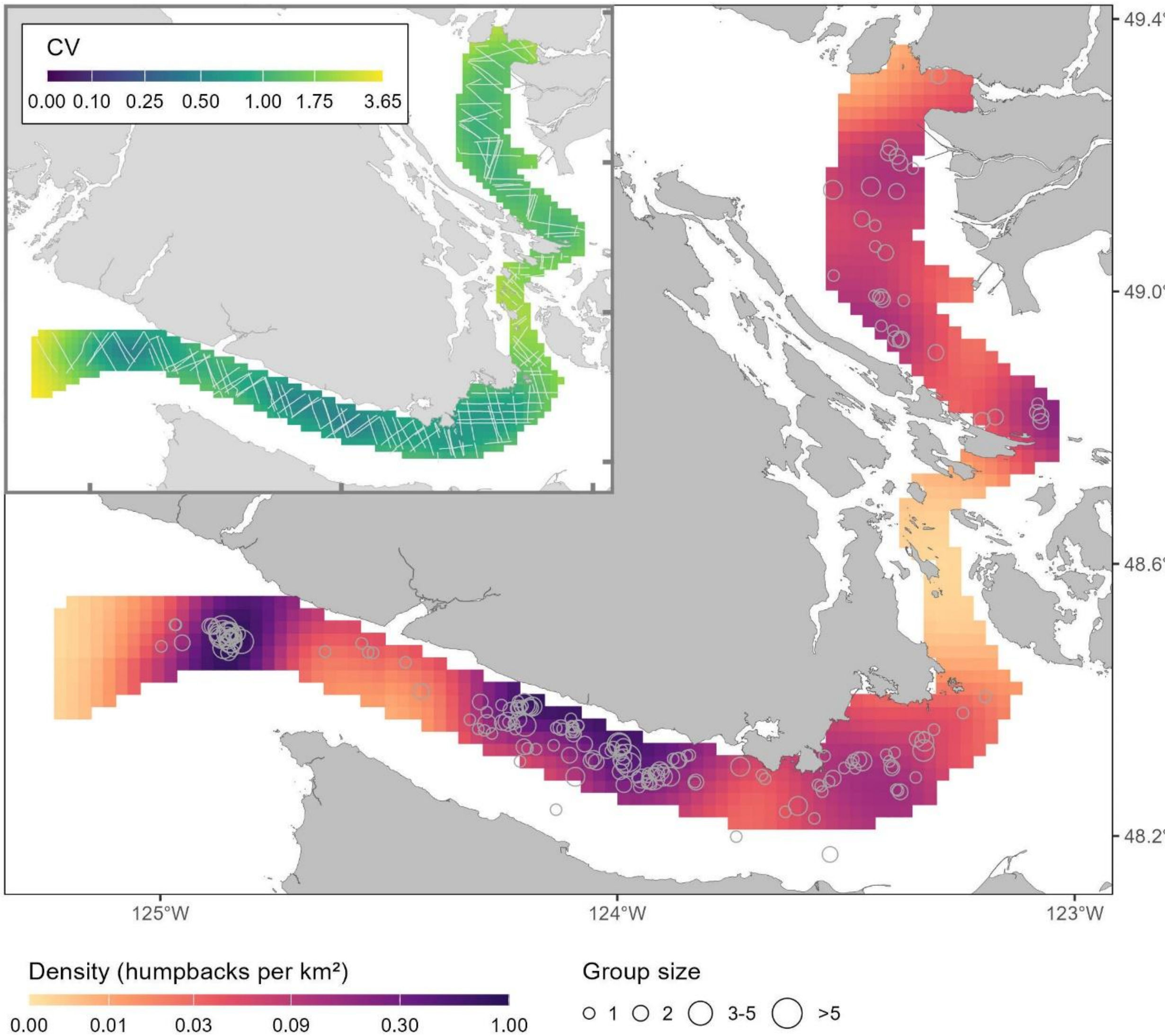

Figure 13. Humpback whale density (whales per km^2) during fall (October, November, December), as predicted by a Tweedie GAM with a bivariate thin plate regression spline spatial smooth, sea surface temperature as a linear term, and year as a factor. Total estimated abundance of humpback whales during fall was 347 (CV = 0.18). Fall sightings of humpback whales (n = 185) are indicated as open circles, relative size of circles indicates humpback whale group size. Inset: spatially-varying CVs per 4 km^2 grid cell for the selected fall humpback whale DSM. Completed fall survey effort is indicated by the grey transect lines.

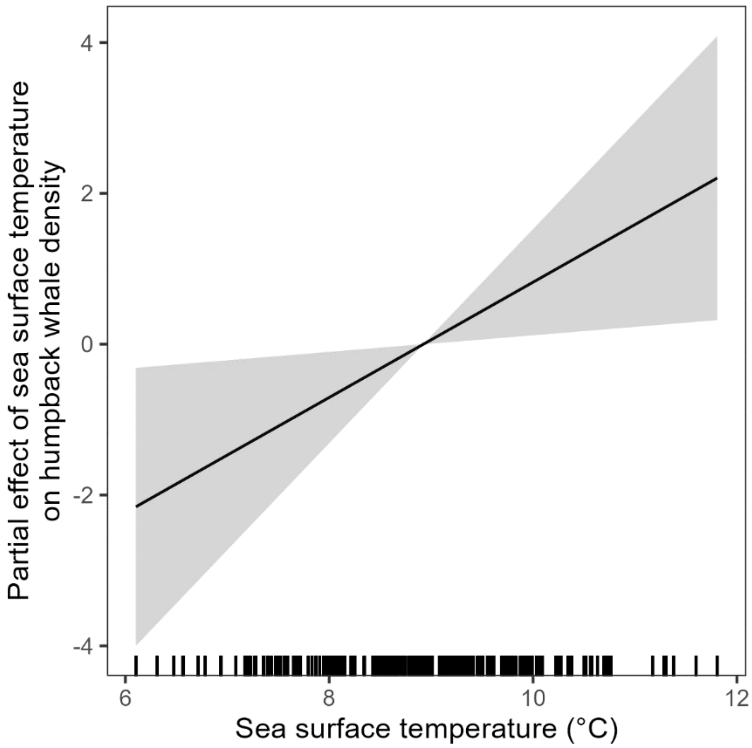

Figure 14. Partial effect plot for sea surface temperature (°C) from the selected fall humpback whale DSM. Shaded bands represent 95% confidence intervals. The rug plot along the x-axis indicates the distribution of values for sea surface temperature.

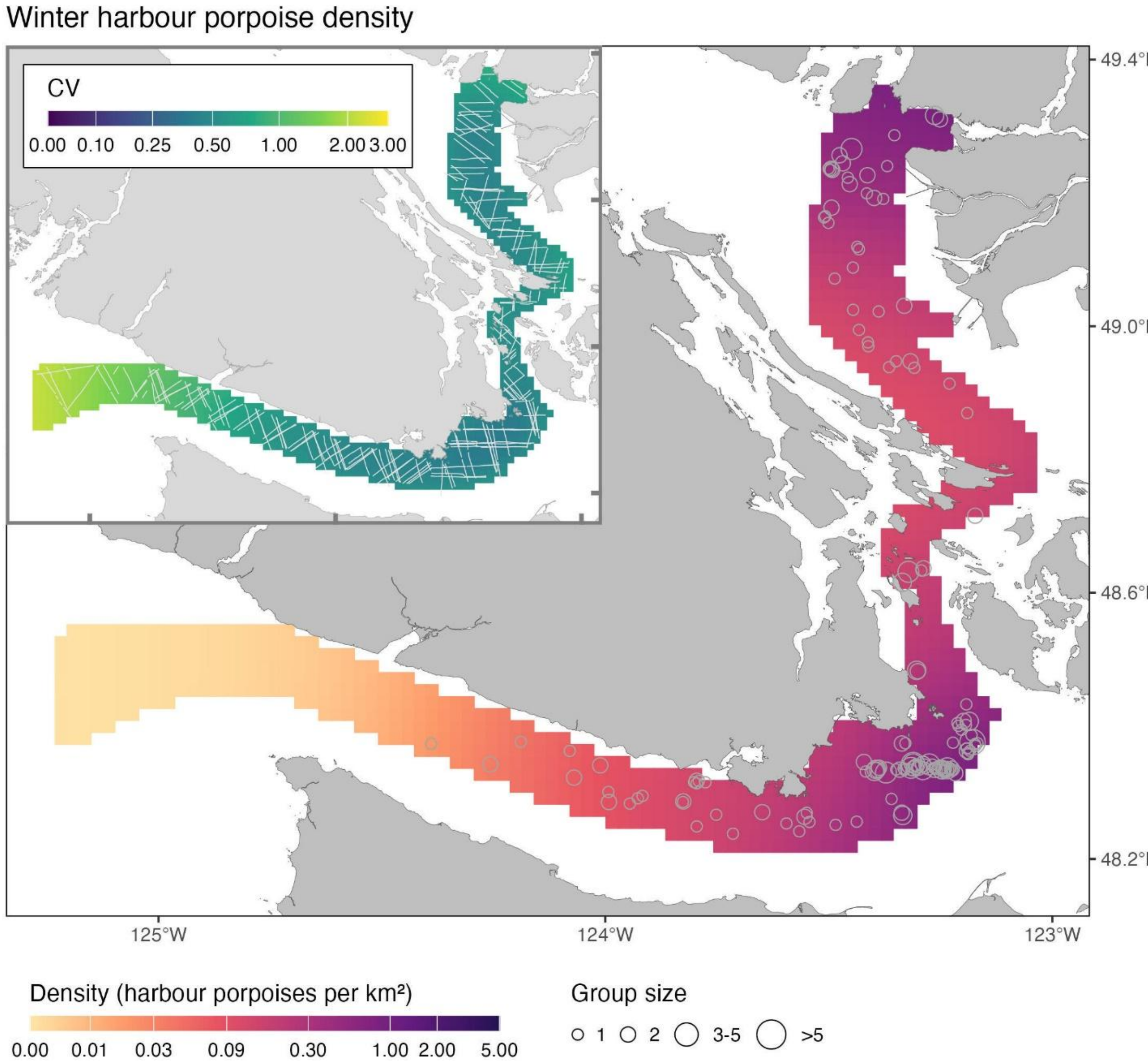

Figure 15. Harbour porpoise density (porpoises per km^2) during winter (January, February, March), as predicted by a negative binomial GAM with a bivariate thin-plate regression spline spatial smoother and month as a factor. Total estimated harbour porpoise abundance during winter was 637 (CV = 0.29). Sightings of harbour porpoises during this period (n = 139) are indicated as open circles, relative size of circles indicates harbour porpoise group size. Inset: spatially-varying CVs per 4 km^2 grid cell for the selected winter harbour porpoise DSM. Completed winter survey effort is indicated by the grey transect lines.

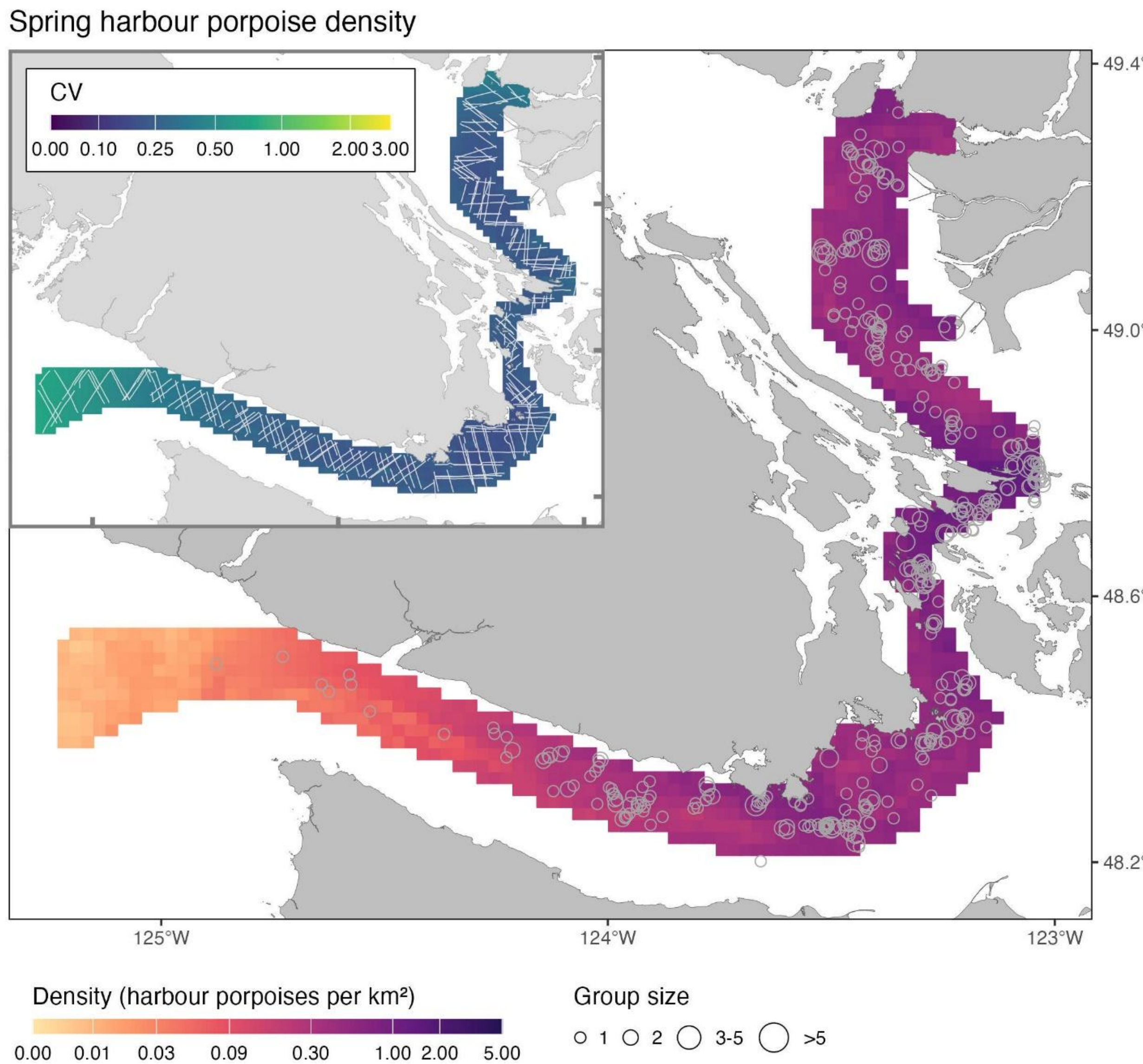

Figure 16. Harbour porpoise density (porpoises per km^2) during spring (April, May, June), as predicted by a negative binomial GAM with a bivariate thin-plate regression spline spatial smoother and rugosity as a linear term. Total estimated harbour porpoise abundance during spring was 1,335 (CV = 0.11). Sightings of harbour porpoises during this period (n = 361) are indicated as open circles, relative size of circles indicates harbour porpoise group size. Inset: spatially-varying CVs per 4 km^2 grid cell for the selected spring harbour porpoise DSM. Completed spring survey effort is indicated by the grey transect lines.

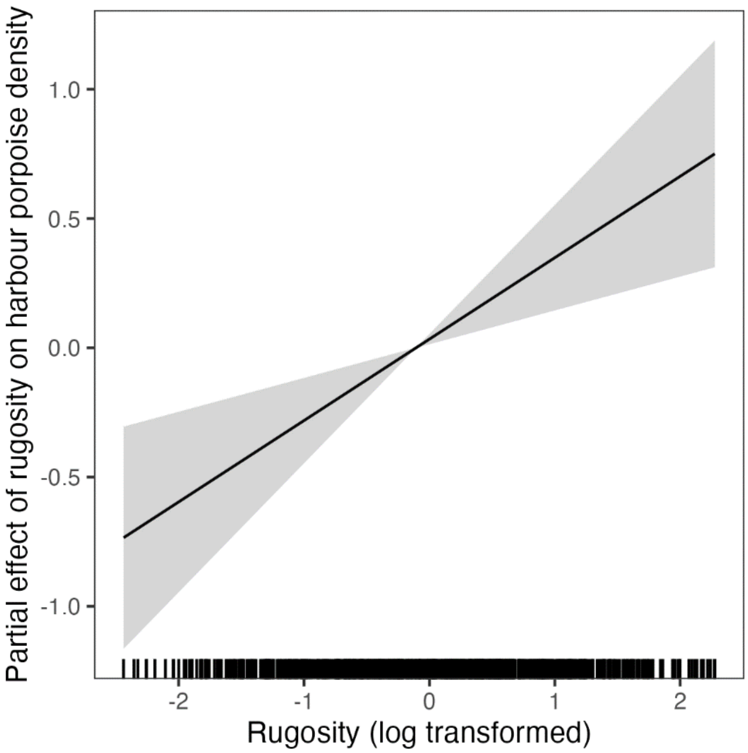

Figure 17. Partial effect of rugosity (log transformed) from the selected spring harbour porpoise DSM. Shaded bands represent 95% confidence intervals. The rug plot along the x-axis indicates the distribution of values for rugosity.

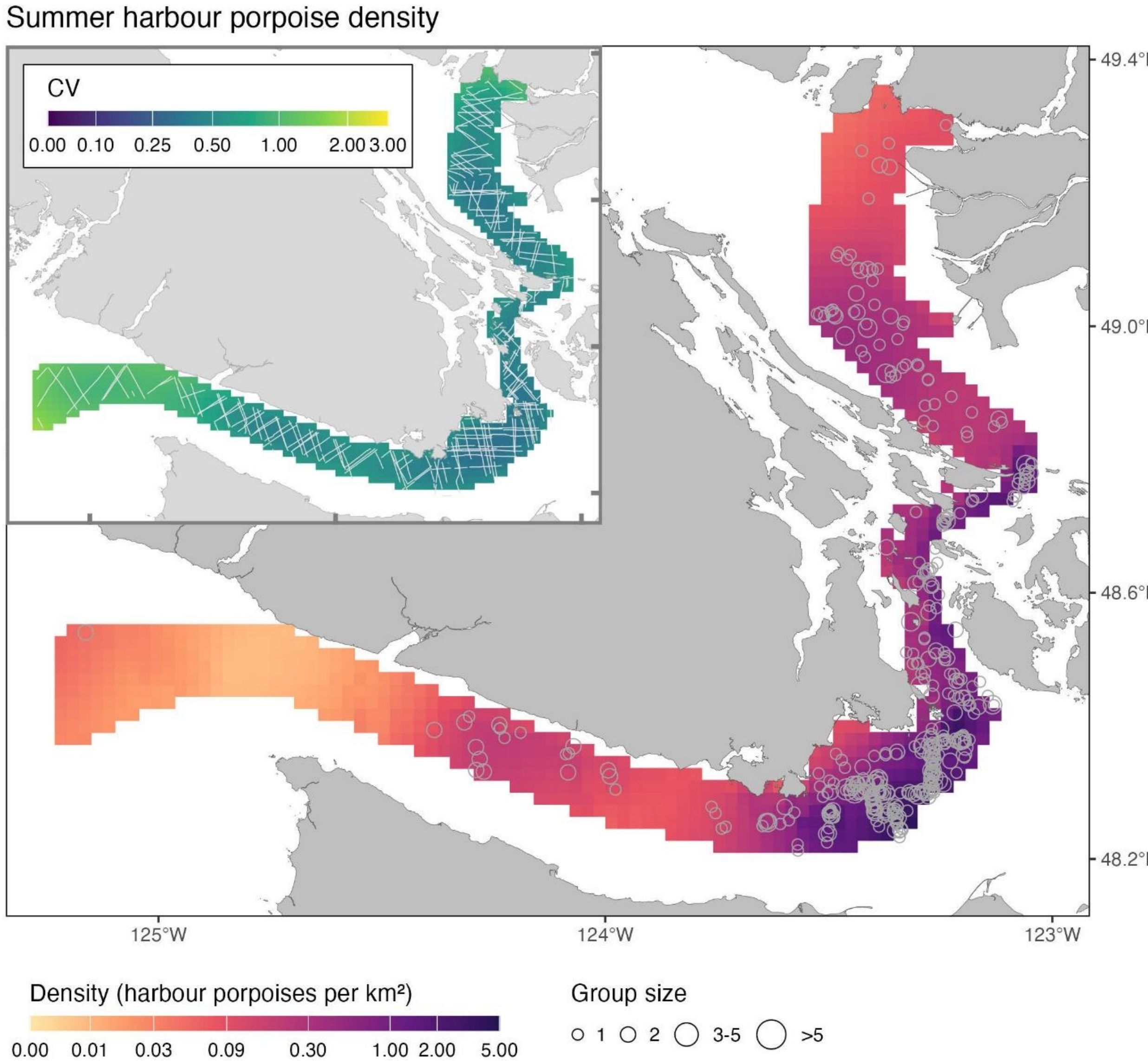

Figure 18. Harbour porpoise density (porpoises per km^2) during summer (July, August, September), as predicted by a Tweedie GAM with a bivariate thin-plate regression spline spatial smoother, average tidal current speed as a linear term, and year as a factor. Total estimated harbour porpoise abundance during summer was 1,192 (CV = 0.17). Sightings of harbour porpoises during this period (n = 384) are indicated as open circles, relative size of circles indicates harbour porpoise group size. Inset: spatially-varying CVs per 4 km^2 grid cell for the selected summer harbour porpoise DSM. Completed summer survey effort is indicated by the grey transect lines.

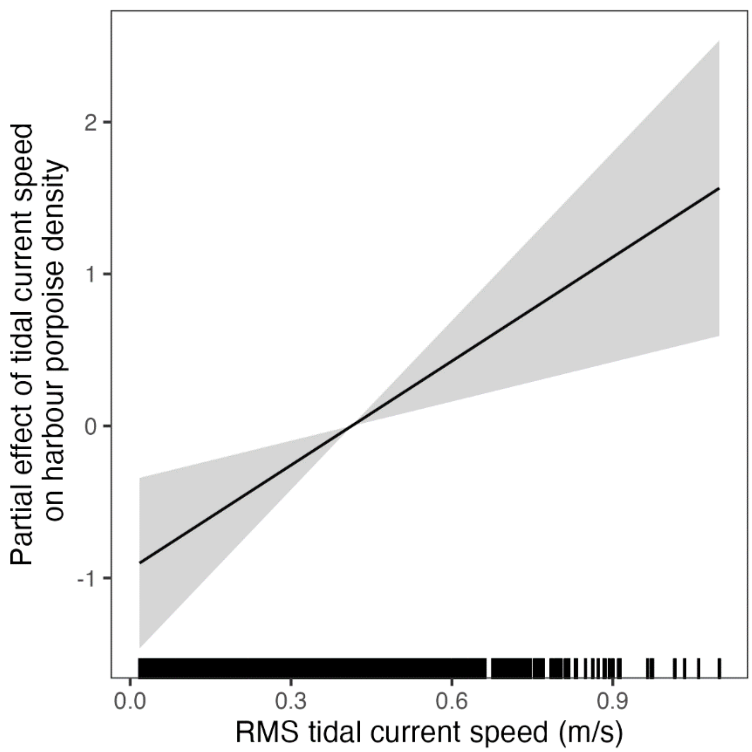

Figure 19. Partial effect plot of root mean square (RMS) tidal current speed from the selected summer harbour porpoise DSM. Shaded bands represent 95% confidence intervals. The rug plot along the x-axis indicates the distribution of values for RMS tidal current speed.

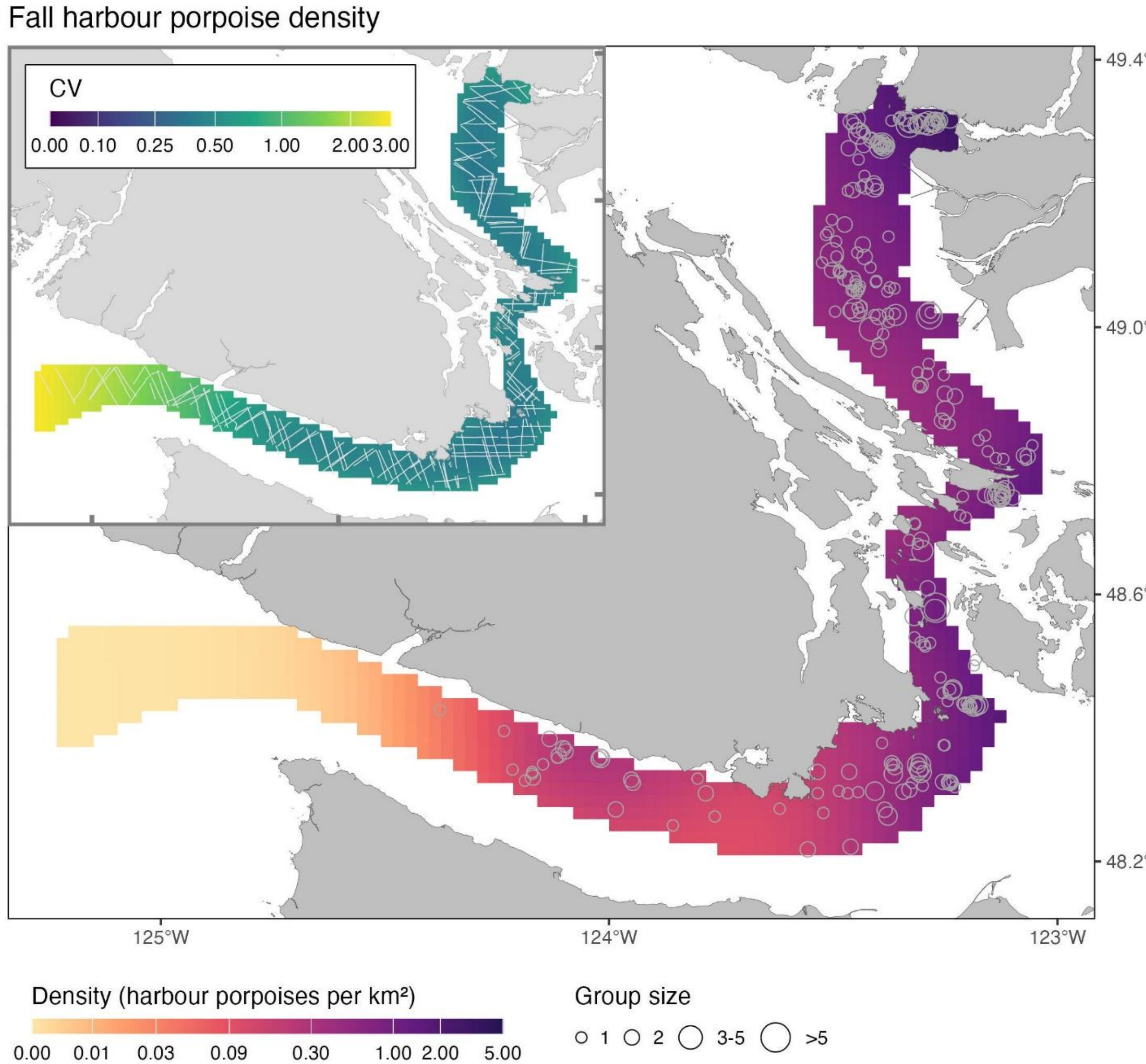

Figure 20. Harbour porpoise density (porpoises per km^2) during fall (October, November, December), as predicted by a negative binomial GAM with a bivariate thin-plate regression spline spatial smoother and month as a factor. Total estimated harbour porpoise abundance during fall was 1,552 (CV = 0.23). Sightings of harbour porpoises during this period (n = 249) are indicated as open circles, relative size of circles indicates harbour porpoise group size. Inset: spatially-varying CVs per 4 km^2 grid cell for the selected fall harbour porpoise DSM. Completed fall survey effort is indicated by the grey transect lines.

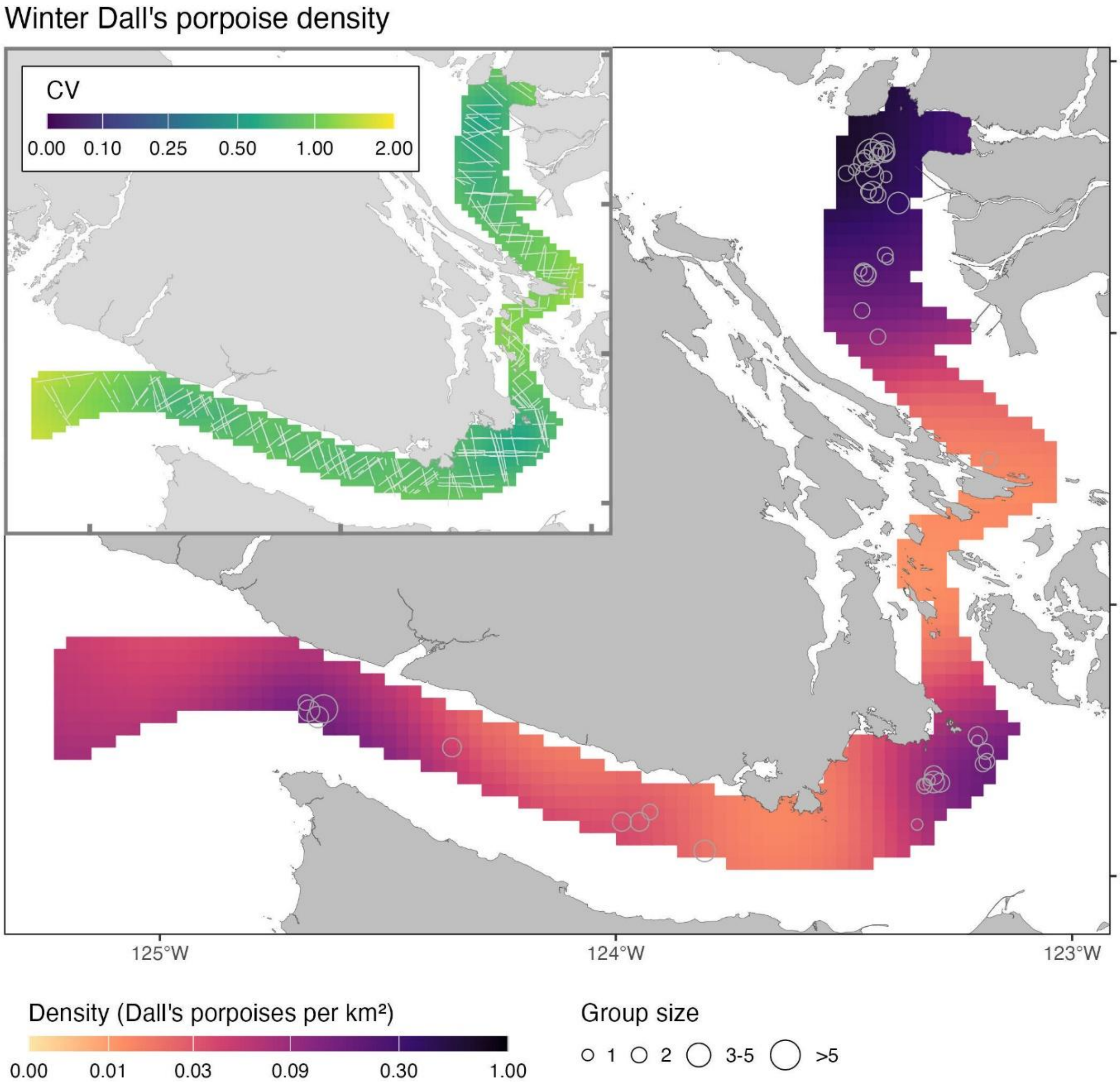

Figure 21. Dall's porpoise density (porpoises per km^2) during winter (January, February, March), as predicted by a Tweedie GAM with a bivariate spatial smoother and a smooth of sea surface temperature, fit using Duchon splines. Total estimated Dall's porpoise abundance in winter was 336 (CV = 0.40). Sightings of Dall's porpoises during this period (n = 49) are indicated as open circles, relative size of circles indicates Dall's porpoise group size. Inset: spatially-varying CVs per 4 km^2 grid cell for the selected winter Dall's porpoise DSM. Completed winter survey effort is indicated by the grey transect lines.

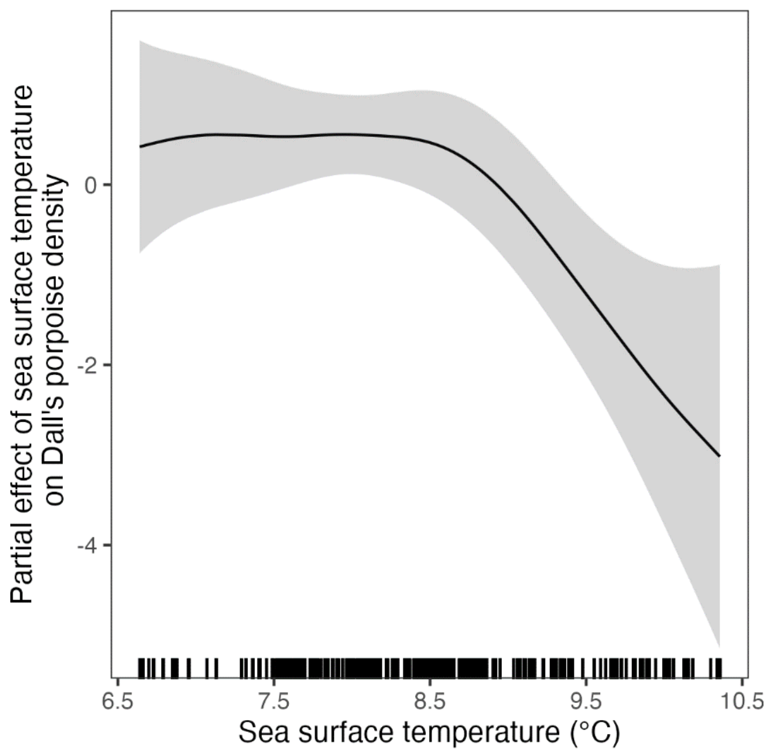

Figure 22. Partial effect of the smooth of sea surface temperature from the selected winter Dall's porpoise DSM. Shaded bands represent 95% confidence intervals. The rug plot along the x-axis indicates the distribution of sampled sea surface temperature values.

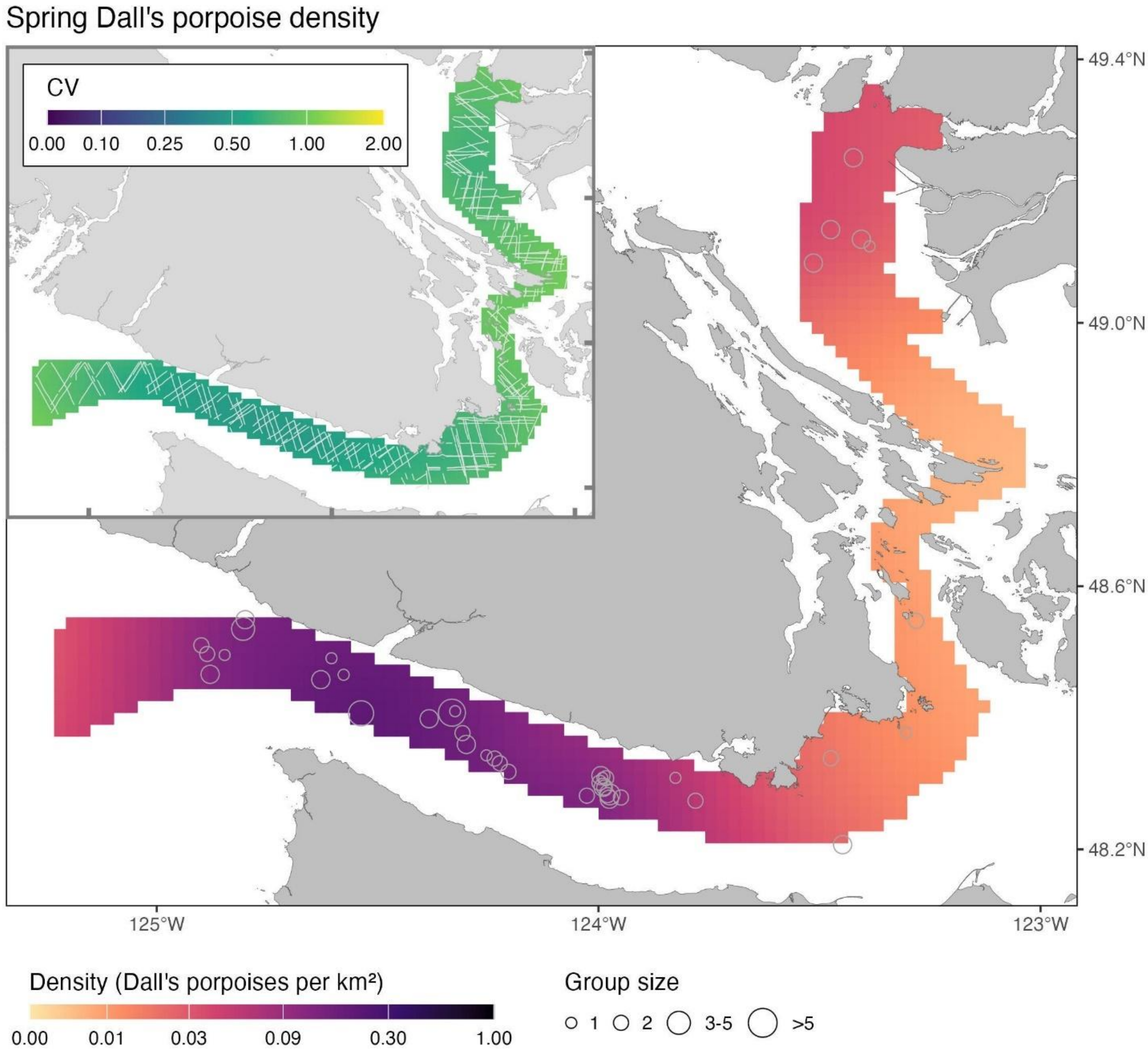

Figure 23. Dall's porpoise density (porpoises per km^2) during spring (April, May, June), as predicted by a Tweedie GAM with a bivariate spatial smooth, fit using a Duchon spline and including month as a factor. Total estimated Dall's porpoise abundance in spring was 201 (CV = 0.22). Sightings of Dall's porpoises during this period (n = 42) are indicated as open circles, relative size of circles indicates Dall's porpoise group size. Inset: spatially-varying CVs per 4 km^2 grid cell for the selected spring Dall's porpoise DSM. Completed spring survey effort is indicated by the grey transect lines.

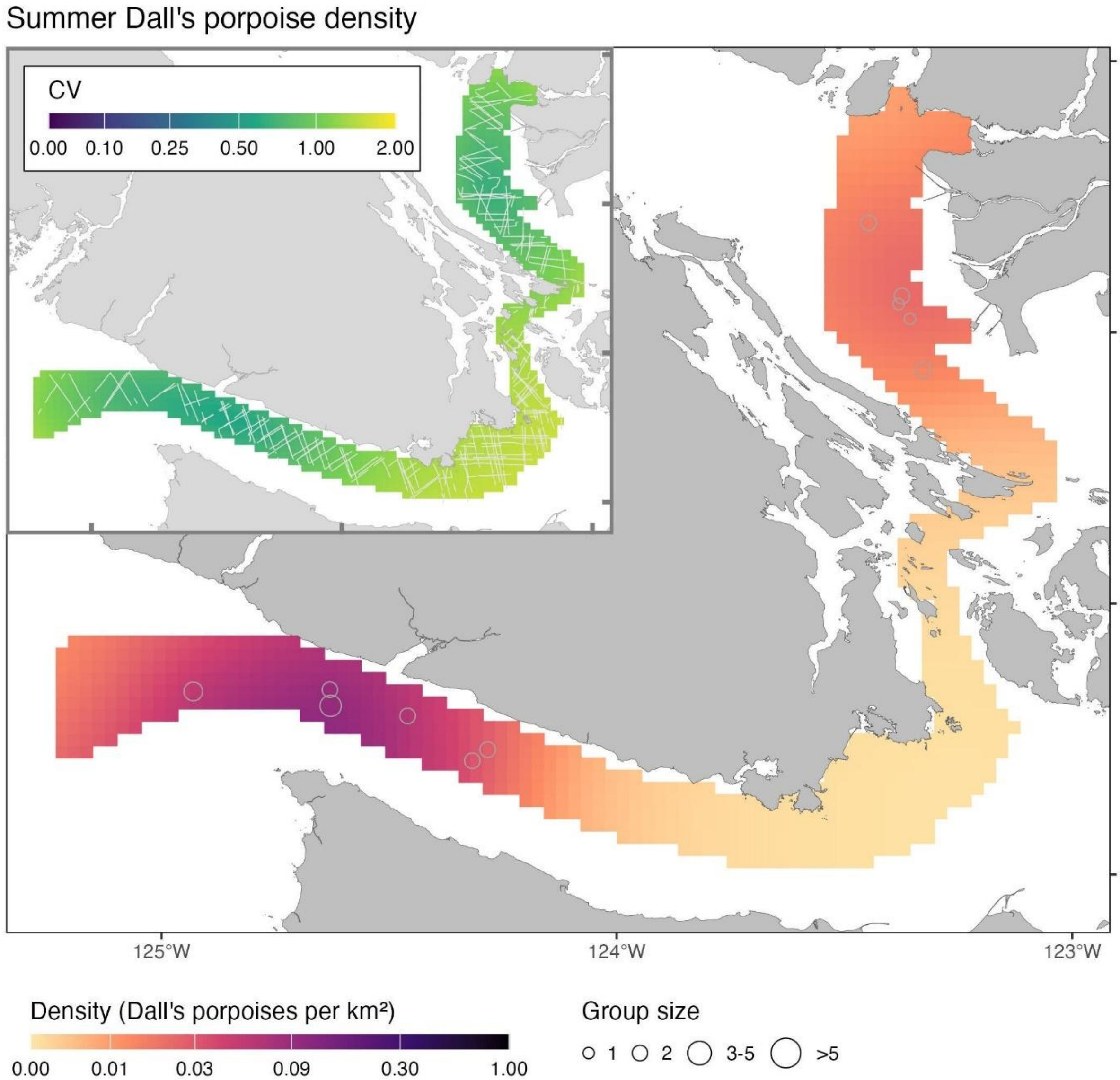

Figure 24. Dall's porpoise density (porpoises per km^2) during summer (July, August, September), as predicted by a Tweedie GAM with a bivariate spatial smooth as the only covariate and fit using a Duchon spline. Total estimated Dall's porpoise abundance in summer was 76 (CV = 0.35). Sightings of Dall's porpoise during this period (n = 11) are indicated as open circles, relative size of circles indicates Dall's porpoise group size. Inset: spatially-varying CVs per 4 km^2 grid cell for the selected summer Dall's porpoise DSM. Completed summer survey effort is indicated by the grey transect lines.

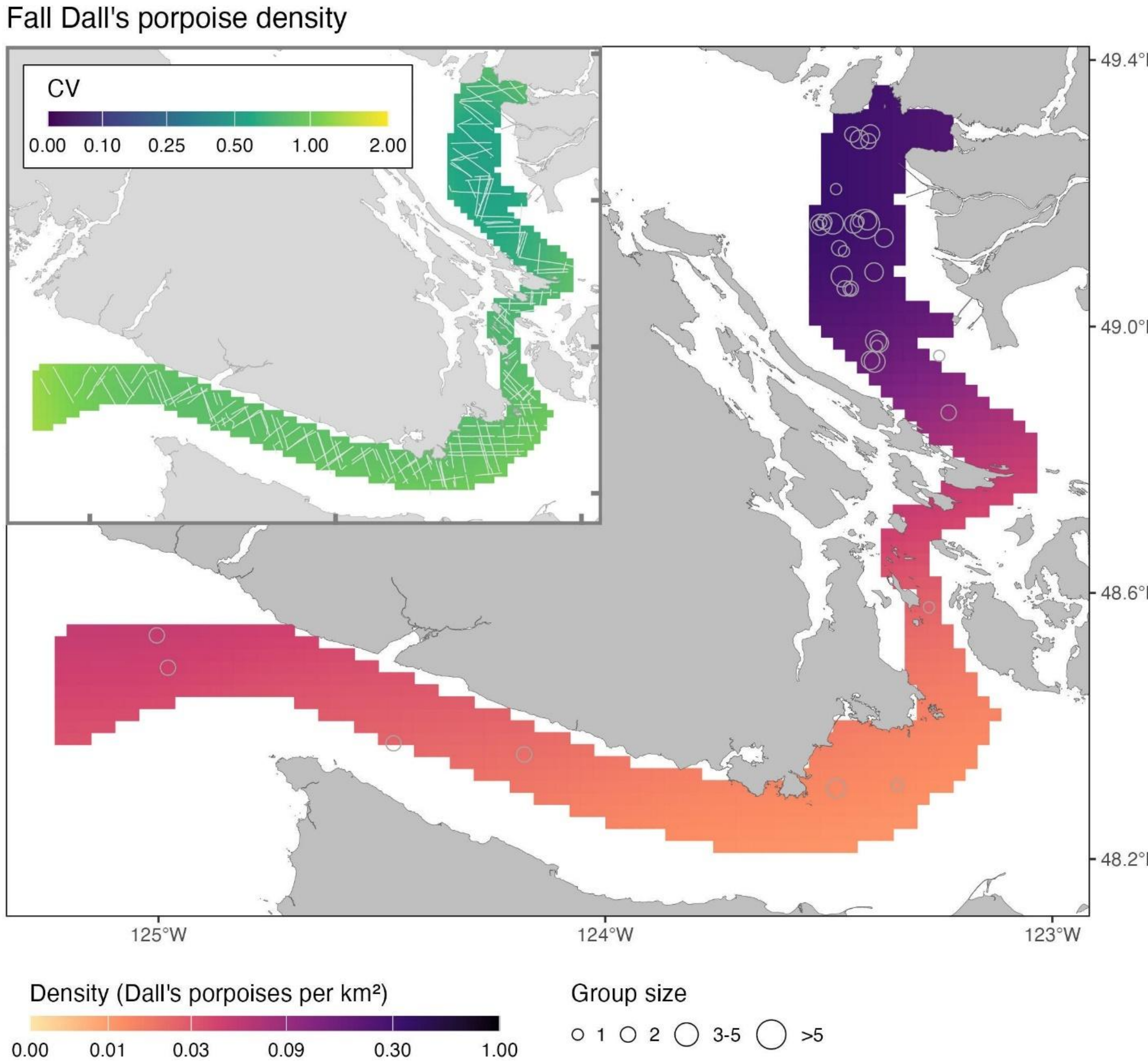

Figure 25. Dall's porpoise density (porpoises per km^2) during fall (October, November, December), as predicted by a Tweedie GAM with a bivariate spatial smooth, fit using a Duchon spline and including year as a factor. Total estimated Dall's porpoise abundance in fall was 283 (CV = 0.47). Sightings of Dall's porpoises during this period (n = 37) are indicated as open circles, relative size of circles indicates Dall's porpoise cluster size. Inset: spatially-varying CVs per 4 km^2 grid cell for the selected fall Dall's porpoise DSM. Completed fall survey effort is indicated by the grey transect lines.

APPENDIX A. ENVIRONMENTAL COVARIATES

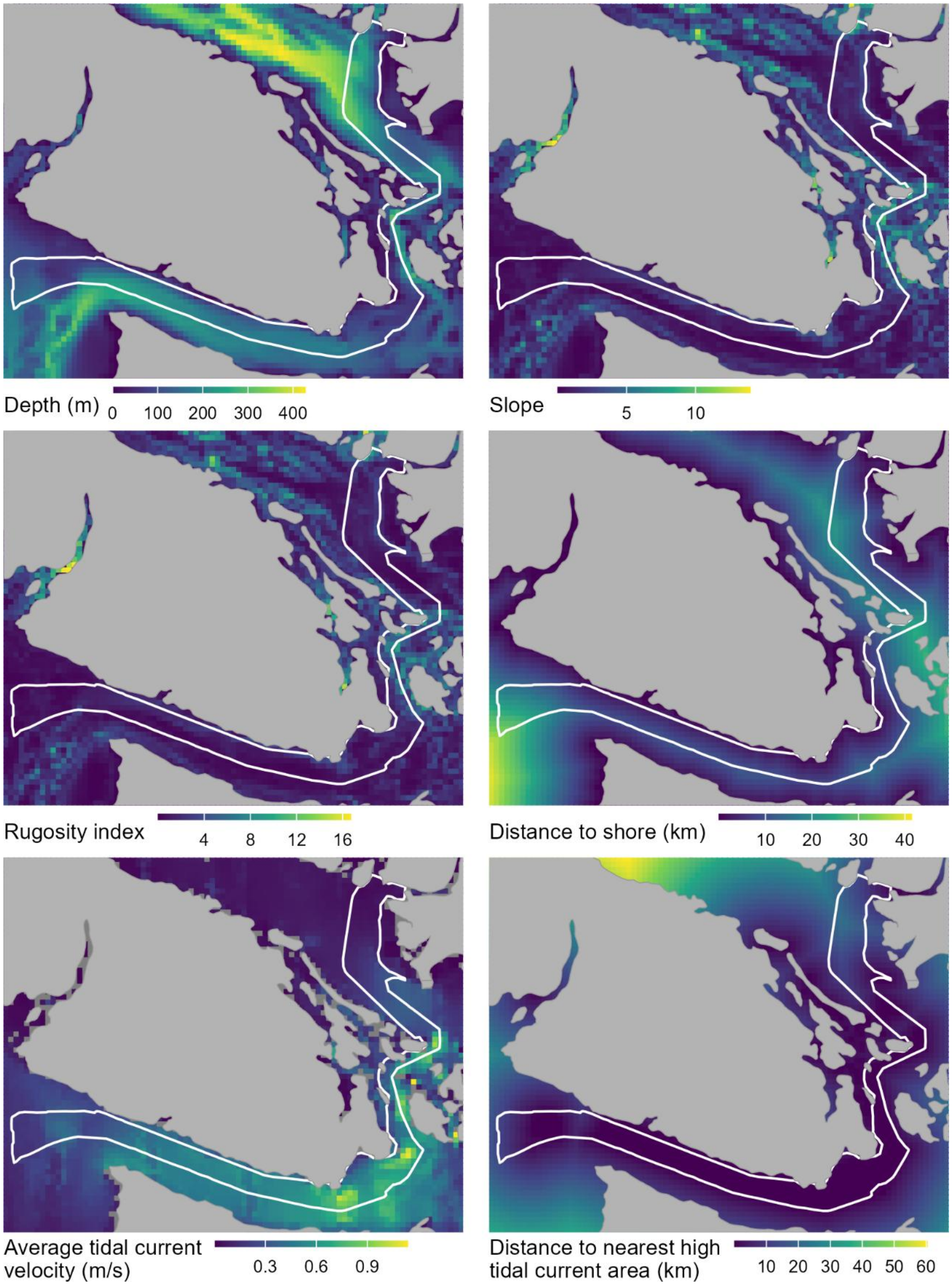

Figure A1. Static environmental covariates considered in candidate density surface models for humpback whales, harbour porpoises, and Dall's porpoises. The study area is delineated by the white outline.

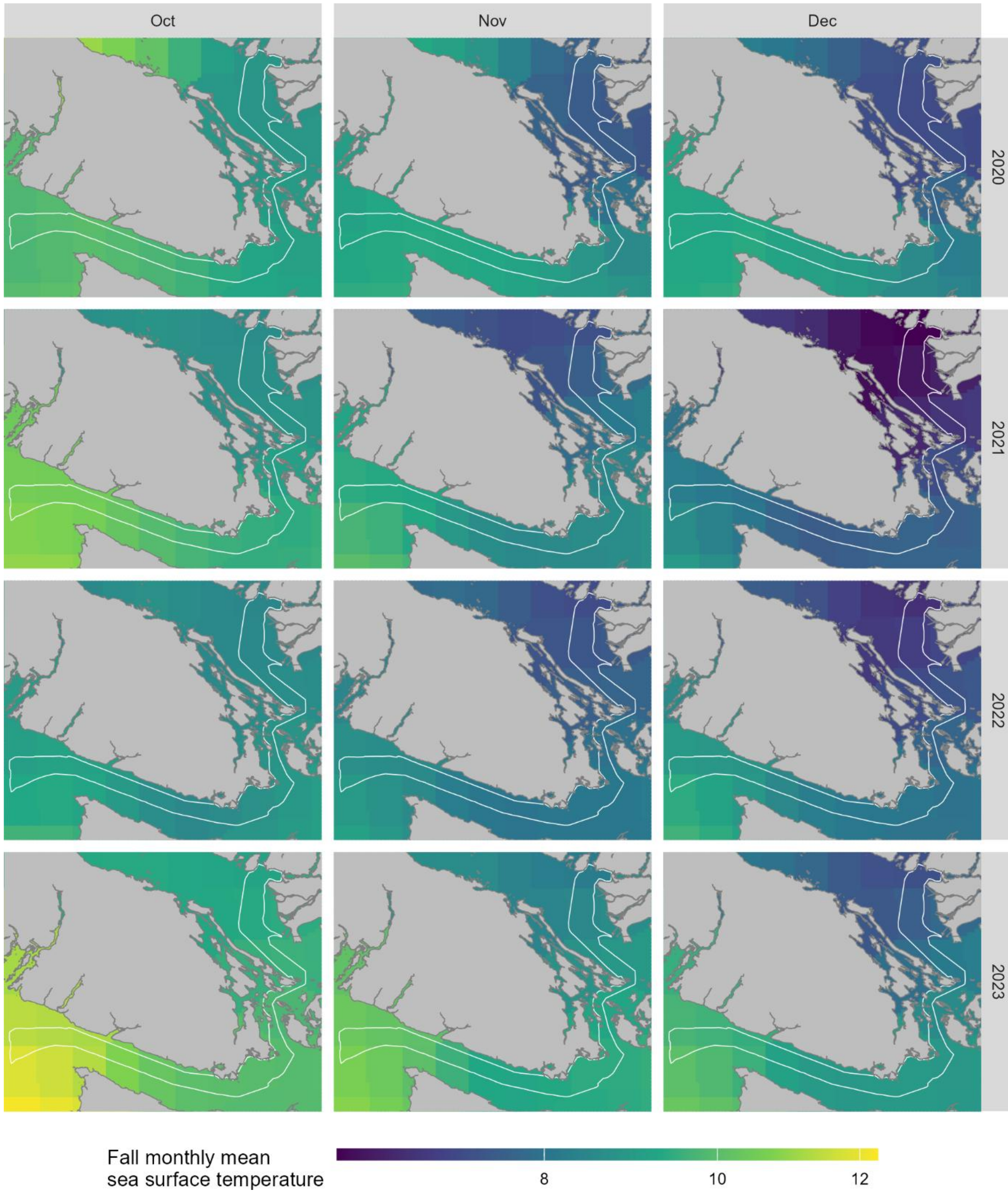

Figure A2. Spatially-varying sea surface temperature (°C), averaged by month, for fall months from 2020-2023. The study area is delineated by the white outline.

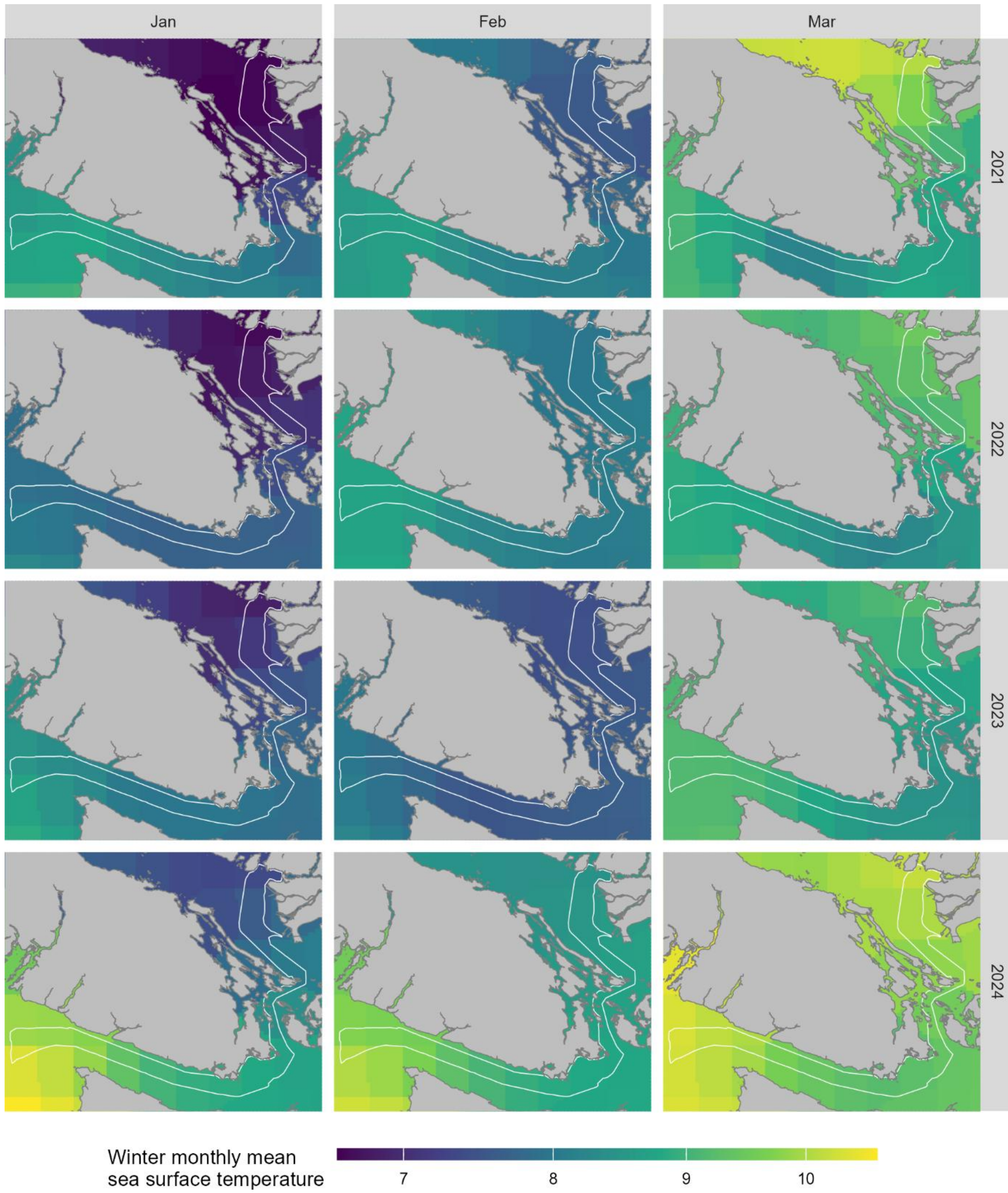

Figure A3. Spatially-varying sea surface temperature (°C), averaged by month, for winter months from 2021-2024. The study area is delineated by the white outline.